

# Mechanisms of co-translational protein targeting by mammalian SRP

Thesis by  
Jae Ho Lee

In Partial Fulfillment of the Requirements for  
the degree of  
Doctor of Philosophy

The Caltech logo, featuring the word "Caltech" in a bold, orange, sans-serif font, centered within a light yellow rectangular background.

CALIFORNIA INSTITUTE OF TECHNOLOGY  
Pasadena, California

2019  
(Defended May 22, 2019)

© 2019

Jae Ho Lee

ORCID: 0000-0002-8663-3209

## ACKNOWLEDGEMENTS

I would like to first thank my advisor, Dr. Shu-ou Shan. I had virtually no background in biochemistry prior to entering graduate school. She was patient with me and gave me time to learn and develop. Her genuine interest and dedication to research really motivated me to try to do the same. All the research would have not been possible without her training and guidance. I was fortunate to have had a chance to work with her.

I also want to thank my thesis committee, Dr. Andre Hoelz, Dr. Bil Clemons, and Dr. Douglas Rees, for their support throughout my graduate school and helpful discussions during committee meetings.

I would not have survived through my degree without the help from the Shan lab. They were not merely co-workers, but friends and family. I first want to thank past and present members of the lab for all the support and discussions: Aileen Ariosa, Sowmya Chandrasekar, Un Seng Chio, Yu-Hsien Hwang Fu, Hyunju Cho, Shuai Wang, Hao-Hsuan Hsieh, Chien-I Yang, Alex Siegel, Meera Rao, George Liang, David Akopian, Camile McAvoy, and Xin Zhang. Particularly, Aileen Ariosa for mentoring me in the beginning, and Sowmya Chandrasekar for mentoring and working with me to help us get through the early stages of the project. All my work would not have been possible without Sowmya Chandrasekar. Also, Un Seng Chio for helping me whenever I needed and spending much time with me outside of the lab. Along with Un Seng Chio, I want to give special thanks to Yu-Hsien Hwang Fu, Hyunju Cho, and Shuai Wang. It was great to have people who joined the lab at similar time. We had more time to bond and more common subjects for discussion as we went through similar phases. It really helped me especially when I was going through difficult times. Finally, I mention Hao-Hsuan Hsieh for helping me so much with optimizing single-molecule assays past few months.

I also had a lot of support from scientists in other labs. I want to first thank SangYoon Chung and Yazan Alhadid in Dr. Shimon Weiss lab at UCLA for dedicating a large fraction of their time to

help me with ALEX measurements. I also want to thank Nagai lab, Gilmore lab, Strub lab, and Zwieb lab for sharing expression constructs and purification protocols of human SRP proteins and RNA. Also, Ajay Sharma for sharing protocols and advice for in vitro translation in Rabbit Reticulocyte Lysate, and Dr. Harris Bernstein for sharing canine pancreatic microsomes. Finally, I want to thank Ahmed Jomaa and Dr. Nenad Ban for fruitful collaboration projects and sharing porcine microsomes.

I was privileged to grow up in a scholarly family. My father, Chang-Hee Lee, who is a professor in chemistry, sparked my interests in science and inspired me to follow his footsteps even when I was young. My mother, Ae-Ju Kim, also has a PhD, and her constant motivation to learn new things shaped my personality as I was growing up. My older brother, Jayhun Lee, also received his PhD few years ago and he is currently a post-doctoral fellow in Dr. Phil Newmark lab. It is great to be in an environment where all my family members know exactly what I am going through, so that I can frequently talk to them about any problems or concerns. I really want to thank them for their ample support and advice throughout my graduate school.

I went through an important phase of life during my graduate school. I was lucky to get married to my wife, Chae Ri Jung. Having her in my life naturally gave me bigger motivation to work harder. My personality also changed learning from her brave personality, not fearing failure, and constantly challenging herself. These changes and her sincere support really allowed me to get through graduate school and will continue to help me succeed in the future.

## ABSTRACT

Proper biogenesis of nascent protein is essential for cell survival. Signal recognition particle (SRP) is an essential and universally conserved factor involved in biogenesis of ~30% of the proteome through co-translational targeting of nascent proteins to Endoplasmic Reticulum (ER). Despite its importance, the mechanisms by which eukaryotic SRP ensure selective and efficient delivery of substrates to ER is poorly understood. Here, we reconstituted human SRP and SRP receptor (SR) to study the interaction between human SRP and SR, and conformational dynamics of SRP and SRP-SR targeting complex through biochemical and biophysical methods. We find that signal sequence and ribosomal components of the substrate sequentially activate human SRP. Especially, presence of signal sequence pre-organizes SRP conformation for efficient recruitment of SR, allowing specific and efficient targeting. In addition, we discover two essential roles of a conformational change in SR, where it is required not only for bringing targeting complex near the ER membrane, but also for inducing subsequent conformational changes of SRP-SR complex that ensures proper delivery of substrates to Sec61 translocon on ER membrane.

## PUBLISHED CONTENT AND CONTRIBUTIONS

Lee, J. H., Chandrasekar, S., Chung, S., Hwang Fu, Y.H., Liu, D., Weiss, S., Shan, S.-o. (2018). “Sequential activation of human signal recognition particle by the ribosome and signal sequence drives efficient protein targeting.” In: *Proceedings of the National Academy of Sciences U.S.A.* 115(24): E5487-E5496. doi: 10.1073/pnas.1802252115.

J.H.L. designed research with S.-o. S. and S.W. and performed research with S. Chandrasekar, S. Chung, Y.H. Hwang Fu, and D. L.. J.H.L. analyzed data and prepared all the figures. J.H.L. and S.-o. S. wrote the paper.

Kobayashi, K., Jomaa, A., Lee, J.H., Chandrasekar, S., Boehringer, D., Shan, S.-o., Ban, N. (2018). “Structure of a prehandover mammalian ribosomal SRP•SRP receptor targeting complex.” In: *Science* 360: 323-327. doi: 10.1126/science.aar7924

J.H.L. prepared samples for functional assays and performed them. Contributed to Figures 3C and 3D, Figure S12, Figure S13, and Figure S14.

## TABLE OF CONTENTS

Acknowledgements.....	iii
Abstract .....	v
Published Content and Contributions.....	vi
Table of Contents.....	vii
List of Illustrations and/or Tables.....	viii
Nomenclature.....	x
Chapter I: Sequential activation of human signal recognition particle by the ribosome and signal sequence drives efficient protein targeting .....	1
Introduction.....	2
Results.....	5
Discussion.....	20
Materials and Methods .....	27
Supplementary Figures .....	40
Chapter II: Dual role of SRP receptor compaction during membrane targeting steps of mammalian SRP pathway .....	50
Introduction.....	51
Results.....	54
Discussion.....	67
Materials and Methods .....	72
Supplementary Figures .....	75
References.....	81

## LIST OF ILLUSTRATIONS AND/OR TABLES

<i>Figures</i>	<i>Page</i>
1.1 Summary of the individual steps in the GTPase cycles of human SRP and SR.....	6
1.2 The ribosome and signal sequence activates SRP-SR GTPase cycle.....	8
1.3 Ribosome and signal sequence stabilize and accelerate SRP-SR complex formation .....	10
1.4 A functional signal sequence on the RNC stimulates the SRP-SR GTPase cycle and accelerates complex formation .....	13
1.5 Comparison of the activities of human SRP and hybrid SRP.....	16
1.6 Signal sequence and the ribosome exert different effects on the conformation of SRP.....	17
1.7 Comparison of <i>E.coli</i> and human SRP, and model for sequential conformational activation of mammalian SRP during targeting .....	21
S1.1 Large scale reconstitution of human SRP and SR .....	40
S1.2 Basal GTPase activities of hSRP, hSR, and their controls .....	42
S1.3 Schematic depiction of substrates used in this work and Measurement of hSRP binding to ribosomal complexes .....	43
S1.4 Fluorescence labeling does not substantially affect the activity of hSRP and hSR Large scale reconstitution of human SRP and SR.....	44
S1.5 Characterization of the mutant hSR(R458A).....	45
S1.6 Additional FRET measurements of the hSRP-SR interaction.....	46
S1.7 Schematic and control experiments for smFRET measurements.....	47
2.1 Distinct steps during conformational change from proximal to distal conformation .....	53
2.2 FRET probes to monitor NG-complex detachment and distal docking .....	55
2.3 FRET probes to monitor SR compaction .....	57
2.4 SR mutations and their effects on the conformation of SRP-SR complex....	59
2.5 Targeting and GTP hydrolysis activity of SR mutants .....	64
2.6 GTPase inhibition of active site residues in mammalian SRP system .....	66

2.7 Model for mammalian SRP pathway .....	71
S2.1 SRP-SR complex in distal conformation with SR mutations highlighted....	75
S2.2 smFRET histograms of distal docking activity of SR mutants .....	76
S2.3 smFRET histograms of NG-complex detachment activity of SR mutants ..	77
S2.4 smFRET histograms of SR compaction activity of SR mutants .....	78
S2.5 Structural model showing SRP-SR complex docked at the proximal site ...	79
S2.6 Details of GTPase active site mutations.....	80
<i>Tables</i>	<i>Page</i>
S1.1 Summary of the rate constants from measurements of the stimulated GTPase reaction between human SRP and SR .....	49
S1.2 Summary of the rate and equilibrium constants of the SRP-SR interaction measured using the FRET assay .....	49

## NOMENCLATURE

**$\beta$ ME.**  $\beta$ -mercapto ethanol

**4.5S RNA.** Bacterial SRP RNA

**4A10L.** Model signal sequence (LALALLLLLALAL)

**7SL RNA.** Mammalian SRP RNA

**80S.** Eukaryotic ribosome

**ALEX.** Alternating laser excitation

**Comp.** Compaction FRET probes

**Dist.** Distal FRET probes

**DTT.** Dithiothreitol

**E\*.** FRET efficiency

**ER.** Endoplasmic Reticulum

**FLAG.** Affinity tag used for purification of RNCs

**FRET.** Fluorescence resonance energy transfer

**GDP.** Guanosine diphosphate

**GppNHp.** Guanosine 5'-[ $\beta$ ,  $\gamma$ -imido] triphosphate. Non-hydrolysable GTP analogue.

**GTP.** Guanosine triphosphate

**hSR.** Human SR

**hSRP.** Human SRP

**mRNA.** Messenger RNA

**NAC.** Nascent polypeptide associated complex

**NIKKOL.** Octaethylene glycol monododecyl ether. A detergent shown to activate bacterial SRP.

**PDB.** Protein data bank

**pdf.** Probability density function

**pPL.** Preprolactin. A model SRP substrate.

**Prox.** Proximal FRET probes

**RM.** ER microsomes

**RNA.** Ribonucleic acid

**RNC.** Ribosome nascent chain complex

**smFRET.** Single molecule FRET

**SR.** Signal recognition particle receptor

**SRP.** Signal recognition particle

**SS.** Signal sequence

**TKRM.** Trypsin digested, high-salt washed ER microsomes

**TMD.** Transmembrane domain

*Chapter 1***SEQUENTIAL ACTIVATION OF HUMAN SIGNAL RECOGNITION PARTICLE BY THE RIBOSOME AND SIGNAL SEQUENCE DRIVES EFFICIENT PROTEIN TARGETING**

A version of this chapter was first published as: Lee, J. H., Chandrasekar, S., Chung, S., Hwang Fu, Y.H., Liu, D., Weiss, S., Shan, S.-o. (2018). “Sequential activation of human signal recognition particle by the ribosome and signal sequence drives efficient protein targeting.” In: *Proceedings of the National Academy of Sciences U.S.A.* 115(24): E5487-E5496. doi: 10.1073/pnas.1802252115.

Signal recognition particle (SRP) is a universally conserved targeting machine that mediates the targeted delivery of ~30% of the proteome. The molecular mechanism by which eukaryotic SRP achieves efficient and selective protein targeting remains elusive. Here, we describe the first quantitative analysis of completely reconstituted human SRP and SRP receptor. Enzymatic and fluorescence analyses showed that the ribosome together with a functional signal sequence on the nascent polypeptide are required to activate SRP for rapid recruitment of the SRP receptor, thus delivering translating ribosomes to the ER. Single molecule fluorescence spectroscopy combined with cross-complementation analyses reveal a sequential mechanism of activation, wherein the ribosome unlocks the human SRP from an auto-inhibited state and primes SRP to sample a variety of conformations. The signal sequence further pre-organizes the mammalian SRP into the optimal conformation for efficient recruitment of the SRP receptor. Finally, the use of a signal sequence to activate SRP for receptor recruitment is a universally conserved feature to enable efficient and selective protein targeting, while the eukaryote-specific components confer upon the mammalian SRP the ability to sense and respond to ribosomes.

## 1.1 INTRODUCTION

Proper localization of nascent proteins is essential for maintaining compartmentalization and protein homeostasis in all cells (Hartl, Bracher, & Hayer-Hartl, 2011). The universally conserved signal recognition particle (SRP) pathway is responsible for the targeted delivery of approximately 30% of the newly synthesized proteome to the eukaryotic endoplasmic reticulum (ER), or the bacterial plasma membrane. SRP recognizes an N-terminal transmembrane domain (TMD) or hydrophobic signal sequence as a nascent protein emerges from the translating ribosome. Through interaction with the SRP receptor (SR), SRP delivers translating ribosomes to the Sec61p (or SecYEG) translocase on the target membrane. Bacteria contain the simplest SRP, comprised of the universally conserved SRP54 protein bound to the 4.5S SRP RNA. SRP54 is a multi-domain protein that contains an M-domain that binds the SRP RNA and recognizes signal sequences on the nascent polypeptides, and a special GTPase domain, termed the NG-domain, that contacts the ribosome and binds to a homologous NG-domain in SR (termed FtsY in bacteria) (Akopian, Shen, Zhang, & Shan, 2013; Zhang & Shan, 2014). Extensive biochemical and biophysical studies demonstrated how an SRP-dependent signal sequence or transmembrane domain (TMD) in a ribosome•nascent chain complex (RNC) regulates the GTP-dependent interaction of SRP with SR and their reciprocal GTPase activation, thus enabling efficient and specific co-translational protein targeting in bacteria (Kuang Shen et al., 2013; Zhang, Rashid, Wang, & Shan, 2010; Zhang, Schaffitzel, Ban, & Shan, 2009).

SRP undergoes an extensive expansion in size and complexity during evolution. The eukaryotic SRP contains a larger 7SL SRP RNA and six protein subunits (SRP9, SRP14, SRP19, SRP54, SRP68, and SRP72). Eukaryotic SR is a heterodimer of SR $\alpha$  and SR $\beta$  subunits. SR $\alpha$  contains an NG domain homologous to that in bacterial FtsY, and an additional X-domain that binds the cytosolic domain of SR $\beta$ . SR $\beta$  contains an additional N-terminal TMD that anchors the eukaryotic SR at the ER membrane (Akopian et al., 2013). The complexity of the mammalian SRP has limited its in-depth mechanistic analyses, and the mechanism by which the eukaryotic SRP pathway achieves efficient and selective protein targeting remains unclear. Microarray and ribosome-profiling analyses of SRP-associated RNCs in yeast (Alamo et al., 2011; Chartron, Hunt, & Frydman, 2016) suggested that the eukaryotic SRP can associate with translating ribosomes without or before the emergence of a signal sequence, raising questions as to the timing and specificity of cargo recognition by SRP. On the other hand, proximity-ribosome profiling experiments in yeast and mammalian cells showed that most ER-associated ribosomes targeted by SRP contain TMD targeting signals (Costa, Subramanian, Nunnari, & Weissman, 2018; Jan, Williams, & Weissman, 2014), suggesting that eukaryotic SRP maintains high targeting selectivity. A potential resolution of these observations is that molecular events after ribosome binding govern the selectivity of this pathway. As SRP has a limited time window to complete the targeting reaction before the nascent polypeptide reaches a critical length (Flanagan et al., 2003; Siegel & Walter, 2018), cargo recognition by SRP must be coupled to efficient delivery to the ER membrane, a process mediated by the direct interaction between the NG-domains of SRP54 and SR $\alpha$ . However, limited information is available on this critical step in the eukaryotic

SRP pathway. Previous work showed that an RNC stimulates the GTPase activity of mammalian SRP and SR, presumably when they form a complex (Bacher, Lütcke, Jungnickel, Rapoport, & Dobberstein, 1996). Nevertheless, an empty ribosome was also found to stimulate the SRP-SR interaction and their GTPase activity (Mandon, Jiang, & Gilmore, 2003), and direct interactions between the mammalian SR and ribosome have been detected (Jadhav et al., 2015). These observations raise questions as to whether the recruitment of SR is specific to SRPs bound to RNCs bearing SRP-dependent substrates. The roles and contributions of the ribosome and signal sequence in regulating the membrane targeting step in the eukaryotic SRP pathway are unresolved, nor the mechanism by which these regulations are exerted.

To address these questions, we reconstituted functional human SRP and SR from recombinant components, which enabled their mechanistic interrogation at high resolution. We found that both the ribosome and a functional signal sequence are necessary for the most efficient assembly and reciprocal GTPase activation between mammalian SRP and SR. Single-molecule FRET (smFRET) measurements showed that the signal sequence plays a dominant role in inducing a ‘proximal’ conformation of SRP that is optimal for the recruitment of SR, whereas the ribosome unlocks SRP from an auto-inhibited mode and allows SRP to sample a variety of conformations. These results, together with cross-complementation analyses, showed that the use of signal sequence to activate SRP for receptor recruitment is a universally conserved feature of SRP pathways, but the mammalian specific components enable the SRP to also sense and be primed by the ribosome.

## 1.2 RESULTS

### *Ribosome and signal sequence together activate the hSRP-hSR GTPase cycle.*

Previous biochemical work on the mammalian SRP pathway (Bacher et al., 1996; Powers & Walter, 1995) has largely relied on native SRP and SR. The low quantity and inability to perturb the system limited in-depth mechanistic investigations. To overcome this barrier, we assembled human SRP (hSRP) from recombinantly purified components using modifications of published procedures (Fig. S1.1A) (Gowda et al., 1998; Huck, 2004; Menichelli, Isel, Oubridge, & Nagai, 2007; Walker, Black, & Zwieb, 1995). Holo-SRP was selectively purified using DEAE-Sephacel, which effectively removes free 7SL RNA and incompletely assembled SRPs (Huck, 2004) (Fig. S1.1B-D). We also expressed and purified a soluble human SR (hSR) complex comprised of full-length hSR $\alpha$  and hSR $\beta\Delta$ TM, in which the dispensable N-terminal TMD in SR $\beta$  was removed (Fig. S1.1E, F) (Ogg, Barz, & Walter, 1998). The reconstituted hSRP and hSR $\alpha\beta\Delta$ TM are highly active in mediating the co-translational targeting and insertion of a model SRP substrate, preprolactin (pPL), into trypsin-digested rough ER microsomes (TKRM) that lacks endogenous SRP and SR (Shan, Chandrasekar, & Walter, 2007) (Fig. S1.1G, H), with efficiency comparable to that of native SRP (Nilsson et al., 2015).

To understand how the GTPases in the mammalian SRP and SR regulate protein targeting, we defined a rigorous kinetic and energetic framework for their GTPase cycle that includes the basal GTPase cycles of free hSRP and hSR (Fig. 1.1A, upper triangles), their assembly with one another (Fig. 1.1A, step 4), and GTP hydrolysis in the hSRP•hSR complex (Fig. 1.1A, step 5). The basal GTPase cycle of hSRP (or hSR) was determined by measuring

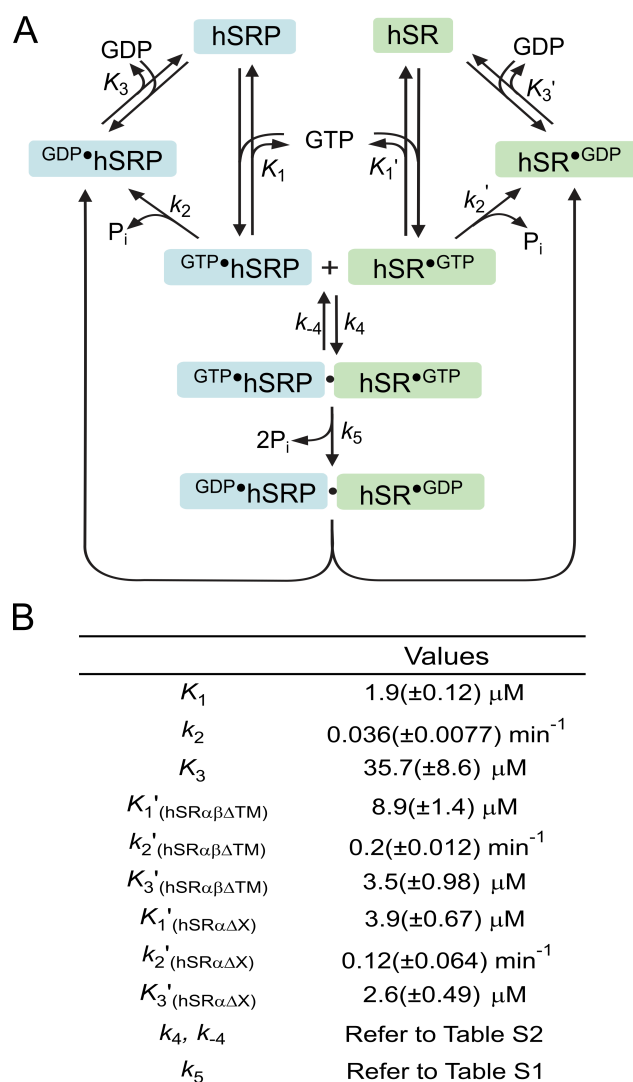


**Figure 1.1** Summary of the individual steps in the GTPase cycles of human SRP and SR. **(A)** Scheme of the GTPase cycles of hSRP (blue) and hSR (green). Superscripts depict the nucleotide bound to each protein. The triangular cycles on the top left and right depict the basal GTPase cycles of hSRP54 and hSR, respectively. Binding of GTP and GDP to hSRP (or SR) are characterized by the equilibrium dissociation constants  $K_1$  and  $K_3$  (or  $K_1'$  and  $K_3'$ ), respectively. Rate constants for GTP hydrolysis from free hSRP and hSR are denoted by  $k_2$  and  $k_2'$ , respectively. Complex formation between hSRP and hSR is characterized by the association rate constant  $k_4$  and dissociation rate constant  $k_{-4}$ . Bound GTPs are hydrolyzed from the  $\text{GTP}\cdot\text{hSRP}\cdot\text{hSR}\cdot\text{GTP}$  complex, represented collectively by the rate constant  $k_5$ , followed by dissociation of the  $\text{GDP}\cdot\text{hSRP}\cdot\text{hSR}\cdot\text{GDP}$  complex. **(B)** Summary of the kinetic parameters described in A. Determination of the individual rate and equilibrium constants is described in the Materials and Methods section.

GTP hydrolysis rates under single turnover conditions with the enzyme in excess of GTP. The slow observed  $k_{\text{cat}}$  ( $0.00060 \text{ s}^{-1}$  and  $0.0033 \text{ s}^{-1}$  for hSRP and hSR, respectively) and  $k_{\text{cat}}/K_m$  ( $3.2 \times 10^2 \text{ M}^{-1}\text{s}^{-1}$  and  $3.7 \times 10^2 \text{ M}^{-1}\text{s}^{-1}$  for hSRP and hSR, respectively) values in the basal GTPase reactions strongly suggest that equilibrium binding of GTP occurs before GTP hydrolysis. Thus, the value of  $K_m$  equals  $K_1$  (or  $K_1'$ ), the equilibrium dissociation constant of GTP for hSRP (or hSR). The binding affinity of GDP for hSRP (or hSR) was determined using GDP as a competitive inhibitor of the basal GTPase reactions. The interaction and reciprocal activation between hSRP and hSR was initially assessed by measuring the rates of the reciprocally stimulated GTPase reaction using a small, fixed amount of hSRP and varying concentrations of excess hSR. As validated by independent fluorescence-based measurements of the hSRP-hSR interaction (next section), the value of  $k_{\text{cat}}/K_m$  in this reciprocally stimulated GTPase reaction equals  $k_4$ , the rate constant for hSRP-hSR assembly, and the value of  $k_{\text{cat}}$  reports on the rate constant of GTP hydrolysis from the most stable hSRP•hSR complex that accumulates during GTP turnover.

Analogous to their bacterial homologues, hSRP and hSR $\alpha\beta\Delta\text{TM}$  by themselves displayed weak nucleotide affinities and slow basal GTPase rates (Fig. S1.2A-C; Fig. 1.1B,  $K_1$ ,  $k_2$ ,  $K_3$  and  $K_1'$ ,  $k_2'$ ,  $K_3'$ ). Bacterial SRP and SR activate the GTPase activities of one another when they form a complex (Peluso, Shan, Nock, Herschlag, & Walter, 2001; Powers & Walter, 1995). In contrast, this reciprocal GTPase activation was barely detectable when hSRP and hSR $\alpha\beta\Delta\text{TM}$  were incubated together (Fig. 1.2A, black circles), even in the presence of the detergent NIKKOL (Octaethylene glycol monododecyl ether, C<sub>12</sub>E<sub>8</sub>) that stimulated the GTPase cycle of bacterial SRP and SR (Fig. S1.2D) (Bradshaw, Neher, Booth,

& Walter, 2009). We therefore searched for potential regulators that stimulate the GTPase cycle of mammalian SRP and SR. Given the observation that fusion of a signal peptide to the C-terminus of the SRP54 M-domain (Hainzl, Huang, Meriläinen, Brännström, & Sauer-Eriksson, 2011) led to structural reorganization of archaeal SRP54 and its stimulated GTPase reaction with SR (Hainzl & Sauer-Eriksson, 2015), we generated mutant hSRP-4A10L in which the C-terminal M-domain of hSRP54 is fused to a model signal sequence, 4A10L (LALALLLLLLLALAL; also see Fig. S1.3A). In addition, we tested the effect of purified 80S ribosome, which was reported to enhance the stimulated GTPase reaction between canine SRP and SR (Bacher et al., 1996; Mandon et al., 2003).

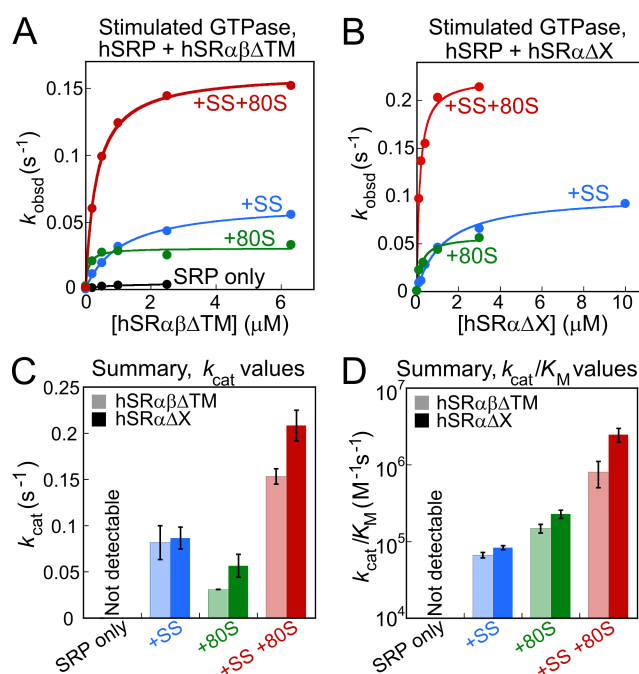


**Figure 1.2.** The ribosome and signal sequence activates the SRP-SR GTPase cycle. **(A, B)** Representative hSR concentration dependences of the reciprocally stimulated GTPase reaction between SRP and hSR $\alpha\beta\Delta$ TM **(A)** or hSR $\alpha\Delta$ X **(B)**. Reactions contained 0.2  $\mu$ M hSRP or hSRP-4A10L, 100  $\mu$ M GTP, and indicated concentrations of hSR. Purified 80S was present at 0.25  $\mu$ M where indicated. The lines are fits of the data to Eq. 2 in Materials and Methods. **(C, D)** Summary of the  $k_{cat}$  **(C)** and  $k_{cat}/K_M$  **(D)** values derived from analysis of the data in parts **A, B** and their replicates. Data are represented as mean  $\pm$  S.D., with  $n \geq 2$ .

Indeed, the presence of either the signal sequence or the 80S ribosome enhanced the reciprocally activated GTPase reaction between hSRP and hSR (Fig. 1.2A). In contrast, the ribosome and signal sequence provided <50% stimulation for free hSRP (Fig. S1.2E, F), indicating that the observed GTPase stimulations are specific to the hSRP•hSR complex. Quantitative analysis of the GTPase data also revealed modest differences in the effects of the signal sequence and the ribosome. The slope at sub-saturating hSR concentrations ( $k_{cat}/K_m$ ), which reports on the assembly between hSRP and hSR (corroborated by fluorescence measurements of the hSRP-hSR interaction later), is more strongly stimulated by the ribosome (Fig. 1.2D and Table S1.1). The rate constant at saturating protein concentration ( $k_{cat}$ ), which reports on the rate constant of GTP hydrolysis from a stably formed hSRP•hSR complex, is more strongly stimulated by the signal sequence (Fig. 1.2C and Table S1.1). When both the ribosome and signal sequence are present, which provides a mimic of the RNC (corroborated by experiments with RNC<sub>4A10L</sub> later), the strongest stimulation was observed for both rate constants (Fig. 1.2, red, and Table S1.1), indicating synergistic actions of both components in activating the GTPase cycle of the mammalian SRP and SR.

***A functional signal sequence confers kinetic privilege to hSRP during hSR recruitment.***

To directly monitor complex formation between hSRP and hSR, we developed a Förster Resonance Energy Transfer (FRET) assay. A donor dye (Cy3B) was labeled at an engineered cysteine (C47) using thiol-specific maleimide chemistry in cyslite hSRP54, in which all the solvent-exposed native cysteines were removed (C36T, C136S, and C229A) (Fig. 1.3A). The two remaining native cysteines in hSRP54 were buried and not labeled

under our experimental conditions. An acceptor dye (ATTO 647N) was conjugated to the C-terminus of hSR $\alpha$  via sortase-mediated ligation (Fig. 1.3A) (Guimaraes et al., 2013).

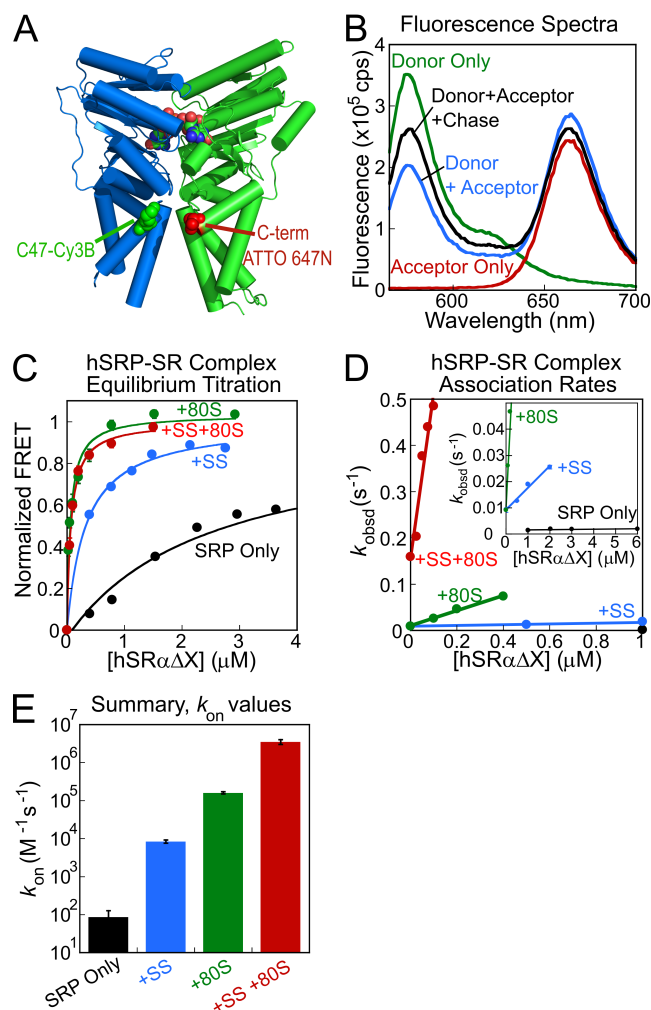


**Figure 1.3.** Ribosome and signal sequence stabilize and accelerate SRP-SR complex formation. **(A)** The positions of FRET probes are shown on the crystal structure of the NG domain complex between hSRP (blue) and hSR $\alpha$  (green) (PDB: 5L3Q) (Wild et al., 2016). **(B)** Fluorescence emission spectra of 20 nM Cy3B-labeled hSRP-4A10L before (*green*) and after addition of 400 nM ATTO 647N-labeled hSR $\alpha$  $\Delta$ X (*blue*), and of 400 nM ATTO 647N-labeled hSR $\alpha$  $\Delta$ X alone (*red*). Addition of 2  $\mu$ M unlabeled hSR $\alpha$  $\Delta$ X (*black*) to a preformed hSRP-SR complex restores the donor fluorescence and reduces acceptor fluorescence, confirming that a large fraction of the observed fluorescence change arises from FRET. The reactions also contained 40 nM 80S to facilitate complex assembly. **(C)** Representative equilibrium titrations of SRP-SR complex formation using the FRET assay. Titrations used 12.5 nM hSRP or hSRP-4A10L, indicated concentrations of hSR, and 2 mM GTP. Where indicated, 300 nM and 40 nM 80S were used for titrations with hSRP and hSRP-4A10L,

respectively. The lines are fits of the data to Eq. 7 in Materials and Methods, and the obtained  $K_d$  values are summarized in Table S1.2. All measurements were repeated at least twice. **(D, E)** FRET-based measurements of SRP-SR association kinetics. Reactions contained the same concentrations of all the factors as in C. The data were fit to Eq. 5 in Materials and Methods, and the obtained  $k_{on}$  values are summarized in part E and Table S1.2. Error bars denote S.D., with  $n \geq 2$ .

Incubation of labeled hSRP and hSR resulted in a significant reduction in donor fluorescence and increase in acceptor fluorescence, and these fluorescence changes can be competed away by unlabeled SR (Fig. 1.3B), indicating FRET between the dye pair. The mutations and fluorescence labeling did not substantially affect the GTPase activity of hSRP and hSR, or their protein targeting activity (Fig. S1.4). In the course of these experiments, we found that a simpler hSR construct hSR $\alpha\Delta X$ , in which the X-domain of SR $\alpha$  and SR $\beta$  are removed (Fig. S1.1E, F), displayed SRP-SR assembly, GTPase activation, and preprotein targeting activities that are comparable to or slightly higher than hSR $\alpha\beta\Delta TM$  (Figs. S1.1G, H, 1.2B-D, and Fig. S1.2). This is consistent with previous observations using canine SRP and SR (Hortsch, Avossa, & Meyer, 1985; Lauffer et al., 1985; Mandon et al., 2003; Meyer, 1982) and indicated that hSR $\alpha\Delta X$  provides a fully functional mimic of hSR for studying the initial assembly between hSRP and hSR. Hence, all subsequent fluorescence measurements of the hSRP-hSR interaction were carried out with hSR $\alpha\Delta X$ . Finally, to block GTP hydrolysis from the hSRP•hSR complex, which would provide an alternative pathway for complex dissociation (via the less stable  $GDP^*SRP \cdot SR^*GDP$  complex (Connolly, Rapiejko, & Gilmore, 1991)), we introduced the R458A mutation in hSR, which disrupts catalytic interactions at the composite active site between hSRP and hSR (Fig. S1.5A). As expected, this mutant was catalytically dead in the reciprocally activated GTPase reaction between hSRP and hSR (Fig.

S1.5B) but effectively competed with wildtype hSR for interaction with hSRP (Fig. S1.5C), indicating that mutant hSR $\alpha\Delta X$  (R458A) still allows rapid and stable hSRP•hSR complex assembly but specifically blocks GTPase activation in the complex.

Using this FRET assay, we tested how the kinetics and equilibrium of hSRP•hSR complex formation are regulated. Equilibrium titrations showed that the interaction between hSRP and hSR was weak by themselves, with an equilibrium dissociation constant ( $K_d$ ) in the micromolar range (Fig. 1.3C and Table S1.2). The hSRP•hSR complex was stabilized ~8-fold by the signal sequence and ~40-fold by the ribosome (Fig. 1.3C and Table S1.2). With both signal sequence and ribosome present, the equilibrium stability of the complex was 56 nM, similar to that with the ribosome (Fig. 1.3C and Table S1.2). Independent determination of  $K_d$  values from the ratio of dissociation and association rate constants ( $k_{off}/k_{on}$ ) yielded similar conclusions (Fig. S1.6A and Table S1.2). On the other hand, kinetic analysis of hSRP-hSR complex assembly showed that this reaction was intrinsically slow, with an association rate constant ( $k_{on}$ ) of  $<10^2 \text{ M}^{-1}\text{s}^{-1}$ . Assembly was accelerated ~ $10^2$ -fold by the signal sequence (Fig. 1.3D, E). The ribosome also provided a ~ $10^3$ -fold stimulation, and the additional presence of the signal sequence further accelerated hSRP-hSR assembly 20-fold, bringing the  $k_{on}$  value to  $>10^6 \text{ M}^{-1}\text{s}^{-1}$  (Fig. 1.3D, E). These results are consistent with the effect of the ribosome and signal sequence on the  $k_{cat}/K_m$  values measured in the GTPase assay (Fig. 1.2D and Table S1.1). Thus, although the ribosome appears to dictate the equilibrium stability of the hSRP•hSR complex, the signal sequence provides a significant additional stimulation for the kinetics of hSRP-hSR complex formation.

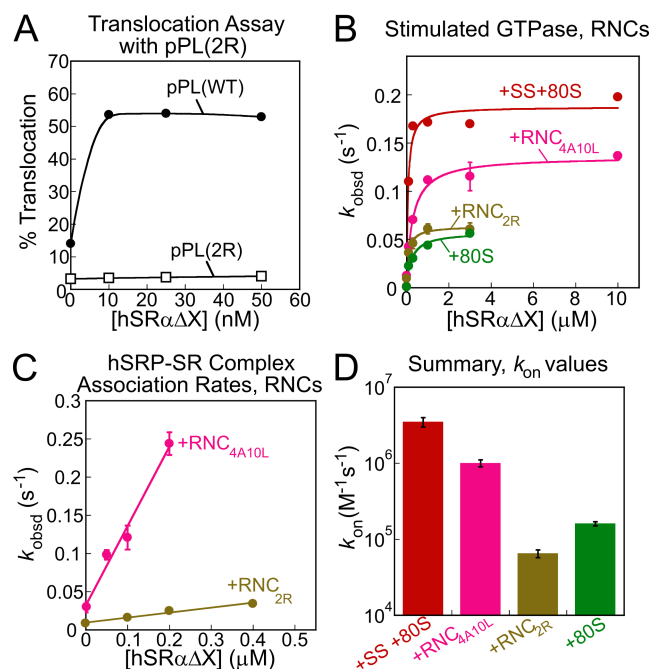


**Figure 1.4.** A functional signal sequence on the RNC stimulates the SRP-SR GTPase cycle and accelerates SRP-SR complex formation. **(A)** Introduction of the 2R mutation in the pPL signal sequence abolished co-translational targeting by hSRP and hSR. Targeting reactions were carried out as described in Materials and Methods using 50 nM hSRP and indicated hSR concentrations. **(B)** Reciprocally stimulated GTP hydrolysis reactions between hSRP and hSR were measured in the presence of 0.3  $\mu$ M RNC $_{4A10L}$  (magenta) or RNC $_{2R}$  (olive). All other reaction conditions are the same as in Fig. 1.2A. The reactions with hSRP-4A10L and 80S (red) were performed in parallel for direct comparison. The reaction with 80S (green) was taken from Fig. 1.2B for comparison. The lines are fits of the data to Eq. 2 in Materials and Methods, and the obtained rate constants are summarized in Table S1.1. **(C)** FRET-based measurements of hSRP-SR association kinetics in the presence of RNC $_{4A10L}$  or RNC $_{2R}$ , carried out under the same conditions as in Fig. 1.3C. **(D)** Summary of the hSRP-SR association rate constants obtained from analysis of the data in part C and their replicates. The data with ribosome and SRP-4A10L were from Fig. 1.3 and shown for comparison. All error bars denote S.D., with  $n \geq 2$ .

To verify that the combination of ribosome and signal sequence fusion to hSRP54 provides a reasonable mimic for the physiological SRP substrate, we generated stalled RNCs by *in vitro* translation of a truncated mRNA encoding the first 90 amino acids of pPL without a stop codon (Fig. S1.3A) (Voorhees & Hegde, 2015). The signal sequence in pPL was

replaced by 4A10L to allow direct comparison with hSRP-4A10L. As a negative control, we inserted two arginines into the pPL signal sequence to generate RNC<sub>2R</sub> (Fig. S1.3A) (Nilsson et al., 2015). *In vitro* targeting assay confirmed that the 2R mutation disrupted SRP-dependent protein targeting (Fig. 1.4A and Fig. S1.3B). RNC<sub>4A10L</sub> and RNC<sub>2R</sub> were affinity purified via a 3xFLAG tag N-terminal to the pPL coding sequence followed by a sucrose gradient to isolate a homogenous population of monosomes bearing the nascent polypeptide. Binding of hSRP to RNC<sub>4A10L</sub> and to the 80S ribosome was confirmed by a binding assay based on microscale thermophoresis (Fig. S1.3C), and saturating concentrations of the RNC and ribosome with respect to their hSRP binding constants were used for the measurements below.

Purified RNCs were tested for their ability to stimulate hSRP-hSR complex assembly and subsequent GTPase activation. In the GTPase assay, the reactions with RNC<sub>4A10L</sub> behaved more similarly to those of signal sequence-fused hSRP in the presence of the ribosome, whereas the reactions with RNC<sub>2R</sub> were more similar to that of hSRP with empty ribosomes (Fig. 1.4B). In the FRET assay, RNC<sub>4A10L</sub> induced rapid hSRP-hSR assembly, with a rate constant similar to that observed with the combination of signal sequence and ribosome, and 10- and 20-fold faster than the assembly rates observed with empty ribosome and RNC<sub>2R</sub>, respectively (Fig. 1.4C, D and Table S1.2). Although RNC<sub>2R</sub> presumably binds hSRP more weakly, the RNC<sub>2R</sub>-induced stimulation of hSRP-hSR assembly and GTPase activation indicated that binding between hSRP and RNC<sub>2R</sub> occurred. Furthermore, the observed GTPase rate constant was not substantially enhanced by increasing the concentration of RNC<sub>2R</sub> beyond 300 nM (Fig. 1.4B and Fig. S1.3E), indicating that an RNC<sub>2R</sub>•hSRP complex is completely formed under our experimental conditions. Thus, the

20-fold faster hSRP-hSR assembly rates with RNC<sub>4A10L</sub> than with RNC<sub>2R</sub> cannot be attributed to incomplete binding of hSRP by RNC<sub>2R</sub>, and instead reflects the kinetic advantage in SR recruitment provided by a functional signal sequence.

***The ribosome relieves auto-inhibition in mammalian SRP.***

Compared to the bacterial SRP system, the ribosome plays a much larger role during the receptor recruitment of mammalian SRP ((Bacher et al., 1996; Mandon et al., 2003) and this work). To understand the mechanism underlying these differences, we carried out cross-complementation analyses by making a hybrid SRP comprised of human SRP54 bound to the 4.5S SRP RNA from *E. coli*. GTPase assays revealed surprising similarities and differences between the hybrid and human SRP. First, the hybrid SRP displayed higher intrinsic activity than human SRP in the reciprocally stimulated GTPase reaction with hSR in the absence of external activators (Fig. 1.5B; cf. black lines in Fig. 1.5A vs. Fig. 1.2A). This suggests that the additional components in human SRP inhibit hSRP54 from attaining a conformation conducive to hSR recruitment and GTPase activation. This result also ruled out general defects in the folding or conformation of hSRP54 in the absence of the additional subunits in human SRP. Second, signal sequence fusion to hSRP54 also stimulated the reciprocally stimulated GTPase reaction between the hybrid SRP and hSR, analogous to the hSRP (Fig. 1.5, blue). This indicates that the ability to sense and respond to a signal sequence is an intrinsic property of hSRP54 and can occur independently of the other SRP protein subunits. Finally, in contrast to the human SRP, the ribosome lost most of its stimulatory effects on the interaction and reciprocal GTPase activation between the hybrid SRP and hSR (Fig. 1.5, green), indicating that the mammalian-specific components in human SRP are

required for the ribosome to exert its stimulatory effects. Together with previous work in bacterial and archaeal SRP (Bradshaw et al., 2009; HAINZL, 2005), the results of these cross-complementation analyses suggest that the signal sequence-induced stimulation of SRP recruitment is a universally conserved property of SRP, whereas the ribosome-induced stimulation of this event is a mammalian-specific phenomenon.

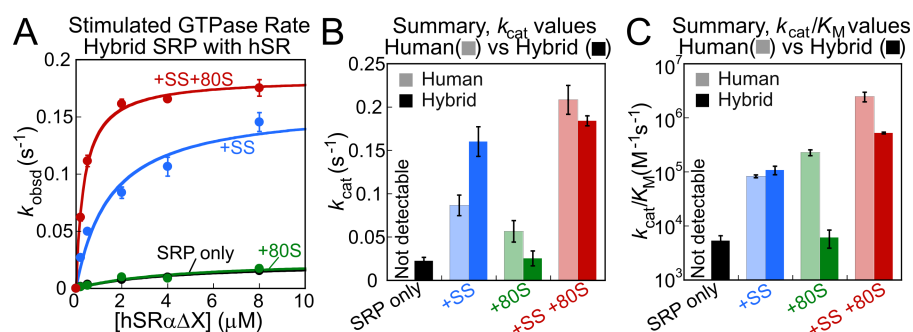


**Figure 1.5.** Comparison of the activities of human SRP and hybrid SRP (hSRP54 bound to 4.5S RNA). **(A)** Reciprocally stimulated GTPase reaction between hybrid SRP and hSR in the presence of indicated factors. Reactions were measured under the same conditions as those in Fig. 1.2A. The lines are fits of the data to Eq. 2 in Materials and Methods. **(B, C)** Summary of the  $k_{cat}$  **(B)** and  $k_{cat}/K_M$  **(C)** values from analysis of the data in **A** and their replicates. All data were represented as mean  $\pm$  SD, with  $n = 3$ . The rate constants for human SRP were from Fig. 1.2 and are shown for comparison.

### ***Signal sequence pre-organizes hSRP into the optimal conformation for hSR recruitment***

To understand the mechanism(s) by which the signal sequence and ribosome activate the interaction between human SRP and SR, we characterized the global conformational changes of hSRP based on FRET measurements between a donor dye (ATTO 550) labeled at SRP19 (C64) and an acceptor dye (ATTO 647N) labeled at SRP54 (C12). Based on the cryo-EM structure of the native hSRP•RNC complex (PDB: 3JAJ) (Voorhees & Hegde, 2015), the distance between the dye pair is  $\sim 44$  Å (Fig. 1.6A). Hence a high FRET efficiency is expected for this dye pair (Förster radius 65 Å) if the SRP54 NG-domain is positioned near

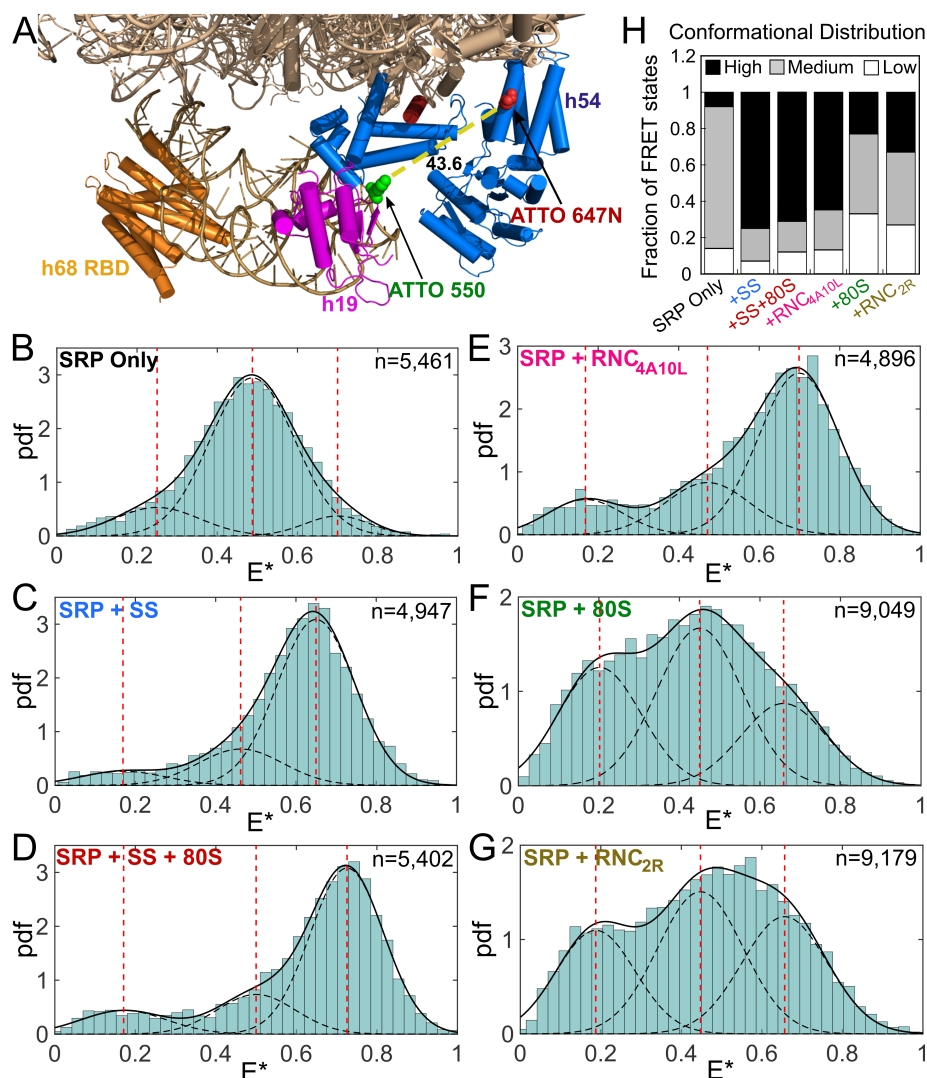


**Figure 1.6.** Signal sequence and the ribosome exert different effects on the conformation of hSRP. **(A)** Approximate positions of fluorescent donor and acceptor dyes on hSRP19 (magenta) and hSRP54 (blue), shown on a cryo-EM structure of the mammalian RNC•SRP complex. (PDB: 3JAJ) (Voorhees & Hegde, 2015) **(B-G)** smFRET histograms of hSRP in the presence of different ligands. Pdf denotes the probability density function, and  $E^*$  denotes uncorrected FRET efficiency. ‘n’ denotes the number of bursts used to construct each histogram, obtained from at least five independent measurements. The data were fit with the sum (solid line) of three Gaussian functions (dotted lines), and the dotted red lines denote the peak  $E^*$  value for each population. **(H)** Summary of the fraction of SRPs in the Low, Medium, and High-FRET states under the respective conditions.

SRP19, which we term the ‘proximal’ conformation. FRET was measured at single molecule resolution (smFRET) based on Fluorescence-aided Molecular Sorting using Alternating Laser Excitation Spectroscopy (ALEX) (Kapanidis et al., 2004), which optically purifies doubly-labeled single SRPs diffusing through a femtoliter-scale observation volume and extracts uncorrected FRET efficiencies ( $E^*$ ) for individual particles (Fig. S1.7A-C) (Kapanidis et al., 2005). Diffusion of the labeled molecules through the femtoliter-scale observation volume is estimated to take  $\sim 1$  milliseconds. Thus, different conformations that exchange on the millisecond or longer timescale can be resolved as discrete populations in a FRET histogram (Torella, Holden, Santoso, Hohlbein, & Kapanidis, 2011).

smFRET measurements showed that hSRP by itself exhibits a FRET distribution that is dominated by a medium-FRET population with a peak  $E^*$  value of  $\sim 0.5$  (Fig. 1.6B). With signal sequence fused hSRP, the FRET distribution shifted and peaked at a higher  $E^*$  value ( $\sim 0.65$ ; Fig. 1.6C). The presence of both the signal sequence and ribosome further shifted the distribution to higher FRET, with  $E^*$  peaking at  $\sim 0.7$  (Fig. 1.6D). This predominantly high FRET distribution was also observed with hSRP bound to RNC<sub>4A10L</sub> (Fig. 1.6E), providing additional evidence that the combination of ribosome and signal sequence fusion provides a reasonable mimic of the effects of a signal sequence-bearing RNC. In contrast, empty ribosomes and RNC<sub>2R</sub> induced significant conformational heterogeneity in hSRP (Fig. 1.6F, G). The FRET distributions of hSRP became broad, and could be accounted for by at least three populations with Low ( $E^* \sim 0.2$ ), Medium ( $E^* \sim 0.5$ ), and High ( $E^* \sim 0.7$ ) FRET values. Quantitative analyses of the FRET distributions further showed that, while free hSRP is dominated by the Medium FRET population ( $\sim 80\%$ ), hSRP bound to the ribosome and RNC<sub>2R</sub> are approximately equally distributed amongst all three conformations, whereas the

High FRET population becomes dominant whenever a functional signal sequence is present (Fig. 1.6H). These results provide strong evidence that a correct cargo displaying an SRP-dependent signal sequence induces SRP into the proximal conformation, and that the signal sequence, rather than the ribosome, plays a dominant role in inducing this conformation.

To exclude possible artifacts due to local environmental perturbations on the photophysics of fluorophores, we repeated these measurements after swapping the position of donor and acceptor dyes in hSRP. smFRET measurements using this swapped dye pair yielded similar signal sequence- and ribosome-induced changes in the FRET distributions of hSRP (Fig. S1.7D-H). In addition, the presence of various interaction partners did not affect the dye photophysics in a way that would alter the FRET distributions (Fig. S1.7I-N). These data strongly suggest that our observed FRET changes can be attributed to the global conformational transitions of hSRP.

In summary, the smFRET data show that human SRP by itself adopts a conformation (or conformations) in which the SRP54-NG domain is positioned away from the proximal site where SRP19 and the SRP54 M-domain are located. In the presence of empty ribosomes or signal-less RNCs, hSRP explores a variety of alternative conformations in which the SRP54 NG-domain can be proximal to or further away from SRP19. In contrast, a functional signal sequence plays a dominant role in inducing the mammalian SRP into the proximal conformation.

### 1.3 DISCUSSION

Efficient and selective targeting of nascent proteins by SRP is essential for the proper functioning of the endomembrane system in eukaryotic cells. Although the mechanism of the simplest bacterial SRP has been deciphered at high resolution (Kuang Shen et al., 2013; Zhang et al., 2010, 2009), our understanding of the more complex eukaryotic SRP has lagged behind. Previous fluorescence measurements suggested that mammalian SRP exhibits significant binding to empty ribosomes, with a  $K_d$  value ( $\sim 80$  nM) significantly below the *in vivo* SRP concentration ( $\sim 500$  nM in mammalian cells) (Flanagan et al., 2003; Kulak, Pichler, Paron, Nagaraj, & Mann, 2014). Substantial signal-independent association of eukaryotic SRP with translating ribosomes was also observed in global analyses in yeast cells (Alamo et al., 2011; Chartron et al., 2016). These observations raise questions as to whether SRP-RNC binding is sufficient to ensure selective co-translational protein targeting in eukaryotic cells. In the bacterial SRP pathway, substrate selection relies heavily on kinetic discrimination during the recruitment of SR, a step that is over  $10^2$ -fold faster with RNCs bearing SRP-dependent than SRP-independent substrates. Whether this mechanism is conserved in mammalian SRP has been unclear, especially given previous observations that the 80S ribosome by itself can bind mammalian SR and enhance its GTPase activity together with SRP (Jadhav et al., 2015; Mandon et al., 2003). In this work, biochemical and biophysical analyses provide the first evidence that a functional signal sequence provides a kinetic advantage during SR recruitment in the mammalian SRP pathway, and suggest a molecular model for the mechanism of SRP activation by the ribosome and signal sequence.

Co-translational protein targeting by SRP kinetically competes with translation elongation, as RNCs lose the competence to be targeted by SRP when the nascent

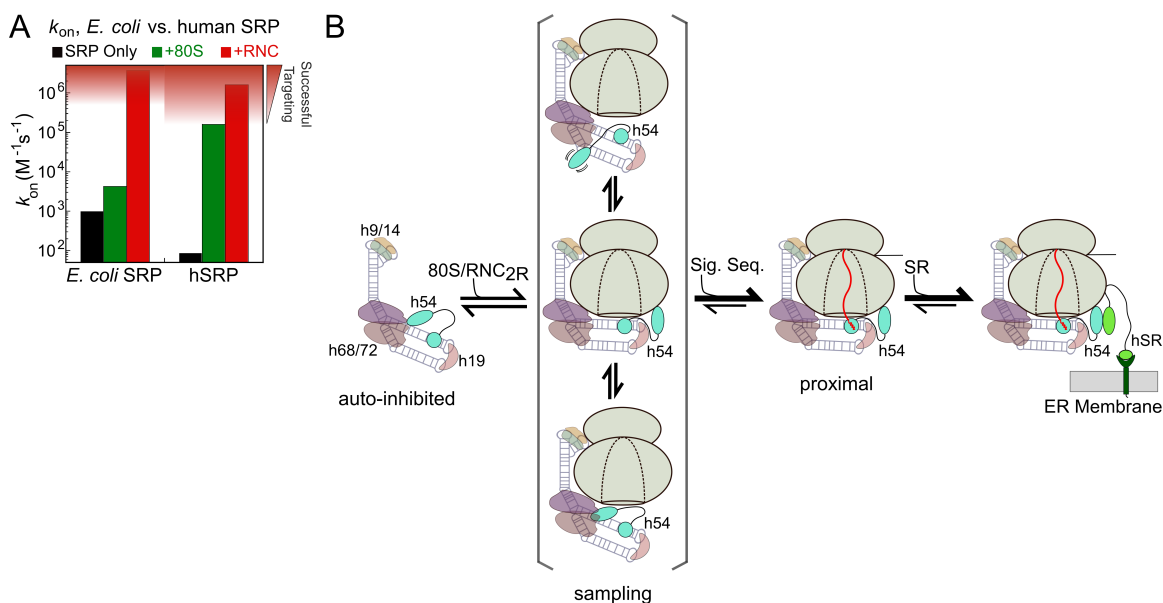


**Figure 1.7.** Comparison of the *E. coli* and human SRP, and model for sequential conformational activation of mammalian SRP during targeting. **(A)** Comparison of the SRP-SR assembly rate constants between *E. coli* and human SRP in the absence (*black*) and presence of the ribosome (*green*) or RNC (*red*). The  $k_{on}$  values for *E. coli* SRP were from reference (K. Shen, Zhang, & Shan, 2011). The shaded area with increasing red denotes SRP-SR interaction rates that are increasingly targeting-competent. The threshold for targeting competent SRP-SR assembly rates was determined using a time window of 5 sec for bacterial SRP and 13 sec for mammalian SRP to complete the targeting reaction and an SR concentration of 500 nM. **(B)** Sequential conformational activation of mammalian SRP by the ribosome and signal sequence for efficient SR recruitment. Free hSRP is in an (or an ensemble of) ‘auto-inhibited’ conformation(s). Upon binding to the ribosome and in the absence of a signal sequence, hSRP is unlocked and samples a variety of alternative conformations (‘sampling’). The emergence of the signal sequence drives most of the hSRP into the ‘proximal’ conformation that allows rapid assembly with hSR for efficient targeting to the ER.

polypeptide exceeds a critical length (~120 amino acids from the start of signal sequence or TMD; (Flanagan et al., 2003; Siegel & Walter, 2018)). Proximity-specific ribosome profiling in yeast further suggest that ER localization of ribosomes were attained immediately after the emergence of signal sequence from the ribosome (~60 amino acids from the start of signal sequence (Jan et al., 2014)). Considering the elongation rate of 6–10 amino acids/second in

mammalian cells (Ingolia, Lareau, & Weissman, 2011; Karpinets, Greenwood, Sams, & Ammons, 2006), a limited time window of  $\leq 12$  sec is imposed on the eukaryotic SRP to complete a targeting cycle (Fig. 1.7A). Although ribosomes and signal-less RNCs also substantially accelerate SRP-SR association, the measurements here suggest that the recruitment of SR at physiological concentrations ( $\sim 0.5 \mu\text{M}$  (Kulak et al., 2014)) would require at least  $\sim 13$  sec for empty ribosomes and  $\sim 32$  sec for RNC<sub>2R</sub>. The crowded cytosolic environment and competition from other ribosome-associated factors could further delay the bi-molecular association between SRP and SR. The additional presence of a signal sequence brings the timescale of SR recruitment to  $\leq 2$  sec, a timescale sufficient to meet the demands for co-translational protein targeting (Fig. 1.7A). In addition, the weaker affinity of SRP for empty ribosomes than signal sequence-bearing RNCs (Flanagan et al., 2003) (Fig. S1.3C) suggests that SRP dissociates more quickly from the former. Together with the difference in SR recruitment rates, this would allow most of the RNCs bearing SRP-dependent substrates to be successfully delivered to the ER membrane, whereas a larger fraction of signal-less ribosomes could dissociate from SRP before SR is recruited.

The ribosome is much more stimulatory during SR recruitment, whereas the additional kinetic advantage provided by the signal sequence on this event is much smaller, in the mammalian SRP system compared to its bacterial homologue (Fig. 1.7A, *green vs. red*). This suggests that additional strategies are used to maintain the fidelity of co-translational protein translocation in eukaryotes, for example by using the Sec61p translocase to discriminate against mutant signal sequences (Hessa et al., 2005, 2007; Jungnickel & Rapoport, 1995). On the other hand, the observation that the ribosome alone brings the SR recruitment rate to the threshold of a targeting-competent timescale raises additional

possibilities of regulation, wherein other ribosome-interacting factors could drive a nascent protein into or out of the SRP pathway by tuning the relative rates of SR recruitment versus protein synthesis. This may include ribosome-associated chaperones that alter the conformational landscape of ribosome-bound SRP, such as the nascent polypeptide associated complex (NAC) (Alamo et al., 2011; Gamerdinger, Hanebuth, Frickey, & Deuerling, 2015; Lauring, Kreibich, & Weidmann, 1995), as well as *cis* regulatory elements or trans-interacting factors that tune translation elongation rates, such as codon usage and arrest sequences at strategic locations on the mRNA (Pechmann, Chartron, & Frydman, 2014). Compared to its bacterial homologue, the mammalian SRP may be more poised for diverse mechanisms of regulation by external factors. The same concept and considerations may be extended to evaluate the possibility of pre-emptive targeting, a model suggested by previous observations that SRP can associate with translating ribosomes before a signal sequence or TMD emerges from the nascent polypeptide exit tunnel (Alamo et al., 2011; Berndt, Oellerer, Zhang, Johnson, & Rospert, 2009; Chartron et al., 2016; Mercier, Holtkamp, Rodnina, & Wintermeyer, 2017). An outstanding question regarding this model is whether productive SRP-SR interaction can initiate before the emergence of the targeting signal from the ribosome, and if so, whether the targeting is specific for SRP substrates. The eukaryote-specific large stimulatory effect of the ribosome during SR recruitment suggests that pre-emptive targeting might play a more significant role in the mammalian than the bacterial SRP pathway.

Cross-complementation analyses and smFRET measurements of the global conformation of hSRP further suggest a molecular model by which the ribosome and signal sequence activate the hSRP-hSR interaction. The weak affinity and extraordinarily slow

association rate of the hSRP-hSR complex indicate that human SRP by itself exists in a conformation inactive for receptor recruitment. The higher activity of the hybrid SRP compared to human SRP further suggests that the eukaryote-specific components in mammalian SRP are responsible, at least in part, for this auto-inhibition. smFRET measurements further showed that free hSRP predominately adopts a conformation in which the dye pair between hSRP19 and hSRP54-NG exhibits medium FRET efficiency, indicating that the hSRP54-NG domain is positioned away from the proximal site of hSRP in this auto-inhibited state (Fig. 1.7B). Importantly, a signal sequence-bearing RNC induces hSRP to predominantly adopt the ‘proximal’ conformation, in which the hSRP54-NG domain is close to hSRP19 (Fig. 1.7B). Although it is intuitive to envision that the dual interactions of the hSRP54 M-domain with the signal sequence and the hSRP54 NG-domain with the uL23/uL29 ribosomal proteins (Voorhees & Hegde, 2015) could induce this conformation, the finding here that signal sequence fusion to hSRP54 is sufficient to induce a near-proximal state of hSRP indicate that signal sequence occupancy in the hSRP M-domain plays a major role in bringing hSRP54-NG near the proximal site. This is in good agreement with crystallographic analyses in archaeal SRP (Hainzl & Sauer-Eriksson, 2015) and suggests that binding of a signal sequence in the human SRP54 M-domain induces re-structuring of the GM linker to reposition its NG domain.

We found here a strong correlation between the acquirement of the proximal conformation of human SRP and faster SRP-SR assembly rates (all else held equal), suggesting that this conformation is optimal for SR recruitment. On the other hand, cryo-EM analyses of both the bacterial and mammalian RNC•SRP•SR complexes indicate that, in the presence of SR, the density of the SRP54 NG-domain is no longer visible near the ribosomal

tunnel exit (Halic, 2006; von Loeffelholz et al., 2015). In the bacterial SRP system, the NG-domain complex further moves to an alternative docking site near the 5', 3'-distal end of the 4.5S RNA (Ataide et al., 2011; Kobayashi et al., 2018). These observations strongly suggest that complex formation with SR induces detachment of SRP54-NG from the vicinity of the ribosome exit site in both SRP systems. Nevertheless, the results here provide strong kinetic evidence that initial SRP-SR assembly occurs near the ribosome exit tunnel, predicting an early RNC•SRP•SR intermediate prior to rearrangement of the NG-domain complex. The structure, dynamics, and interactions of this initial targeting intermediate remain to be defined.

The large stimulatory effect of the ribosome on SRP-SR assembly is a eukaryote-specific phenomenon (Zhang et al., 2010). Previous work showed that the ribosome also binds the mammalian SR and suggested that it could provide a template that brings SRP and SR together for assembly (Jadhav et al., 2015; Mandon et al., 2003). Although this model is highly probable, the loss of ribosome-induced stimulation in the reaction of hybrid SRP with human SR indicates that additional mechanisms are necessary to account for all the stimulatory effects from the ribosome, and the results here suggested a new allosteric mechanism. smFRET measurements showed that, in contrast to the predominantly Medium-FRET state observed with free hSRP, the ribosome induces multiple alternative conformations in which hSRP54-NG can be close to or even further away from the hSRP proximal site. In the simplest model, the stimulated recruitment of hSR could arise solely from the sub-population of ribosome-bound hSRP in the proximal conformation. It is plausible that the Low-FRET state observed with 80S-bound hSRP could also recruit hSR, but the correlation between assembly rates and smFRET data strongly suggest that SR

recruitment in this state is slower than in the proximal conformation. Together, the results here suggest that the ribosome unlocks hSRP from the auto-inhibited state and allows it to dynamically sample more active conformations, thus priming SRP for subsequent receptor recruitment (Fig. 1.7B, ‘sampling’).

In summary, our work provides a new model for how a correct cargo activates the mammalian SRP for targeting to the ER membrane (Fig. 1.7B). In the absence of translating ribosomes, the eukaryote-specific components retain SRP in an auto-inhibited conformation where its interaction with SR is extremely slow. Binding of the ribosome relieves SRP from this auto-inhibited state and enables SRP to sample multiple alternative conformations, including the ‘proximal state’ conducive to assembly with SR. The direct interaction of the ribosome with SR provides an additional mechanism that can bring SRP and SR together to facilitate their assembly (Jadhav et al., 2015). SRPs bound to signal-less ribosomes remain largely in the sampling mode, in which SR recruitment, though accelerated, does not occur on a biologically relevant timescale. In contrast, the emergence of a signal sequence from the ribosome exit tunnel drives the majority of SRP into the proximal conformation in which SR recruitment can occur rapidly, thus delivering the translating ribosome to the ER membrane. Compared to the bacterial SRP, the use of signal sequence to activate SRP for receptor recruitment is a universally conserved feature of the co-translational protein targeting pathway; in contrast, the mammalian SRP evolved the unique ability to sense and be primed by the ribosomes, which may poise the pathway for additional layers of regulation.

## 1.4 MATERIALS AND METHODS

**Vectors.** pET15b-h19 and pET23d-h54 for expression of hSRP19 and hSRP54, respectively, were gifts from C. Zwieb (Gowda et al., 1998; Walker et al., 1995). pET3b-h9 and pET9a-h14 for expression of hSRP9 and hSRP14, respectively, and pS7CA for *in vitro* transcription of the 7SL SRP RNA were gifts from K. Strub (Huck, 2004; Mary et al., 2010). pRS426-h68/72 vector and BCY123 yeast strain for expression of hSRP68/72 were gifts from K. Nagai (Menichelli et al., 2007). Commercially available cDNA clones for human SR $\alpha$  (Origene) and mouse SR $\beta$  (SINO Biological) were subcloned to construct pET28a-hSR $\alpha$ , pET15b-SR $\beta$  $\Delta$ TM, and bicistronic pET28a-hSR $\alpha$ -SR $\beta$  $\Delta$ TM using Gibson cloning for co-expression of hSR $\alpha$  $\beta$  $\Delta$ TM. The X-domain of SR $\alpha$  was removed from pET28a-hSR $\alpha$  using fastcloning to construct pET28a-hSR $\alpha$  $\Delta$ X. Cyslite hSRP54, cysless hSRP19, and single cysteine mutants of hSRP54 and hSRP19 for fluorescence labeling were generated by QuikChange mutagenesis (Stratagene). pET23d-h54-4A10L for expression of signal sequence fused hSRP54 was constructed using fastcloning. Sortase-tagged hSR $\alpha$  $\Delta$ X was constructed by adding the sortase tag and (GS)<sub>6</sub> linker at the C-terminus using fastcloning.

### ***Biochemical Preparations.***

*hSRP19.* Rosetta pLysS cells harboring pET-h19 were grown to OD<sub>600</sub> = 0.6 at 25 °C. Expression was induced with 1 mM IPTG for 16 hrs at 25 °C. Cells were resuspended in Lysis Buffer (50 mM KHEPES (pH 7.5), 300 mM NaCl, 10% glycerol, 4 mM  $\beta$ ME, and protease inhibitor cocktail (ProBlock Gold (Gold Bio), 1X)) and lysed by two passes through French press at 18,000 psi. Clarified lysate was incubated for 1 hr with Ni-NTA resin (2ml/L

of cells) equilibrated with Lysis Buffer. The resin was washed with 20 CV of Wash buffer (50 mM KHEPES (pH 7.5), 1 M NaCl, 5% glycerol, and 4 mM  $\beta$ ME) containing 10 mM Imidazole, and protein was eluted with Lysis buffer supplemented with 250 mM Imidazole. Eluted protein was dialyzed in SP Buffer (50 mM Tris-HCl (pH 7.5), 150 mM NaCl, 2 mM EDTA, 5% glycerol, and 2mM DTT), and further purified over SP-sepharose ion-exchange column using a gradient of 150–500mM NaCl over 20CV. Purified hSRP19 was stored in 20% glycerol at  $-80^{\circ}\text{C}$ .

*hSRP9/14*. hSRP9 and hSRP14 were expressed separately in BL21(DE3) pLysS cells grown in LB media with 0.4% glucose at  $37^{\circ}\text{C}$ . Expression was induced at  $\text{OD}_{600} = 0.6$  using 0.4 mM IPTG for 3 hours. Cells were resuspended in Lysis buffer (50 mM Tris-HCl (pH 7.5), 50 mM NaCl, 0.25 M  $\text{NH}_4\text{Cl}$ , 10 mM  $\text{MgCl}_2$ , 20 mM EDTA, 10% glycerol, 10 mM DTT, and 2 mM AEBSF) and lysed by sonication. Clarified lysate containing SRP9 and SRP14 were mixed at 1:1 ratio and stirred gently for 30 minutes. The mixture was loaded onto Heparin-sepharose resin (10 ml/L of cells) equilibrated with Heparin Buffer (50 mM KHEPES (pH 7.5), 50 mM NaCl, 0.25 M  $\text{NH}_4\text{Cl}$ , 1 mM EDTA, 10% glycerol, 10 mM DTT, and 2 mM AEBSF). The resin was washed with 10 CV of Heparin Buffer with 250 mM KOAc. Proteins were eluted using a gradient of 250 mM – 1.5 M KOAc. Peak fractions were dialyzed in Buffer A (50 mM KHEPES (pH 7.5), 300 mM KOAc, 1 mM EDTA, 0.01% Nikkol, 10% glycerol, 10 mM DTT, and 1 mM AEBSF) and further purified over a MonoS cation-exchange column using a gradient of 300 mM – 650 mM KOAc over 20CV. Purified hSRP9/14 was stored in 20% glycerol at  $-80^{\circ}\text{C}$ .

*hSRP54*. hSRP54 or hSRP54-4A10L were expressed in Rosetta pLysS cells grown at  $37^{\circ}\text{C}$  to  $\text{OD}_{600} = 0.6$ . Cells were chilled to  $25^{\circ}\text{C}$  in a water bath for 15 minutes, and

expression was induced using 1 mM IPTG for 2 hours at 25 °C. Cells were resuspended in Lysis Buffer (50 mM KHEPES (pH 7.5), 100 mM NaCl, 4 mM  $\beta$ ME, 1 mM AEBSF, and Protease Inhibitor cocktail) and lysed by sonication. Clarified lysate was incubated with Ni-Sepharose resin (1.5 ml/L of cells) equilibrated in Lysis Buffer for 1 hr. The resin was washed with 20CV of Ni-buffer (50 mM KHEPES (pH 7.5), 500 mM NaCl, 40 mM Imidazole, 10% glycerol, 4 mM  $\beta$ ME, and 1 mM AEBSF). Protein was eluted with Lysis buffer containing 300 mM NaCl and 300 mM Imidazole. Eluted protein was dialyzed to MonoS buffer (50 mM Tris-HCl (pH 7.5), 2 mM EDTA, 10% glycerol, and 2 mM DTT) with 150 mM NaCl, and purified over a MonoS column using a gradient of 150–600 mM NaCl over 20CV. Purified hSRP54 or hSRP54-4A10L was stored in 20% glycerol at  $-80^{\circ}\text{C}$ .

*hSRP68/72*. hSRP68 and C-terminally His<sub>6</sub>-tagged hSRP72 were co-expressed in BCY123 yeast cells grown in SD-Ura + 2% glucose media at 30 °C. 25 mL of this culture was inoculated into 1L of SD-Ura + 2% raffinose media and cells were grown to OD<sub>600</sub> = 0.9. Expression was induced by adding 2% galactose for 16 hours. Cells were washed twice with ice-cold water and flash frozen in droplets. Frozen cells were ground to powder in liquid nitrogen using Cryomill (Retsch), and mixed with Lysis buffer (50 mM K-Phosphate (pH 7.4), 1 M NaCl, 0.5 M Urea, 4 mM  $\beta$ ME, 10% glycerol, and Protease inhibitor cocktail), and centrifuged at 42,000rpm in Ti45 rotor for 40 minutes. Clarified lysate was incubated with Ni-Sepharose resin (1.5ml/L of cells) equilibrated in Equilibration buffer (50 mM K-Phosphate (pH 7.4), 500 mM NaCl, 0.5 M Urea, 4 mM  $\beta$ ME, and 10% glycerol) for 1 hour. The resin was washed with 20CV of Equilibration buffer containing 35 mM imidazole. Protein was eluted using Equilibration buffer containing 500 mM Imidazole, and eluted

hSRP68/72 was further purified over a MonoS column using a gradient of 0.5 – 1 M NaCl over 20CV. Purified hSRP68/72 was stored in 50% glycerol at  $-30^{\circ}\text{C}$ .

*hSR $\alpha$  $\beta$  $\Delta$ TM and hSR $\alpha$  $\Delta$ X.* To express hSR $\alpha$  $\beta$  $\Delta$ TM, pET28 vector encoding N-terminally His<sub>6</sub>-tagged hSR $\alpha$  and hSR $\beta$  $\Delta$ TM [hSR $\beta$ (57-269)], and pET15 vector encoding hSR $\beta$  $\Delta$ TM were co-transformed into BL21(DE3\*). For hSR $\alpha$  $\Delta$ X, pET28 vector encoding N-terminally His<sub>6</sub>-tagged hSR $\alpha$  $\Delta$ X [hSR $\alpha$ (131-638)] was transformed into BL21(DE3\*). Cells were grown at 30 °C to OD<sub>600</sub> = 0.6, and expression was induced with 0.5 mM IPTG for 4 hours. Cells were resuspended in Lysis Buffer (50 mM KHEPES (pH 8.0), 500 mM NaCl, 10% glycerol, 4 mM  $\beta$ ME, and protease inhibitor cocktail) and lysed by two passages through French press at 18,000 psi. Clarified lysate was incubated with Ni-Sepharose resin (3 ml/L of cells) equilibrated in Lysis Buffer for 1 hr. The resin was washed with 15CV of Wash Buffer (50 mM KHEPES (pH 7.5), 500 mM NaCl, 35 mM Imidazole, 10% glycerol, and 4 mM  $\beta$ ME). Bound protein was eluted with Wash Buffer containing 500 mM imidazole. Fractions containing target protein were diluted to 60 mM NaCl with Dilution Buffer (50mM KHEPES (pH 8.0) and 20% glycerol) and incubated with CM-Sepharose resin (5ml/L of cells) equilibrated in CM Buffer (50 mM KHEPES (pH 8.0), 10% glycerol, and 2 mM DTT) containing 100 mM KOAc for 1hr. The resin was washed with 10CV of CM-Buffer containing 100 mM KOAc, and protein was eluted with CM Buffer containing 350 mM KOAc. Peak fractions were pooled, concentrated, and further purified on a Superdex200 size-exclusion column in S200 Buffer (50 mM KHEPES (pH 7.5), 300 mM KOAc, 5 mM Mg(OAc)<sub>2</sub>, 10% glycerol, 0.02% Nikkol, and 2 mM DTT). Purified hSR was stored in 20% glycerol at  $-80^{\circ}\text{C}$ .

*SRP RNA. S7CA*, a circularly permuted version of human 7SL SRP RNA for improved SRP assembly, was *in vitro* transcribed using T7 RNA polymerase as described (Huck, 2004). Transcribed RNA was acid phenol extracted and purified over a denaturing polyacrylamide gel (100 mM Tris, 89 mM Boric Acid, 1.3 mM EDTA, 7 M Urea, and 10% acrylamide(29:1)) (Travers, Boyd, & Herschlag, 2007). RNA extracted from the gel was dialyzed in 20 mM Tris-HCl (pH 7.5), flash frozen in liquid nitrogen, and stored at  $-80^{\circ}\text{C}$ .

*80S purification.* Rabbit Reticulocyte Lysate (RRL) was treated with micrococcal nuclease (Nuclease S7; Roche) as described before (Sharma, Mariappan, Appathurai, & Hegde, 2010). 20 mL nuclease treated RRL was ultracentrifuged at 42,000 rpm on TI70 rotor for 3.5 hours. The ribosome pellet was carefully resuspended with 6 mL HS Buffer (50 mM KHEPES (pH 7.5), 500 mM KOAc, 10 mM  $\text{Mg}(\text{OAc})_2$ , and 2 mM DTT) and layered on 1M sucrose cushion (1M Sucrose in HS Buffer) and centrifuged at 95,000 rpm in a TLA100.3 rotor for 90 minutes. The ribosome pellet was resuspended with 6ml of HS Buffer and 1ml sample was layered on a 40 ml 10–50% sucrose gradient in HS Buffer. The gradient was ultracentrifuged at 23,000 rpm in a SW32 rotor for 12 hours. The monosome peak was collected and centrifuged at 95,000 rpm in a TLA100.3 rotor for 90 minutes. The ribosome pellet was gently washed once with SRP Assay buffer, and resuspended in SRP Assay buffer without Nikkol to desired concentration. Aliquots were flash frozen in liquid nitrogen and stored at  $-80^{\circ}\text{C}$ .

*RNC purification.* mRNA encoding the nascent chains on RNC was translated in Rabbit Reticulocyte Lysate for 30 minutes at  $32^{\circ}\text{C}$  (Voorhees & Hegde, 2015). 1.8 mL of translation reactions was layered on a 1 mL 0.5M Sucrose cushion (50 mM KHEPES (pH 7.1), 100 mM KOAc, 15 mM  $\text{Mg}(\text{OAc})_2$ , 0.5 M Sucrose, 0.1% Triton, and 20  $\mu\text{g}/\text{ml}$

Cycloheximide) and centrifuged at 100,000 rpm for 1 hour at 4 °C in a TLA100.3 rotor. The pellet was resuspended with Resuspension Buffer (50 mM KHEPES (pH 7.1), 100 mM KOAc, 15 mM Mg(OAc)<sub>2</sub>, and 20 µg/ml Cycloheximide) and incubated with anti-FLAG resin (anti-FLAG M2 Magnetic Beads (Sigma), 5 µL/mL translation) for 1-2 hours. The resin was washed with 20 CV of Wash 1 Buffer (50 mM KHEPES (pH 7.1), 100 mM KOAc, 15 mM Mg(OAc)<sub>2</sub>, 0.1% Triton, and 20 µg/ml Cycloheximide) followed by 20 CV of Wash 2 Buffer (50 mM KHEPES (pH 7.1), 300 mM KOAc, 15 mM Mg(OAc)<sub>2</sub>, and 20 µg/ml Cycloheximide). RNC was eluted three times with 2 CV of Elution Buffer (50 mM KHEPES (pH 7.1), 150 mM KOAc, 15 mM Mg(OAc)<sub>2</sub>, 1 mg/ml 3xFLAG peptide, and 20 µg/ml Cycloheximide). Eluted RNCs were layered on a 4.8 mL 10–30 % sucrose gradient (in 50 mM KHEPES (pH 7.1), 500 mM KOAc, 10 mM Mg(OAc)<sub>2</sub>, 2 mM DTT, 20 µg/ml Cycloheximide, and 0.3 mg/ml BSA) and ultracentrifuged at 50,000 rpm for 100 minutes at 4 °C in a SW55 rotor (Verma, Oania, Kolawa, & Deshaies, 2013). 200 µL fractions were collected from the top of the gradient. The monosome peak fractions were combined and centrifuged at 95,000 rpm for 95 minutes at 4 °C in a TLA100.3 rotor. The RNC pellet was resuspended in SRP Assay Buffer, flash frozen in liquid nitrogen, and stored at –80°C.

### ***Fluorescence labeling***

*hSRP54*. There are five native cysteines in hSRP54. The three exposed cysteines in hSRP54 were mutated (C36T, C136S, and C229A) to generate ‘cyslite’ hSRP54, which did not show any labeling with maleimide dyes (data not shown). An engineered cysteine (C47 or C12) was introduced into cyslite hSRP54 for site-specific labeling using maleimide chemistry (Zhang, Kung, & Shan, 2008). 50 µM hSRP54 or hSRP54-4A10L was treated

with 2 mM TCEP for 4 hours at room temperature. A 15-fold excess of Cy3b (or ATTO 550 or ATTO 647N) maleimide was added and incubated at room temperature for 4 hours. Labeled protein was separated from free dye by size exclusion chromatography on a G-25 column (Zhang et al., 2008). Labeled protein was concentrated and stored in 20% glycerol at  $-80^{\circ}\text{C}$ . Labeling efficiency was 70–80%.

*hSRP19*. The native cysteines in hSRP19 were mutated (C3S, C17V, C53L, and C94S) to generate cysless hSRP19, into which a single cysteine (K64C) is introduced. 50  $\mu\text{M}$  hSRP19 (K64C) was treated with 2 mM TCEP for 4 hours at room temperature. A 10-fold excess of ATTO 550 or ATTO 647N maleimide was added and incubated at room temperature for 2 hours. Labeled hSRP19 was separated from free-dye by size exclusion on a G-25 column. Labeled protein was stored in 20% glycerol at  $-80^{\circ}\text{C}$ . Labeling efficiency was  $\sim 80\%$ .

*hSR*. A sortase-tag (LPETG) with (GS)<sub>6</sub> linker was added to the C-terminus of hSR $\alpha\Delta\text{X}$  (Guimaraes et al., 2013). A sortase peptide (GGGC) was labeled with ATTO 647N via maleimide chemistry, and labeled peptide was purified by HPLC using a C18 column. To label SR, 1:4:8 molar ratio of sortase-tagged SR $\alpha\Delta\text{X}$  or SR $\alpha\beta\Delta\text{TM}$ , sortase, and labeled peptide was mixed in Sortase Buffer (50 mM Tris-HCl (pH 7.5), 150 mM NaCl, 10 mM CaCl<sub>2</sub>, 10% glycerol, 1 mM DTT, and 0.02% Nikkol) and incubated for 3-4 hours at room temperature. The reaction mixture was purified on Ni-Sepharose resin to remove untagged-sortase and free peptides. Labeling efficiency was 60–70%. Labeled protein was concentrated and stored in 20% glycerol at  $-80^{\circ}\text{C}$ .

***Biochemical assays.***

All proteins except for SRP were centrifuged at 4 °C, 100,000 rpm in TLA100 rotor for 30 minutes to remove aggregates before the assay. GTPase reactions were performed in SRP Assay Buffer (50 mM KHEPES (pH 7.5), 150 mM KOAc, 5 mM Mg(OAc)<sub>2</sub>, 10% glycerol, 2 mM DTT, and 0.04% Nikkol) at 25 °C. Reactions were followed and analyzed as described before (Peluso et al., 2001) except that PEI cellulose thin layer chromatography were run in 1 M formic acid / 0.5 M LiCl. Observed rate constants were determined as described before (Peluso et al., 2001).

Steady-state fluorescence measurements to analyze the SRP-SR interaction were carried out on a Fluorolog 3-22 spectrofluorometer (Jobin Yvon) and Kintek stopped-flow apparatus (Kintek Inc.) at 25 °C. The binding of SRP to RNC<sub>4A10L</sub> or to 80S was measured using Microscale Thermophoresis (MST; Nanotemper) following manufacturer's instructions.

Co-translational targeting and translocation of <sup>35</sup>S-methionine labeled pPL into salt-washed, trypsinized rough ER microsome (TKRM) was measured in wheat germ extract as previously described (Powers, 1997; Shan et al., 2007). The efficiency of translocation was quantified as:

$$\% \text{Translocation} = \frac{\binom{8}{7} \text{prolactin}}{\binom{8}{7} \text{prolactin} + \text{preprolactin}} \times 100$$

The (8/7) term here corrects for the different number of methionines in pPL versus signal sequence-cleaved prolactin.

*Determination of individual rate and equilibrium constants.* Basal GTPase reactions were measured under single-turnover conditions using varying concentrations of hSRP or hSR in excess of trace  $\gamma$ -<sup>32</sup>P-GTP. The SRP or SR concentration dependence of the observed rate constant ( $k_{\text{obsd}}$ ) were fit to Eq. 1,

$$k_{\text{obsd}} = k_{\text{cat}} \times \frac{[\text{SRP or SR}]}{K_m + [\text{SRP or SR}]} \quad (1)$$

in which  $k_{\text{cat}}$  is basal GTPase rate constants and  $K_m$  is the GTP concentration required to reach half of the maximal observed GTPase rate constant.

The reciprocally stimulated GTPase reaction between SRP and SR were measured under multiple turnover conditions using 0.2  $\mu\text{M}$  hSRP, varying concentrations of excess hSR, and 100  $\mu\text{M}$  GTP doped with trace  $\gamma$ -<sup>32</sup>P-GTP. The SR concentration dependences of observed rate constants were fit to Eq. 2.

$$k_{\text{obsd}} = k_{\text{cat}} \times \frac{[\text{SR}]}{K_m + [\text{SR}]} \quad (2)$$

The binding affinity of GDP for hSRP and hSR were determined using GDP as a competitive inhibitor of the basal GTPase reaction. The GDP concentration dependence of observed rate constants were fit to Eq. 3,

$$k_{\text{obsd}} = k_0 \times \frac{K_i}{[\text{GDP}] + K_i} \quad (3)$$

where  $k_0$  is rate in the absence of GDP and  $K_i$  is inhibition constant.

Inhibition of GTPase activity by hSR $\alpha\Delta\text{X}$ (R458A) was measured in multi-turnover conditions using 0.2  $\mu\text{M}$  of hSRP, 0.5  $\mu\text{M}$  of hSR $\alpha\Delta\text{X}$ , and increasing concentrations of

hSR $\alpha$  $\Delta$ X(R458A). hSR $\alpha$  $\Delta$ X(R458A) concentration dependence of observed rate constants were fit to Eq. 4,

$$k_{\text{obsd}} = k_0 \times \frac{[\text{SR}]}{[\text{SR}] + K_m \times \left(1 + \frac{[\text{SR}_{\text{R458A}}]}{K_i}\right)} \quad (4)$$

where  $k_0$  is the observed reaction rate in the absence of hSR $\alpha$  $\Delta$ X(R458A),  $[\text{SR}] = 0.5 \mu\text{M}$ ,  $K_m$  is the Michaelis constant for the reaction of wildtype hSRP with SR, determined as  $0.06 \mu\text{M}$  from the data in Figure 1.2, and  $K_i$  is the inhibition constant of hSR $\alpha$  $\Delta$ X(R458A).

Association rate constants between hSRP and hSR were measured on a stopped-flow apparatus by rapid mixing of a fixed concentration of Cy3B-labeled hSRP or hSRP-4A10L with varying concentrations of excess ATTO-647N-labeled hSR $\alpha$  $\Delta$ X. The time courses of fluorescence change were fit to exponential functions to extract the observed association rate constants ( $k_{\text{obsd}}$ ). The SR concentration dependences of  $k_{\text{obsd}}$  values were fit to Eq. 5,

$$k_{\text{obsd}} = k_{\text{on}} \times [\text{SR}] + k_{\text{off}} \quad (5)$$

in which  $k_{\text{on}}$  is the bi-molecular association rate constant between hSRP and hSR, and  $k_{\text{off}}$  is the dissociation rate constant of the hSRP•hSR complex. The ribosome or RNC was pre-incubated with hSRP where indicated.

The values of  $k_{\text{off}}$  were also directly determined using pulse chase experiments. Labeled hSRP and hSR were mixed and incubated until it reached equilibrium. Excess amount of unlabeled hSR was added to initiate chase, and the fluorescence signal change over time was measured. Resulting time-courses were fit to exponential functions to extract  $k_{\text{off}}$ .

Equilibrium titrations to measure the equilibrium dissociation constant ( $K_d$ ) of the hSRP•hSR complex were carried out using 15 nM Cy3B labeled SRP, 2mM GTP, and addition of increasing concentrations of ATTO-647N-labeled SR. Donor fluorescence was recorded when equilibrium is reached. 0.6 mg/ml BSA was supplemented in SRP Assay buffer to reduce non-specific adhesion of proteins to surfaces. A control titration with unlabeled hSR was carried out in parallel, and the fluorescence signal change from the control reaction was subtracted. The fluorescence signal was converted to FRET (E) using Eq. 6,

$$E = 1 - \frac{F_{DA}}{F_D} \quad (6)$$

where  $F_{DA}$  and  $F_D$  are the fluorescence signals with and without the acceptor present. E was plotted against hSR concentration and fit to Eq. 7,

$$E = E_{\max} \times \frac{[SR]}{K_d + [SR]} \quad (7)$$

in which  $E_{\max}$  is the value of E at saturating SR concentrations. Independently, the values of  $K_d$  were calculated from:  $K_d = k_{\text{off}} / k_{\text{on}}$ .

Equilibrium binding affinities between hSRP/hSRP-4A10L and 80S/RNCs were measured on Microscale Thermophoresis (MST) instrument (Nanotemper). 15 nM of Cy3B labeled hSRP/hSRP-4A10L was incubated with series of concentrations of either 80S or RNC<sub>4A10L</sub>. Thermophoresis of each sample was measured, and normalized fluorescence change was plotted against 80S/RNC4A10L concentration, and fit to Eq. 8,

$$\Delta F = \frac{[SRP] + [80S/RNC] + K_d - \sqrt{([SRP] + [80S/RNC] + K_d)^2 - 4[SRP] \times [80S/RNC]}}{2 \times [SRP]} \quad (8)$$

where  $\Delta F$  is normalized fluorescence, and  $K_d$  is equilibrium binding constant.

### ***smFRET measurements***

hSRP was diluted to 50–100 pM in SRP Assay Buffer containing 200  $\mu$ M GTP and 1  $\mu$ M 80S, 150 nM RNC<sub>4A10L</sub> or 150 nM RNC<sub>2R</sub> where indicated. Based on independently determined  $K_d$  values (Fig. S1.3), these concentrations of RNC and 80S ensure that all observed hSRP complexes were bound with the indicated partner. Samples were placed in a closed chamber made by sandwiching a perforated silicone sheet (Grace Bio-Labs) with two coverslips to prevent potential evaporation during measurements. Data were collected over 30-60 min using an ALEX-FAMS setup (Kapanidis et al., 2005, 2004) with two single-photon Avalanche photodiodes (Perkin Elmer) and 532 nm and 638 nm continuous wave lasers (Coherent) operating at 150  $\mu$ W and 70  $\mu$ W, respectively.

All smFRET data analyses including burst search, burst selection were performed using FRETbursts, an open-source burst analysis toolkit for confocal smFRET (Ingargiola, Lerner, Chung, Weiss, & Michalet, 2016). A dual-channel burst search (Nir et al., 2006) was performed to isolate the photon streams of particles containing FRET pairs from those containing only the donor or acceptor dye. Each burst (assumed to be the fluorescence signal from an individual SRP particle) was identified as a minimum of 10 consecutive detected photons with a photon count rate at least 10 times higher than the background photon count rate during both donor and acceptor excitation periods. Since the background rate can fluctuate within a measurement, the background rate was computed for every 50 second interval according to maximum likelihood fitting of the inter-photon delay distribution. The

identified bursts were further selected according to the following criteria: (i)  $n_{DD} + n_{DA} \geq 25$ ; and (ii)  $n_{AA} \geq 25$ , where  $n_{DD}$  and  $n_{DA}$  are the number of photons emitted from donor and acceptor during the donor excitation period, respectively, and  $n_{AA}$  is the number of photons emitted from acceptor during the acceptor excitation period.

The uncorrected FRET efficiency ( $E^*$ ) and the Stoichiometry ( $S$ ) for each burst were calculated using the following equations:

$$E^* = \frac{n_{DA}}{n_{DD} + n_{DA}} \quad (9)$$

$$S = \frac{n_{DD} + n_{DA}}{n_{DD} + n_{DA} + n_{AA}} \quad (10)$$

In most cases,  $E^*$  is different from the actual FRET efficiency due to simplifying assumptions (*i.e.*  $lk=0$ ,  $dir=0$ ,  $\gamma=1$ ). However, since the correction factors only depend on the photo-physical properties of fluorophores and the configuration of the optical setup, their contributions to the actual FRET efficiency are constant as long as the same optical set up, FRET pair and labeling position are used throughout all measurements. Importantly, we did not observe any significant changes in the photo-physical properties of both the donor and acceptor dyes by local environments (*i.e.* different conformations, substrates, ligands) (Fig. 1.6 and Fig. S1.7). Therefore, conformational changes in SRP that alter the actual FRET efficiency will also change the  $E^*$  value, and the trend of the changes with different binding partners will be the same. FRET histograms were obtained by 1D projection of the 2D  $E^*$ - $S$  histograms onto the  $E^*$  axis. In this context, we used  $E^*$  in this study to demonstrate the relative conformational change in SRP induced by its binding partners.

## 1.5 SUPPLEMENTARY FIGURES AND TABLES

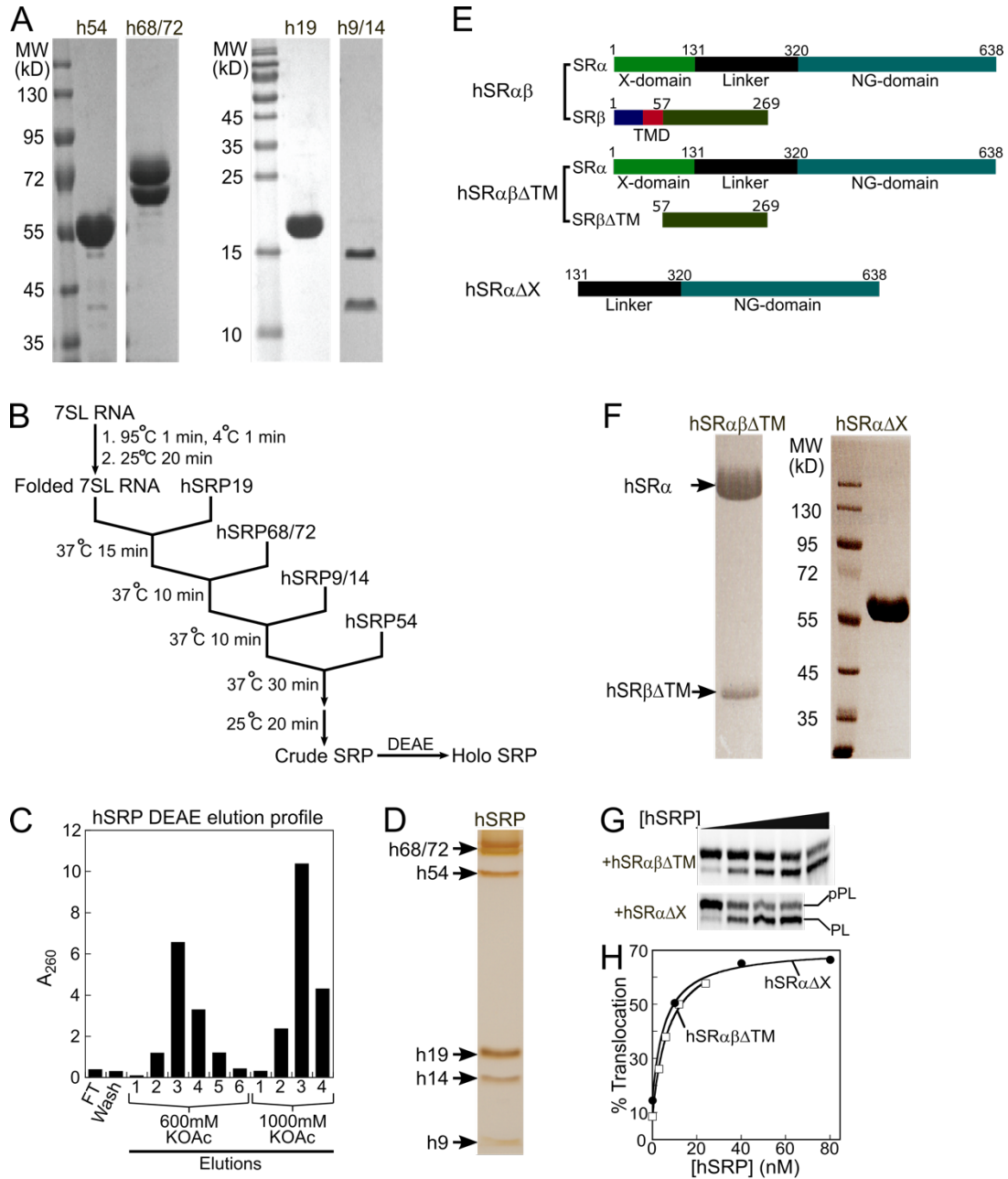


**Figure S1.1.** Large scale reconstitution of human SRP and SR. **(A)** Visualization of purified human SRP proteins by SDS-PAGE and Coomassie blue staining. **(B)** Outline of human SRP assembly based on modifications of published procedures (Huck, 2004; Mary et al., 2010). SRP proteins were ultracentrifuged at 100,000 rpm in TLA100 rotor for 30 minutes to remove aggregates prior to assembly. SRP RNA was refolded by heating at 95 °C for 1 minute and snap cooling on ice for 1 minute, followed by addition of 0.25 volume of 5X Binding Buffer (100 mM Tris-HCl (pH 7.5), 1.5 M KOAc, 25 mM Mg(OAc)<sub>2</sub>, 20 mM DTT,

and 50% glycerol) and incubation at room temperature for 20 minutes. A typical 600  $\mu$ L assembly reaction contained 300  $\mu$ L of 1XHKMN buffer (50 mM KHEPES (pH 7.5), 500 mM KOAc, 5 mM Mg(OAc)<sub>2</sub>, 1 mM DTT, and 0.02% Nikkol) and the remainder with SRP proteins and RNA in 1X Binding Buffer. Refolded SRP RNA at a final concentration of 2.5  $\mu$ M was first incubated with 4-6  $\mu$ M hSRP19 at 37 °C for 15 minutes, followed by addition of 2.5  $\mu$ M hSRP68/72 and 4  $\mu$ M hSRP9/14 and an additional 10 minute incubation. 4  $\mu$ M hSRP54 was added last, and the assembly mixture was incubated at 37 °C for 30 minutes and then at room temperature for 20 minutes. The assembly reaction was chilled on ice and diluted with 0.6 volume of Dilution Buffer (50 mM KHEPES (pH 7.5), 5 mM Mg(OAc)<sub>2</sub>, 1 mM DTT, 0.01% Nikkol, and 20% glycerol). **(C)** A representative A<sub>260</sub> profile of the purification of assembled hSRP using a DEAE-Sephacel column. The assembly mixture from part **B** was centrifuged at 18,000g for 5 minutes to remove large aggregates and loaded twice on 180  $\mu$ l DEAE-sephacel resin pre-equilibrated in 20CV of Equilibration Buffer (50 mM KHEPES (pH 7.5), 250 mM KOAc, 3 mM Mg(OAc)<sub>2</sub>, 0.5 mM EDTA, 1 mM DTT, 0.01% Nikkol, and 10% glycerol). The resin was washed with 5CV of Wash Buffer (50 mM KHEPES (pH 7.5), 350 mM KOAc, 4 mM Mg(OAc)<sub>2</sub>, 0.5 mM EDTA, 1 mM DTT, 0.01% Nikkol, and 10% glycerol). Holo-SRP was eluted using 80  $\mu$ l E600 Buffer (50 mM KHEPES (pH 7.5), 600 mM KOAc, 6.5 mM Mg(OAc)<sub>2</sub>, 0.5 mM EDTA, 1 mM DTT, 0.01% Nikkol, and 10% glycerol) per fraction. Incompletely assembled SRP was eluted with E1000 Buffer (50 mM KHEPES (pH 7.5), 1000 mM KOAc, 6.5 mM Mg(OAc)<sub>2</sub>, 0.5 mM EDTA, 1 mM DTT, 0.01% Nikkol, and 10% glycerol). Peak fractions containing SRP were collected based on A<sub>260</sub> readings. FT denotes Flow-through. **(D)** Visualization of purified Holo-SRP by SDS-PAGE and silver staining. **(E)** Schematic of the hSR constructs used in this work. **(F)** Visualization of purified hSR $\alpha\beta\Delta$ TM and hSR $\alpha\Delta$ X by SDS-PAGE and Coomassie blue staining. **(G)** Representative co-translational targeting and translocation of preprolactin (pPL) mediated by reconstituted hSRP and hSR. pPL was translated in wheat germ extract in the presence of <sup>35</sup>S-methionine, hSRP and hSR, and salt-washed/trypsinized rough ER microsomes (TKRM). Reactions were stopped after 30-40 minutes and analyzed by SDS-PAGE and autoradiography. **(H)** Quantification of the data in part **G** for reactions with hSR $\alpha\beta\Delta$ TM ( $\square$ ) and hSR $\alpha\Delta$ X ( $\bullet$ ).

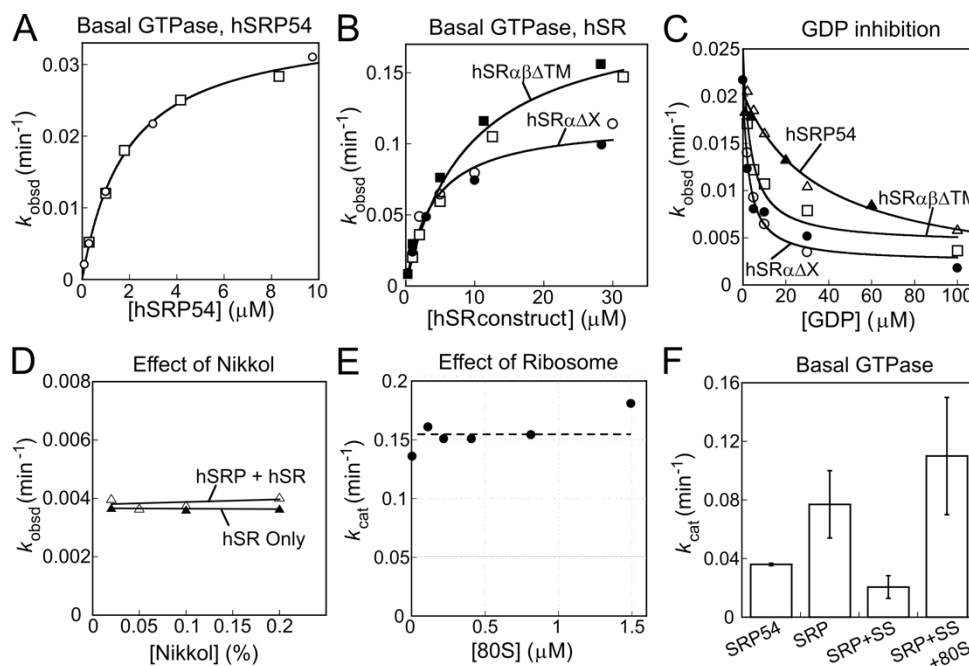


**Figure S1.2.** Basal GTPase activities of hSRP, hSR, and their controls. **(A, B)** The basal GTPase reactions of hSRP54 **(A)**, hSR $\alpha\beta\Delta\text{TM}$  **(B, □■)**, and hSR $\alpha\Delta\text{X}$  **(B, ○●)** were measured under single-turnover conditions with trace  $\gamma\text{-}^{32}\text{P}\text{-GTP}$  and indicated concentrations of proteins. The lines are fits of the data to Eq. 1 in the SI Methods, and the obtained rate constants are summarized in Fig. 1.1B. **(C)** Inhibition assay to measure the binding of GDP to hSRP54 ( $\Delta, \blacktriangle$ ), hSR $\alpha\beta\Delta\text{TM}$  ( $\square$ ), and hSR $\alpha\Delta\text{X}$  ( $\circ, \bullet$ ). Observed rate constants were measured under single-turnover conditions using 1  $\mu\text{M}$  hSRP54 or hSR and indicated concentrations of GDP. The lines are fits of the data to Eq. 3, and the values of  $K_i$  are summarized in Fig. 1.1B. Open and closed symbols denote the data from two independent measurements. **(D)** Increasing concentrations of Nikkol (up to 0.2%) do not affect the basal GTPase activity of hSR ( $\blacktriangle$ ), nor the stimulated GTPase reaction of hSRP with hSR ( $\Delta$ ). **(E)** The basal GTPase activity of hSR was unaffected by the ribosome. The intrinsic GTPase activity of hSR was measured under  $k_{\text{cat}}$  conditions with increasing concentrations of 80S. **(F)** Signal sequence and ribosome did not substantially stimulate the basal GTPase activity of hSRP.

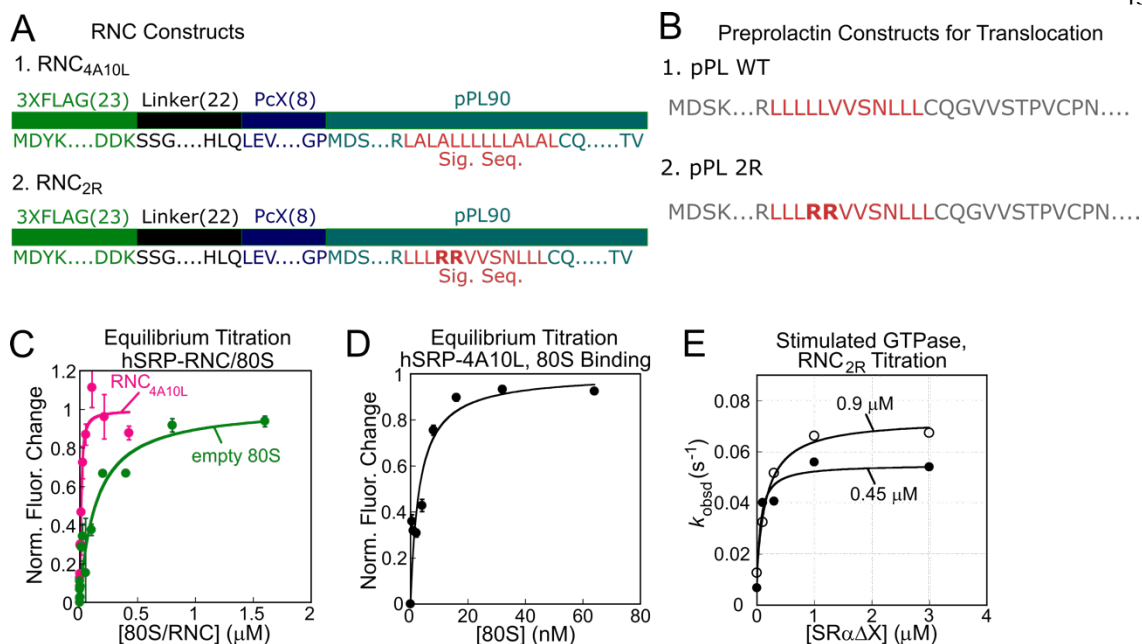


**Figure S1.3.** Schematic depiction of substrates used in this work and measurement of hSRP binding to ribosomal complexes. **(A)** The nascent chain of RNCs were based on the first 90 amino acids of preprolactin (pPL). An N-terminal 3xFLAG tag allows for affinity purification, and is followed by a 20 amino acid flexible linker and a PreScission protease site (PcX) for removing the affinity tag after purification. The pPL signal sequence was mutated to 4A10L or 2R to generate a correct and an incorrect substrate for SRP. **(B)** N-terminal sequences of full-length pPL, a model substrate for SRP-dependent co-translational targeting and translocation, and a 2R mutant of pPL as a negative control. Red highlights the wildtype or mutant signal sequence. **(C)** Equilibrium titration to measure the binding of hSRP to RNC<sub>4A10L</sub> and the 80S ribosome. Measurements were based on Microscale Thermophoresis (MST) using 20 nM of Cy3B labeled hSRP and indicated concentrations of purified 80S or RNC<sub>4A10L</sub>. The lines are fits of the data to Eq. 8, and gave  $K_d$  values of  $5.1 \pm 2.0$  nM and  $120 \pm 29$  nM for RNC<sub>4A10L</sub> and 80S, respectively. **(D)** Equilibrium titration to measure the binding of signal sequence fused hSRP to the 80S ribosome using MST. The data was fit to Eq. 8 and gave a  $K_d$  value of  $3.1 \pm 1.0$  nM. All data are presented as mean  $\pm$  S.D., with  $n = 3$ . **(E)** GTPase activity measured with increasing concentrations of RNC<sub>2R</sub>. Reciprocally stimulated GTPase reaction between hSRP and hSR $\alpha$  $\Delta$ X was measured in the presence of either 0.45  $\mu$ M (closed circle) or 0.9  $\mu$ M (open circle) of RNC<sub>2R</sub>.

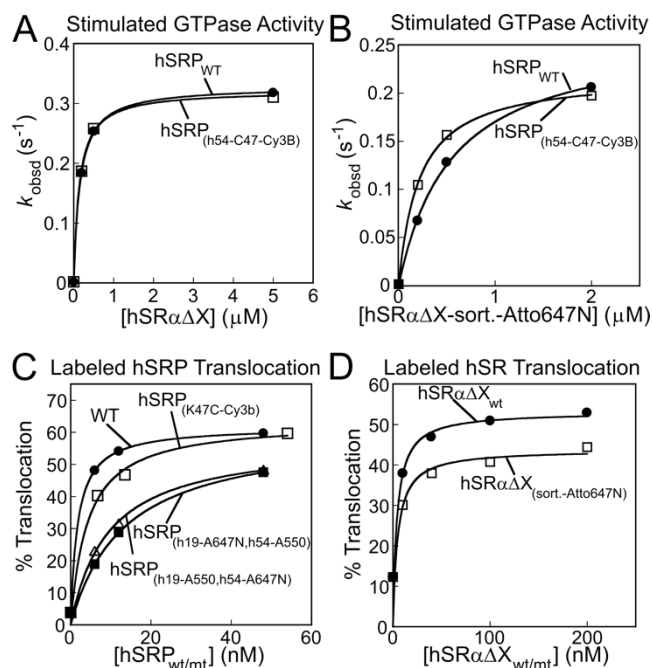


**Figure S1.4.** Fluorescence labeling does not substantially affect the activity of hSRP and hSR. (A, B) Reciprocally stimulated GTPase reactions between hSRP and hSR were measured as in Fig. 1.2A with wildtype hSRP and hSR $\alpha\Delta\text{X}$  (A, open), Cy3B-labeled hSRP and hSR $\alpha\Delta\text{X}$  (A, closed), hSRP and ATTO 647N-labeled hSR $\alpha\Delta\text{X}$  (B, closed), and the combination of dye-labeled hSRP and hSR (B, open). Note the different scales in A and B. (C, D) Co-translational targeting and translocation of pPL was measured as in Fig. S1.1H with fluorescently labeled hSRP (C) and hSR (D). The reactions in C contained 200 nM hSR. The reactions in D used 30 nM hSRP.

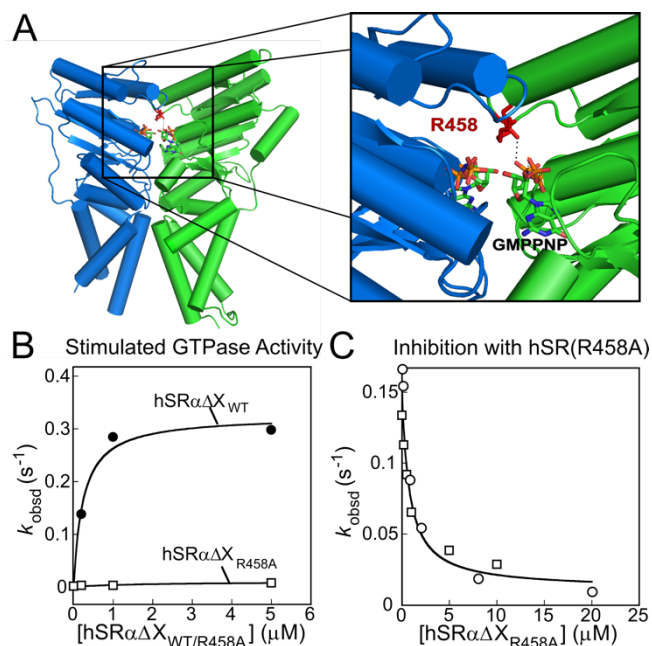


**Figure S1.5.** Characterization of the mutant hSR(R458A). **(A)** R458 in hSR $\alpha$  is highlighted in the crystal structure of the NG-domain complex between hSRP54 (*blue*) and hSR $\alpha$  (*green*; PDB 5L3Q) (Wild et al., 2016). The bound nucleotides are in *stick*, and the dotted line shows the hydrogen bond between R458 and the  $\gamma$ -phosphate of GMPPNP. **(B)** Reciprocally stimulated GTPase reaction of hSRP with hSR $\alpha$  $\Delta$ X (closed symbols) and hSR $\alpha$  $\Delta$ X(R458A) (open symbols), measured as in Fig. 1.2A. **(C)** hSR $\alpha$  $\Delta$ X(R458A) potentially inhibits the interaction between hSRP and hSR $\alpha$  $\Delta$ X. Reciprocally stimulated GTPase reactions were measured with 0.2  $\mu$ M hSRP and 0.5  $\mu$ M hSR $\alpha$  $\Delta$ X in the presence of the indicated concentrations of mutant hSR $\alpha$  $\Delta$ X (R458A). The data were fit to Eq. 4 in the SI Methods, which gave an apparent inhibition constant of  $K_i = 83$  nM. ‘ $\square$ ’ and ‘ $\circ$ ’ denote the data from two independent measurements.

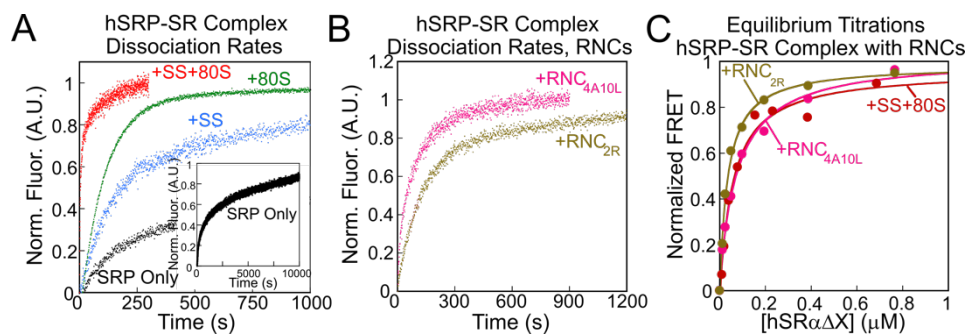


**Figure S1.6.** Additional FRET measurements of the hSRP-SR interaction. **(A)** Representative time traces of hSRP-hSR dissociation in the presence of the indicated SRP ligands. 12.5 nM hSRP or hSRP-4A10L was pre-incubated with labeled hSR (hSR\*) to allow their complex formation, and unlabeled hSR was added to initiate complex dissociation. The following concentrations of labeled and unlabeled hSR were used: 2  $\mu$ M hSR\* and 10  $\mu$ M hSR for the reaction with hSRP only, 0.25  $\mu$ M hSR\* and 2.5  $\mu$ M hSR in the presence of 80S (300 nM), 2  $\mu$ M hSR\* and 8  $\mu$ M hSR for hSRP-4A10L, and 75 nM hSR\* and 375 nM hSR for hSRP-4A10L bound to 80S (40 nM). The data were fit to double exponential functions, and the weighted sum of the observed rate constants were reported in Table S1.2. **(B)** Representative time traces of hSRP-SR dissociation in the presence of RNCs, measured as in part A. The following concentrations of labeled and unlabeled hSR were used: 160 nM hSR\* and 0.8  $\mu$ M hSR for hSRP bound to RNC<sub>4A10L</sub>, and 400 nM hSR\* and 4  $\mu$ M hSR for hSRP bound to RNC<sub>2R</sub>. **(C)** Equilibrium titrations to measure the stability of the hSRP-SR complex in the presence of RNCs. Titrations were carried out under the same conditions as in Fig. 1.3C, except that 300 nM RNCs were used instead of ribosomes.

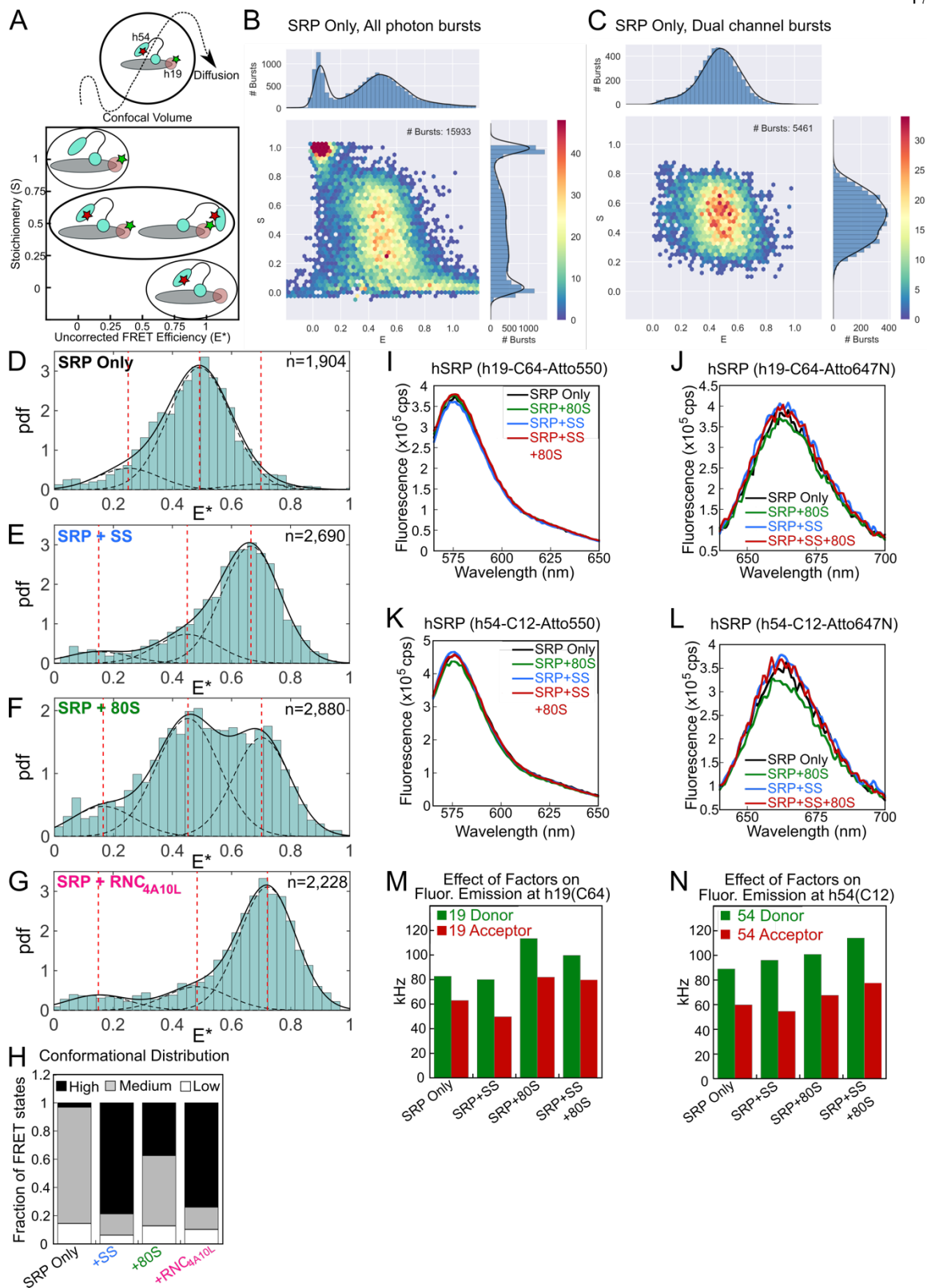


**Figure S1.7.** Schematic and control experiments for smFRET measurements. **(A)** Schematic depiction of the fluorescence-aided molecule sorting measurements using Alternating Laser Excitation Spectroscopy (ALEX). Fluorescently labeled SRPs diffusing through a femtoliter-scale observation volume are alternatively excited with donor (green) and acceptor (red) excitation lasers, and fluorescence emission from both the donor and acceptor dyes are measured to calculate donor-acceptor stoichiometry ( $S$ ) and uncorrected FRET efficiency ( $E^*$ ) to generate a 2-D  $E^*$ - $S$  plot. This allows optical purification of the doubly labeled particles with both donor and acceptor dyes ( $S \sim 0.5$ ), and 1D-projection of the doubly labeled population onto the  $E^*$  axis generates the FRET histogram (Kapanidis et al., 2005). **(B-C)** Representative 2-D  $E^*$ - $S$  plots for free hSRP labeled with ATTO-550 at SRP19(C64) and ATTO-647N at SRP54(C12). Panel **B** shows all the data from the measurement, while panel **C** shows the data for doubly labeled species after optical purification. **(D-G)** FRET histograms for hSRP, labeled with ATTO-550 at SRP54(C12) and ATTO-647N at SRP19(C64), with various binding partners. **(H)** Summary of the fraction of hSRPs containing the SRP54-ATTO550/SRP19-ATTO647N pair in the Low, Medium, and High-FRET populations from the data in **D-G**. Compared to the SRP19-ATTO550/SRP54-ATTO647N pair (Fig. 1.6), switching the position of donor and acceptor dyes did not significantly affect the FRET distribution of hSRP and its regulation by various ligands. Although the High-FRET state was slightly more populated with the SRP19-ATTO647N/SRP54-ATTO550 dye pair, the ribosome and signal sequence-induced changes in FRET distributions are the same between the two dye pairs. **(I-N)** Steady state fluorescence measurements **(I-L)** and median photon emission rate measurements on the ALEX setup **(M, N)** detected no significant effects of the various SRP ligands on the fluorescence of donor and acceptor dyes labeled at either SRP position.

**Table S1.1.** Summary of the rate constants from measurements of the stimulated GTPase reaction between human SRP and SR. N.D, not detectable. Values are reported as mean  $\pm$  S.D., with  $n \geq 2$ .

	<b>hSR<math>\alpha\beta\Delta</math>TM</b>		<b>hSR<math>\alpha\Delta</math>X</b>	
	$k_{cat}$ (s <sup>-1</sup> )	$k_{cat}/K_m$ (M <sup>-1</sup> s <sup>-1</sup> )	$k_{cat}$ (s <sup>-1</sup> )	$k_{cat}/K_m$ (M <sup>-1</sup> s <sup>-1</sup> )
<b>SRP Only</b>	N.D.	N.D.	N.D.	N.D.
<b>+SS</b>	0.082 $\pm$ 0.018	6.7( $\pm$ 0.53) $\times 10^4$	0.087 $\pm$ 0.012	8.3( $\pm$ 0.50) $\times 10^4$
<b>+80S</b>	0.032 $\pm$ 0.00017	1.5( $\pm$ 0.19) $\times 10^5$	0.057 $\pm$ 0.012	2.3( $\pm$ 0.28) $\times 10^5$
<b>+SS+80S</b>	0.15 $\pm$ 0.008	8.0( $\pm$ 3.0) $\times 10^5$	0.21 $\pm$ 0.017	2.5( $\pm$ 0.5) $\times 10^6$

**Table S1.2.** Summary of the rate and equilibrium constants of the SRP-SR interaction measured using the FRET assay. Values are reported as mean  $\pm$  S.D., with  $n \geq 2$ .

	$k_4$ (M <sup>-1</sup> s <sup>-1</sup> )	$k_{-4}$ (s <sup>-1</sup> )	$K_d$ ( $k_{off}/k_{on}$ ) (nM)	Measured $K_d$ (nM)
<b>SRP Only</b>	8.6( $\pm$ 4.1) $\times 10^1$	8.9( $\pm$ 0.14) $\times 10^{-4}$	10350	*2460 $\pm$ 48
<b>+SS</b>	8.4( $\pm$ 0.78) $\times 10^3$	3.3( $\pm$ 1.3) $\times 10^{-3}$	393	326 $\pm$ 13
<b>+80S</b>	1.6( $\pm$ 0.10) $\times 10^5$	9.1( $\pm$ 0.60) $\times 10^{-3}$	57	64 $\pm$ 10
<b>+SS+80S</b>	3.5( $\pm$ 0.50) $\times 10^6$	8.3( $\pm$ 1.1) $\times 10^{-2}$	24	56 $\pm$ 13
<b>RNC<sub>4A10L</sub></b>	1.0( $\pm$ 0.10) $\times 10^6$	1.7( $\pm$ 0.12) $\times 10^{-2}$	17	77 $\pm$ 5
<b>RNC<sub>2R</sub></b>	6.5( $\pm$ 0.76) $\times 10^4$	5.7( $\pm$ 1.0) $\times 10^{-3}$	88	35 $\pm$ 4

\* In the absence of ligands, the  $K_d$  value from the equilibrium titration is less accurate, because saturation could not be reached due to limitations in protein concentration, and because of difficulties in reaching equilibrium at low SR concentrations due to the slow assembly rates.

*Chapter 2***DUAL ROLE OF SRP RECEPTOR COMPACTION DURING MEMBRANE TARGETING STEPS OF MAMMALIAN SRP PATHWAY**

A part of this chapter was first published as: Kobayashi, K., Jomaa, A., Lee, J.H., Chandrasekar, S., Boehringer, D., Shan, S.-o., Ban, N. (2018). “Structure of a prehandover mammalian ribosomal SRP•SRP receptor targeting complex.” In: *Science* 360: 323-327. doi: 10.1126/science.aar7924

Signal recognition particle (SRP) is an essential and universally conserved machinery responsible for biogenesis of ~30% of proteome. How SRP and SRP receptor (SR) mediates co-translational delivery of nascent proteins to Endoplasmic Reticulum (ER) is poorly understood. Here, we observe, for the first time, the details of conformational dynamics of SRP-SR targeting complex by single-molecule fluorescence spectroscopy. Through mutational studies, we identified three distinct conformational changes of targeting complex during membrane targeting steps. Moreover, we discovered two essential roles of SR compaction, where SR compaction not only brings the targeting complex near the membrane, but also induces subsequent conformational changes to expose Sec61 binding site and generate transfer-ready intermediate. Mutations blocking these conformational changes caused significant defect in SRP targeting activity. Interestingly, multiple interactions at this state delays GTP hydrolysis. These results together establish a detailed model for membrane targeting in mammalian SRP pathway and emphasize a crucial role of SR in ensuring proper delivery of substrates to ER membrane.

## 2.1 INTRODUCTION

Proper biogenesis of nascent proteins is essential for maintaining protein homeostasis inside the cell (Hartl et al., 2011). Signal recognition particle (SRP) pathway is a universally conserved pathway that mediates co-translational delivery of ribosomes translating ~30% of proteome to eukaryotic endoplasmic reticulum (ER) or bacterial plasma membrane. SRP recognizes and binds to translating ribosomes with exposed N-terminal signal sequence or transmembrane domain. Through interaction with SRP receptor (SR), SRP delivers translating ribosomes to Sec61p (or SecYEG in bacteria) translocase on ER, where translation continues coupled with translocation through the membrane (Akopian et al., 2013; Zhang & Shan, 2014). Mammalian SRP is an RNA-protein complex composed of six proteins (SRP19, SRP9/14, SRP68/72, and SRP54) bound to 7SL SRP RNA (Peter Walter & Blobel, 1983). SRP54 is a universally conserved subunit that contains M-domain, which binds to the RNA as well as the signal sequence, and NG-domain, which contains the GTPase module required for interaction with SR. Mammalian SR is a heterodimer of SR $\alpha$  and SR $\beta$ . SR $\alpha$  contains homologous NG-domain, which also has a GTPase module for interaction with SRP54 NG-domain, and X-domain, which is the domain interacting with SR $\beta$ . These two domains of SR $\alpha$  is connected through a long unstructured flexible linker (~150 residues) that has been implicated in binding ribosomes (Jadhav et al., 2015). SR $\beta$  is a membrane protein on ER presumably localizing SR heterodimer near the ER membrane (Akopian et al., 2013; Nyathi, Wilkinson, & Pool, 2013).

Previous studies on the initial steps of mammalian SRP pathway found that the presence of correct signal sequence pre-organizes SRP into proximal conformation, where

NG-domain of SRP54 is near the ribosome exit site. Moreover, this pre-organization led to efficient recruitment of SR, implying that SRP-SR NG-complex initially forms at the proximal site (Lee et al., 2018). On the other hand, structural studies of ternary complex of ribosome-nascent chain complex (RNC) bound SRP in complex with SR described a completely different conformation where NG-complex is docked at the opposite end of SRP, the distal site (Halic, 2006; Kobayashi et al., 2018). These two sets of data suggest that the SRP-SR NG-complex undergoes largescale movement from the proximal site to the distal site during the targeting cycle. Although similar movement has been extensively studied in bacterial system (Jomaa et al., 2017; Kuang Shen et al., 2013; Voigts-Hoffmann et al., 2013), such movement has never been observed in mammalian system and its functional relevance remains unknown.

However, structure of SRP-SR complex in distal conformation leads to speculations on its functional role in SRP targeting. First, the NG-complex docked at the proximal site would prevent Sec61p binding and substrate transfer. Thus, it would be essential to induce a movement of NG-complex to distal site in order to expose Sec61p binding site on the ribosome and allow substrate transfer (Halic, 2006; Kobayashi et al., 2018). Secondly, structure of distal conformation (Kobayashi et al., 2018) shows three domains of SR (NG, X, and  $\beta$ ) forming multiple protein-protein interactions at the distal site. As SR $\alpha$ NG and X/ $\beta$  domains are connected through a flexible linker, these two domains can initially be far apart, which puts the SRP bound translating ribosome far from the membrane. Through hypothesized conformational change to reach distal conformation, SR could bring the three domains of SR in contact, which effectively brings the substrate near the membrane for

interaction with Sec61 for transfer (Fig. 2.1). Although these two aspects would be essential for SRP targeting activity, no direct evidence is available to support these hypotheses. Moreover, the precise mechanism of SRP-SR conformational change during membrane targeting steps is entirely unknown.

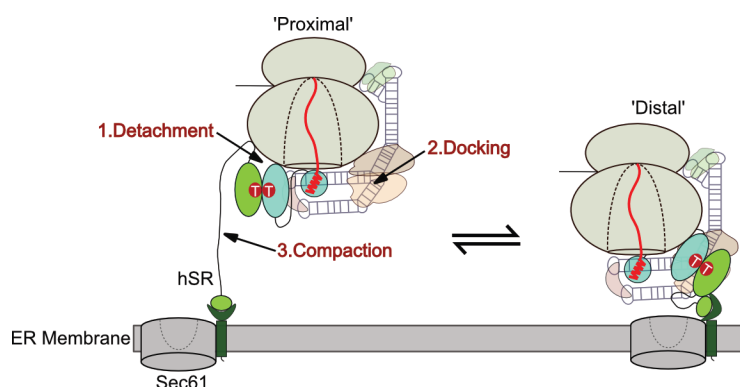


**Figure. 2.1. Distinct steps during conformational change from proximal to distal conformation.** Conformational change from proximal to distal site can be dissected into three distinct steps; 1. Detachment of NG-complex from proximal site (Detachment), 2. NG-complex docking at the distal site (Docking), 3. SR compaction to bring X/ $\beta$  and NG domain together (Compaction).

To address these outstanding questions, we studied the conformations of SRP-SR complex through single-molecule FRET (smFRET) methods and dissected the functional roles of these conformations during SRP targeting cycle. For the first time, we show that the largescale movement of NG-complex indeed occurs in solution upon SRP-SR interaction. Through mutational studies, we found that this NG-complex movement occurs in three distinct steps. Moreover, we discovered dual role of SR compaction where this step not only brings targeting complex near the membrane, but also induces the NG-complex movement. These steps during conformational change was found to be essential for SRP activity, and

importantly, we discovered that interactions at the distal site inhibits GTP hydrolysis. These results elucidate previously unknown mechanistic details during SRP targeting cycle and emphasize the essential role of SR compaction for successful delivery of substrates to ER membrane by SRP and SR.

## 2.2 RESULTS

### *Largescale movement of NG complex occurs upon SRP-SR interaction*

The conformational change of SRP-SR complex from proximal site to distal site can be separated into three distinct steps. First, the NG complex needs to detach from the proximal site. Secondly, the NG complex can dock at the distal site through multiple protein-protein interactions. Finally, the flexible linker of SR connecting X-domain and NG-domain needs to compact to bring two domains together (Fig. 2.1). To directly monitor these distinct steps, we designed three sets of FRET probes. The conformations of SRP and SRP-SR complex were monitored at single-molecule resolution (smFRET) based on Fluorescence-aided Molecular Sorting using Alternating Laser Excitation Spectroscopy (ALEX) (Kapanidis et al., 2005, 2004).

To monitor NG complex detachment, we incorporated a donor dye (Atto550) on SRP19 (C64) and an acceptor dye (Atto647N) on SRP54 (C12) (Proximal Probe) (Lee et al., 2018). Based on the available structure (Voorhees & Hegde, 2015), the distance between the dye pair is  $\sim 44$  Å (Fig. 2.2A), so we would expect high FRET when NG domain is near the proximal site (Förster radius 65 Å). But if NG complex moves away from the proximal site ('Detachment'), we expect loss of high FRET population and increase in low FRET populations (Fig. 2.2B). As shown previously (Lee et al., 2018), in the absence of SR,

substrate-bound SRP shows predominantly high FRET population (Fig. 2.2C). Upon addition of SR, we observed a dramatic change where the FRET population is now dominated by low FRET population (Fig. 2.2D). This result shows that although SRP-SR NG complex initially forms at the proximal site (Lee et al., 2018; Voorhees & Hegde, 2015), it rapidly moves away from the proximal site.

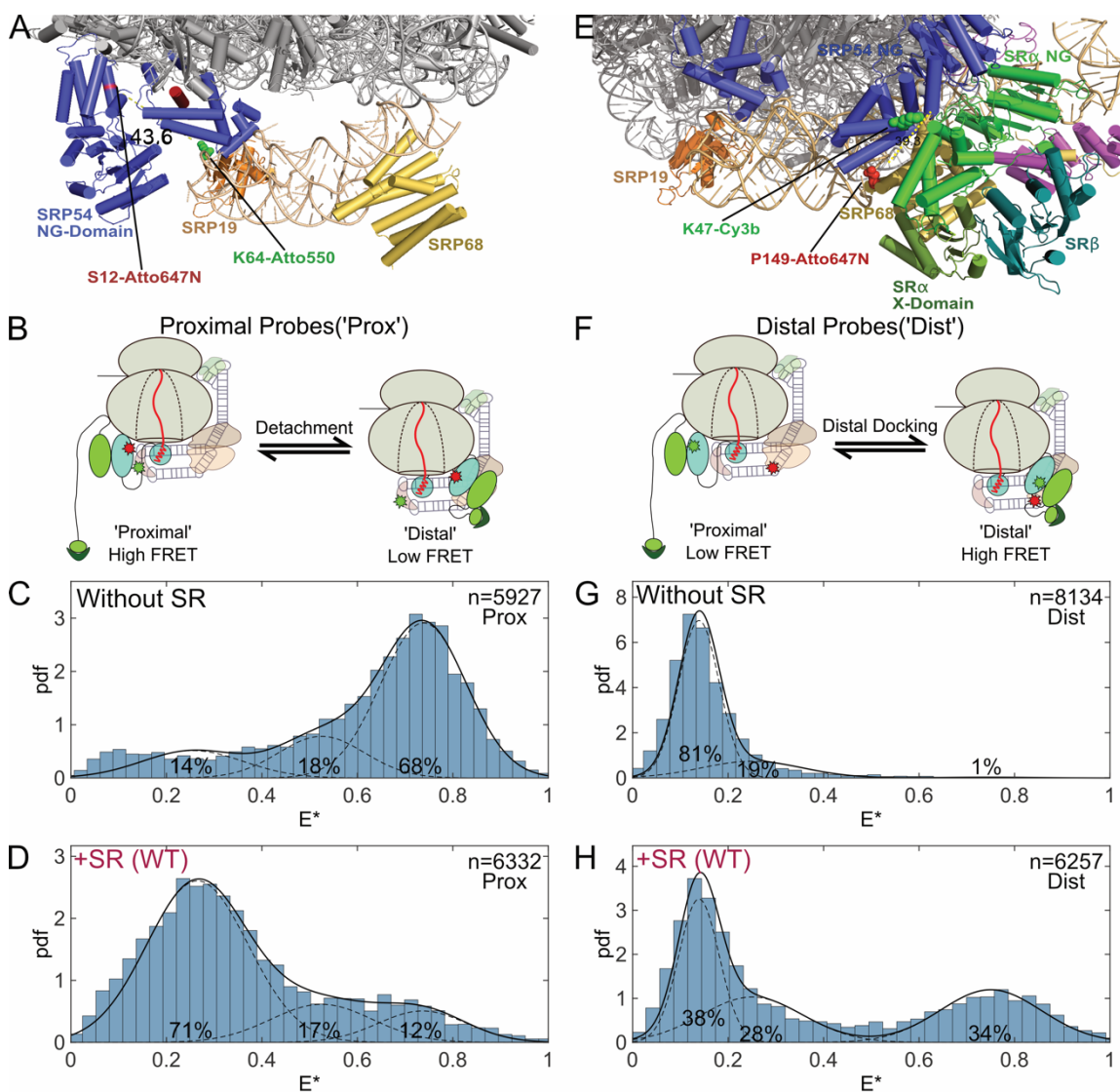


**Figure 2.2. FRET probes to monitor NG-complex detachment and distal docking. (A)** Structure showing SRP in proximal conformation with positions of proximal FRET probes highlighted (PDB: 3JAJ) (Voorhees & Hegde, 2015); SRP19 (orange) with a donor dye

(Atto550) on C64, and SRP54 (blue) with an acceptor dye (Atto647N) on C12 (Lee et al., 2018). **(B)** NG-complex detachment from proximal site (high FRET) to distal site (low FRET). **(C-D)** smFRET histograms of signal sequence fused human SRP with ribosome (Lee et al., 2018) in the absence **(C)** and presence **(D)** of SR $\alpha\beta\Delta$ TM. ‘pdf’ denotes probability density function, ‘n’ is number of data points, and ‘Prox’ denotes proximal probes. [SRP-4A10L]=200pM, [80S]=150nM, [SR $\alpha\beta\Delta$ TM]=2 $\mu$ M. All smFRET histograms are combined data from five to ten independent experiments. **(E)** Structure showing ternary complex of RNC bound SRP-SR complex in distal conformation (PDB: 6FRK) (Kobayashi et al., 2018), with positions of distal FRET probes highlighted; SRP54 (blue) with a donor dye (Cy3B) on C47 and SRP68 (yellow) with an acceptor dye (Atto647N) on ybbr tag inserted after P149 (Yin, Lin, Golan, & Walsh, 2006). **(F)** NG-complex movement from proximal site (low FRET) to distal site docking (high FRET). **(G-H)** smFRET histograms under the same condition as **C-D**, but with distal probes. ‘Dist’ denotes distal probes.

Next, we designed a new set of FRET probes to monitor NG complex docking at the distal site. Instead of SRP19, SRP68, which is at the opposite side of SRP, was used as the target for fluorescent dye incorporation. A short sfp recognition motif (DSLEFI) was inserted into one of the loops of SRP68 (after P149) for site-specific incorporation of CoA-Atto647N conjugate (Yin et al., 2006). A donor dye (Cy3B) was incorporated on SRP54 (C47) (Distal Probe) (Lee et al., 2018). Based on the structure of distal conformation (Kobayashi et al., 2018), the distance between the dye pair is  $\sim 39$  Å (Fig. 2.2E) and we expect high FRET when NG domain is near distal site (Förster radius 62 Å) (Fig. 2.2F). In the absence of SR, substrate-bound SRP showed predominantly low FRET population (Fig. 2.2G), consistent with the data from proximal probe. Upon addition of SR, high FRET population appeared, which is occupied by 34% of the entire population (Fig. 2.2H). This result provides direct evidence that the conformational change from proximal to distal occurs upon SRP-SR interaction and that the distal conformation depicted in the structure exists in solution. The fraction of SRP-SR complex in low FRET with proximal probe (71%) differs from that in high FRET with distal probe (34%). This implies that although most of NG complex detaches

from the proximal site, only half of them actually docks on the distal site, while the other half is localized at another site that is far from both proximal and distal site suggesting existence of an additional conformation that is yet to be characterized.

### ***SR compaction is SRP dependent***

The degree of SR linker compaction can be indirectly measured through the proximity of NG-domain and X/ $\beta$ -domain. To this extent, we designed another set of FRET probe (Compaction Probe) by incorporating a donor dye (Atto550) at the C-terminus of NG-domain through sortase mediated conjugation (Guimaraes et al., 2013; Lee et al., 2018) and an acceptor dye (Atto647N) at the N-terminus of SR $\beta$  through *sfp* mediated conjugation (Yin et al., 2006). Based on the structure of distal conformation (Kobayashi et al., 2018), the distance between the two dyes is very short ( $\sim 36$  Å) (Fig. 2.3A). Thus, even if SRP-SR is not specifically in the distal conformation, when the linker compacts and there is interaction between NG-domain and X/ $\beta$ -domain, we can expect SR to sample high FRET states (Fig. 2.3B).

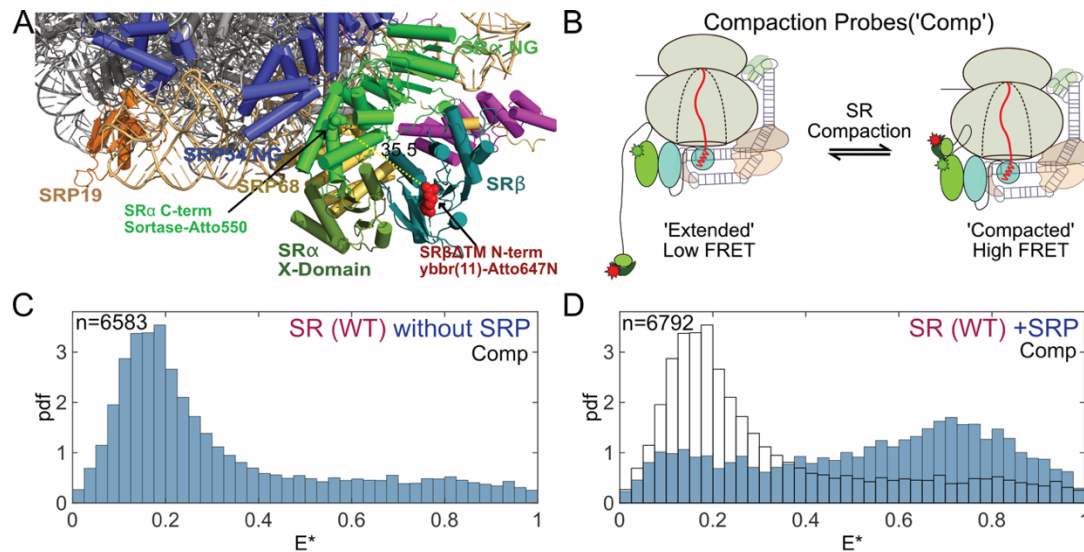


**Figure 2.3. FRET probes to monitor SR compaction.** (A) Structure showing ternary complex of RNC bound SRP-SR complex in distal conformation (PDB: 6FRK) (Kobayashi et al., 2018), with positions of compaction FRET probes highlighted; SR $\alpha$ -NG (green) with a donor dye (Atto550) at the C-terminus and SR $\beta$  (deep blue) with an acceptor dye (Atto647N) at the N-terminus. (B) SR with linker extended (low FRET) compacts to bring SR $\alpha$ -NG and SR $\beta$  in proximity (high FRET); cartoons represent one of many possible conformations. (C-D) smFRET histograms of double-labeled SR $\alpha\beta\Delta$ TM with ribosome in the absence (C) and presence (D) of signal sequence fused SRP. ‘Comp’ denotes compaction probes. [SR]=200pM, [80S]=400nM, and [SRP-4A10L]=300nM.

We first measured the conformation of SR in the presence of ribosome without SRP. Surprisingly, vast majority of SR sampled low FRET state (Fig. 2.3C) showing evidence that the linker is in an extended form and that NG-domain and X/ $\beta$ -domain are far apart. Upon addition of SRP, the SR population was highly biased towards high-FRET state (Fig. 2.3D). This implies a novel mode of regulation. While SR is known to interact with ribosomes (Jadhav et al., 2015), our results show that it does not compact when SR is interacting with ribosome. Rather, SR compacts only when SRP is present implying that SR searches for SRP bound ribosomes to specifically bring them near the membrane through compaction.

### ***Distal movement of SRP-SR NG-complex is initiated by SR compaction***

To gain mechanistic insights on the conformational change of SRP-SR complex, we introduced a series of mutations to SR that are designed to disrupt the distal conformation based on the available structure (Fig. S2.1 and Fig. 2.4A). The mutations can be classified into two major classes; mutations designed to disrupt intramolecular interaction of SR between NG-domain and X/ $\beta$ -domain (Fig. 2.4A, *green*), and mutations disrupting interaction between SRP68/72 subunit of SRP and NG-domain of SR (Fig. 2.4A, *blue*).  $\Delta$ 477



at low and high FRET peaks, calculating fraction in high-FRET state, and normalizing to wild-type (black).

and  $\Delta 572$  mutations were initially identified through sequence analysis where we found two loops that potentially co-evolved with SRP68/72, which is a unique subunit to mammalian system (Fig. 2.4B). This idea is further supported by the structure of distal conformation (Kobayashi et al., 2018), which shows direct contact between loop 572 and SRP68 (Fig. S2.1). These mutations did not significantly affect SRP-SR complex assembly rate (Fig. 2.4C) showing that the mutations did not disrupt interaction with SRP. Thus, all defects that we observe in subsequent analyses are caused by the defect in conformational change, and not by the defect in SRP interaction.

Because these mutations are based on distal conformation, we first analyzed whether the mutations reduce the distal docking activity of SRP-SR complex using ‘Distal Probe’ (Fig. 2.2F). Indeed, all the mutants displayed reduced high FRET population compared to the wild-type (Fig. S2.2 and Fig. 2.2H). High FRET population with each mutant was plotted relative to the wild-type for comparison (Fig. 2.4D). The defect was mild (Fig. S2.2D and E) for some while others showed significant defect (Fig. S2.2A-C). Importantly, the mutations disrupting interactions between NG-domain and X/ $\beta$ -domain of SR showed more significant defect (Fig. 2.4D, *green*).

We next monitored SRP-SR NG-complex detachment from the proximal site using ‘Proximal Probe’ (Fig. 2.2B). In this case, we observed two distinct behaviors of the mutant SRs. One set of mutants showed virtually the same conformational distribution as the wild-type, where majority is in low-FRET state (compare Fig. S2.3D and E, and Fig. 2.2D). On

the other hand, another set of mutants showed significant population still sampling high-FRET state (Fig. S2.3A-C). The fraction of median and high FRET state was combined and plotted relative to the wild-type for comparison (Fig. 2.4E). And surprisingly, these two types of behaviors corresponded well with the type of mutations introduced (Fig. 2.4E, *green* vs *blue*). This result is consistent with the defect we observe in distal docking activity; because NG-complex of mutants in *green* cannot detach efficiently from the proximal site, it cannot dock at the distal site. More importantly, these results show that the intramolecular interaction within SR between NG-domain and X/ $\beta$ -domain is crucial for initiating detachment and subsequent conformational changes.

However, NG-domain and X/ $\beta$ -domain of SR are far apart initially as the linker is in an extended form (Fig. 2.3C), and only compacts upon interaction with SRP (Fig. 2.3D). So how could the interaction between the two domains that are far apart be important for initiating conformational change of SRP-SR complex? This invokes a model where SR compaction must occur first before the other steps (detachment and distal docking) during the conformational change of SRP-SR complex. In fact, SR compaction must be initiating NG-complex detachment from the proximal site as intra-molecular interaction of SR is crucial for NG-complex detachment. Based on this model, we can predict that the mutants showing defect in NG-complex detachment would show defect in SR compaction.

Indeed, when SR compaction activity of the mutants were measured with ‘Compaction Probe’ (Fig. 2.3B), we observed largest defect with  $\Delta 371$  (Fig. S2.4A and Fig. 2.4F), which was also defective in NG-complex detachment (Fig. 2.4E). On the other hand,  $\Delta 572$ , which showed no defect in NG-complex detachment, showed milder defect in SR

compaction compared to  $\Delta 371$  (Fig. S2.4C and Fig. 2.4F). These results support the model where SR compaction initiates NG-complex detachment from proximal site, which subsequently allows the complex to dock at the distal site. R407A shows defect in NG-complex detachment (Fig. 2.4E) but shows similar SR compaction activity as  $\Delta 572$  (Fig. 2.4F and Fig. S2.4B). This implies that R407 residue may not be directly involved in compaction but is rather involved in positioning X/ $\beta$ -domain for specific interaction that leads to NG-complex detachment.

We can also find some structural evidence to support this model. Although there is no available structural information of SRP-SR NG-complex docked at the proximal site, there are existing structures of SRP NG-domain docked at the proximal site (Voorhees & Hegde, 2015), and SRP-SR NG-complex docked at the distal site (Kobayashi et al., 2018). A structural model of NG-complex docked at the proximal site can be derived based on these existing structures by aligning SRP-SR complex from distal structure to the proximal structure using SRP54 NG-domain homology (Fig. S2.5A). In this structural model, X-domain of SR is in very close contact with the proximal site of the ribosome (Fig. S2.5B). Thus, initially when SR linker is extended, SRP-SR NG-complex forms at the proximal site. Subsequently, SR compacts to bring X-domain near the proximal site, which potentially introduces a clash or a specific interaction (Fig. S2.5B) that induces detachment of NG-complex from the proximal site. NG-complex can then dock at the distal site to allow Sec61 binding and substrate transfer.

***SR compaction is essential for SRP activity***

To evaluate the importance of these series of conformational changes of SRP-SR complex in SRP activity, we measured co-translational targeting activity of the mutants that inhibit distinct steps of conformational changes. At saturating concentration of SR, mutants showed different degree of defects (Fig. 2.5A). Distal docking mutants ( $\Delta 477$  and  $\Delta 572$ ) showed about ~20% reduced activity compared to the wild-type (Fig. 2.5A, blue), providing evidence that distal docking activity is indeed an important step during targeting by SRP. On the other hand, R407A, which showed little defect in SR compaction but significant defect in NG-complex detachment from proximal site, showed virtually no defect in targeting activity (Fig. 2.5A, R407A). This implies that the defect in NG-complex detachment of R407A mutant may be rescued by a membrane component.

Importantly, SR compaction mutant ( $\Delta 371$ ) showed largest defect in targeting activity with only ~35% activity compared to the wild-type (Fig. 2.5A,  $\Delta 371$ ). This provides additional support for our current model; as SR compaction is the initial step of membrane targeting after SRP-SR interaction, inhibiting this step would lead to largest defect in overall activity. Moreover, this implies that SR compaction is the essential step that brings the targeting intermediate near the membrane, and without this conformational change, the substrates are not able to reach the membrane or the translocon. Once the targeting intermediate reaches the membrane through SR compaction (R407A,  $\Delta 477$ , and  $\Delta 572$ ), the defect in overall activity is much less (Fig. 2.5A), likely because a membrane component may be able to rescue other defects.

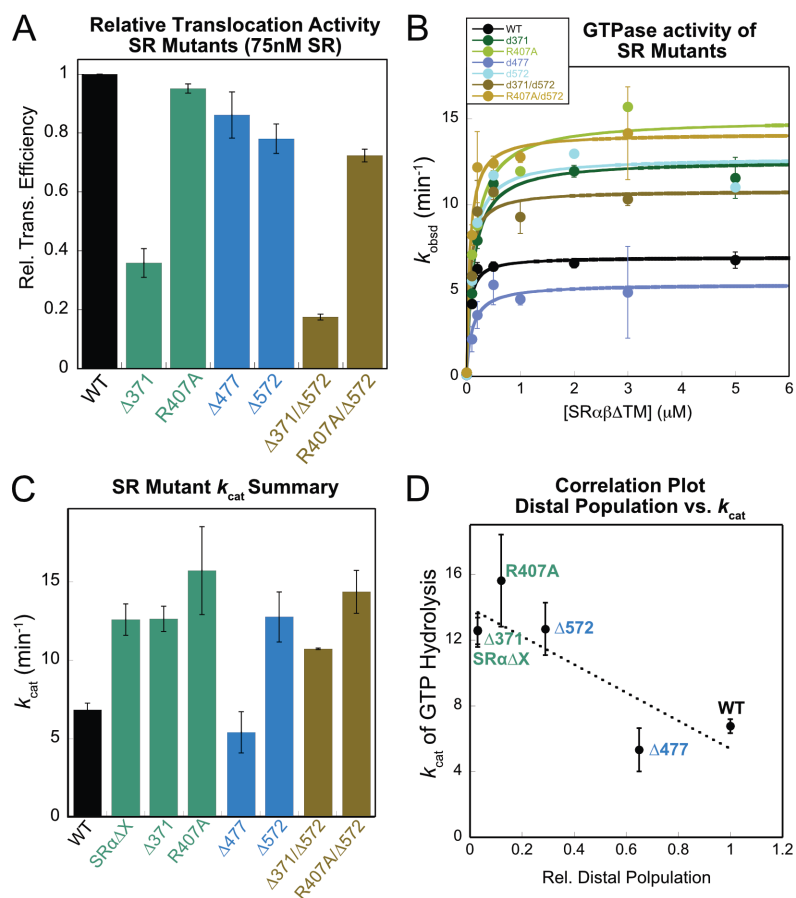


**Figure 2.5. Targeting and GTP hydrolysis activity of SR mutants.** (A) Translocation activity of model SRP substrate, preprolactin, into ER microsomes were measured through standard procedures (Lee et al., 2018; Shan et al., 2007). Efficiency at saturating SR concentration (75nM) was normalized to wild-type (black). Data represented as mean  $\pm$  SD, with n=3. (B) Stimulated GTPase activity of SRP and SR was measured through previously developed procedures (Lee et al., 2018). Data represented as mean  $\pm$  SD, with n=3. (C) Bar graph of  $k_{cat}$  values extracted from fitting in B. Data represented as mean  $\pm$  SD, with n=3. (D) Correlation plot between  $k_{cat}$  and relative fraction of SRP in distal conformation (Fig. 2.4D).

### *Distal site docking of SRP-SR NG-complex inhibits GTP hydrolysis*

Regulation of GTP hydrolysis was an essential regulatory mechanism of the SRP pathway in other organisms (Kuang Shen et al., 2013; Voigts-Hoffmann et al., 2013). To test whether distal conformation has any regulatory role of GTP hydrolysis in mammalian

system, we measured GTPase activity of the SR mutants. Stimulated GTPase activity was measured in SR concentration dependent manner to extract maximal rate of GTP hydrolysis ( $k_{cat}$ ) (Fig. 2.5B) (Lee et al., 2018; Peluso et al., 2001). When we compared  $k_{cat}$  across the mutants, we observed general hyperactivity compared to the wild-type, where most of the mutants showed over 2-fold higher  $k_{cat}$  value (Fig. 2.5C). Moreover, when we plotted correlation between  $k_{cat}$  and distal docking activity of the mutants (Fig. 2.4D), there was a mild negative correlation (Fig. 2.5D). This implies that distal site docking of the NG-complex inhibits GTPase activity. As SRP and SR dissociates upon GTP hydrolysis, the inhibition caused by distal site docking would increase the lifetime of transfer-ready targeting intermediate. This increased lifetime may provide sufficient time window for the substrate to dissociate from SRP and engage Sec61 translocon.

### ***Mechanism of GTPase regulation diverged in mammalian system***

The movement of SRP-SR NG-complex from proximal site to distal site has been studied in other organisms previously (Kuang Shen, Arslan, Akopian, Ha, & Shan, 2012; Kuang Shen et al., 2013). When we compare the active site structure from mammalian (Fig. 2.6A) and bacterial (Fig. 2.6B) system (Jomaa et al., 2017; Kobayashi et al., 2018), the architecture and arrangements are very similar. F456 from mammalian SR and G232 of mammalian SRP RNA are arranged identically to bacterial F332 and G83 (compare Fig. 2.6A and B). G83 in bacteria was found to be essential for activating GTP hydrolysis, and any mutation on this site led to nearly complete abolishment of GTP hydrolysis. Thus, in bacterial system, distal conformation was essential for activating GTP hydrolysis and recycling SRP and SR (Kuang Shen et al., 2013; Voigts-Hoffmann et al., 2013). As G232 in

mammalian system is arranged identically to bacterial G83, we hypothesized that mutating this residue would also abolish GTPase activity. In addition, C-terminus of SRP72 also protrudes into the GTPase active site next to G232 (Fig. 2.6C and D). Thus, we mutated G232 and generated series of C-terminal truncation mutants of SRP72 and measured GTPase activity (Fig. S2.6).

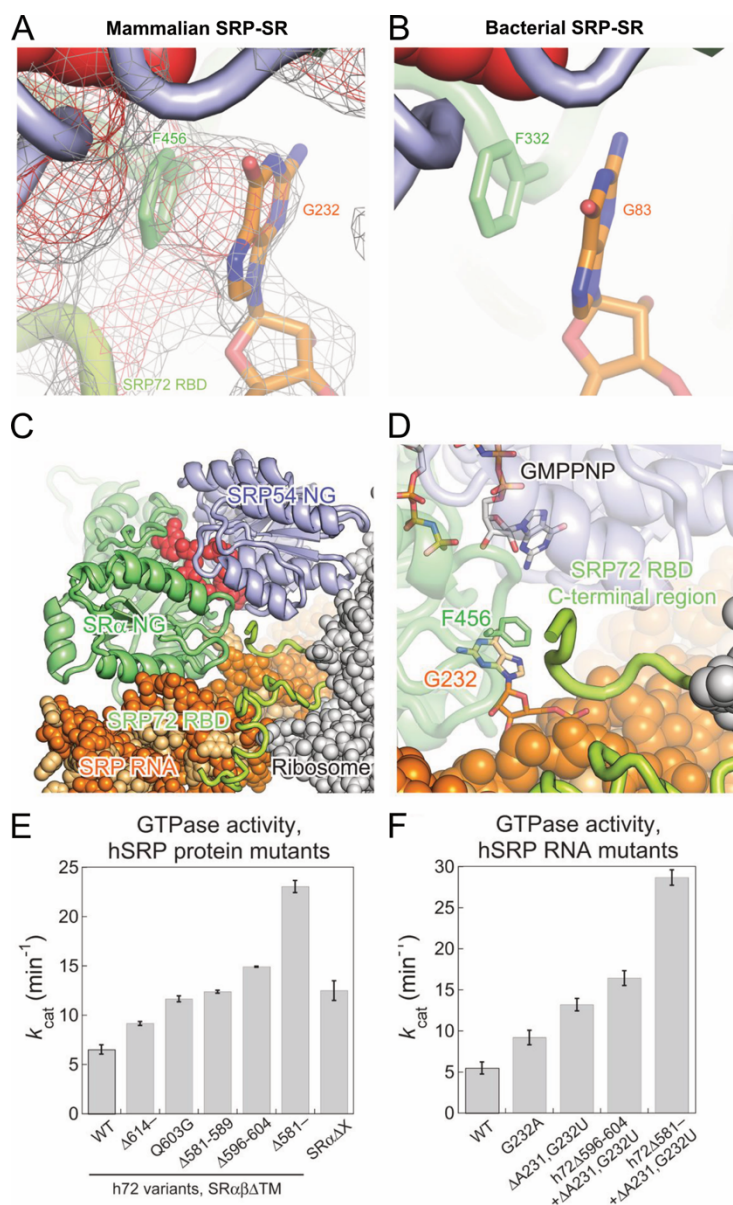


**Figure 2.6. GTPase inhibition of active site residues in mammalian SRP system. (A-B)** Close up view of active site structure of distal conformation from mammalian SRP (**A**) (PDB: 6FRK) (Kobayashi et al., 2018) and bacterial SRP (**B**) (PDB: 5NCO) (Jomaa et al., 2017). Stacking interaction between phenylalanine and RNA base is shown. (**C-D**) View of active site structure of distal conformation from mammalian SRP showing the proximity of G232 as well as C-terminus of SRP72 to the active site (PDB: 6FRK) (Kobayashi et al., 2018). (**E-F**)  $k_{cat}$  was measured for different mutants and plotted on a bar graph. Data represented as mean  $\pm$  SD, with  $n=3$ .

Surprisingly, all C-terminal truncations of SRP72 led to an increase in GTPase activity (Fig. 2.6E and Fig. S2.6A), rather than a decrease which was suggested by previous studies in bacterial system. Moreover, mutation on G232 also led to increase in GTPase activity (Fig. 2.6F and Fig. S2.6B). When RNA and SRP72 mutations were combined, we observed over 5-fold increase in  $k_{cat}$  of GTP hydrolysis (Fig. 2.6F). This is consistent with our previous data with SR mutants, where disruption of distal site interactions leads to an increase in GTPase activity (Fig. 2.5C and D). Thus, interactions at the distal site are designed to inhibit GTP hydrolysis in mammalian system. As discussed in the previous section, this inhibition would increase the lifetime of transfer-ready targeting complex and may provide longer time window for substrate transfer to Sec61. The mechanistic details of what gives rise to the opposite phenotypes in mammalian system compared to bacterial system despite having similar active site structure would require extensive study in the future.

### 2.3 DISCUSSION

Co-translational targeting of nascent proteins by SRP pathway is a multi-step process (Zhang et al., 2010; Zhang & Shan, 2014). After initial substrate recognition and binding by SRP, it recruits SR to deliver targeting intermediate to the membrane (Akopian et al., 2013; Zhang & Shan, 2014). In bacterial system, this step is mediated by the interaction between

the amphipathic helix of FtsY (bacterial SR) and the membrane (Hwang Fu et al., 2017).

On the other hand, how substrates reach membrane after initial SR recruitment has been poorly understood in mammalian system. In this work, we observe, for the first time, multiple conformational changes during membrane targeting by SRP-SR complex and provide a molecular model for membrane targeting steps in mammalian system.

In mammalian SRP system, SR $\beta$  is a membrane protein, and SR $\alpha$  is attached to SR $\beta$  through the X-domain (Nyathi et al., 2013). Thus, mammalian SR is naturally localized near the membrane, and it has been speculated that this proximity is sufficient for delivering translating ribosomes to the membrane. However, SR NG-domain and X-domain is connected through a long unstructured flexible linker. Thus, if the linker is in an extended form, targeting intermediate can be far away from the membrane. Indeed, our data suggests that SR, in the absence of SRP, is in an extended conformation (Fig. 2.3C). Based on the FRET value of low FRET population ( $\sim 0.15$ ), the distance between NG-domain and SR $\beta$  would be at least 90Å, which is quite far for any spontaneous delivery of substrates. Thus, mammalian SRP requires additional regulated mechanism to ensure delivery of targeting intermediates closer to the membrane.

Our smFRET data provides direct evidence that SR compaction mediates membrane targeting. Importantly, SR compaction only occurs after interaction with SRP (Fig. 2.3D). As SR is known to interact with ribosomes by itself (Jadhav et al., 2015), this regulation by SRP is crucial for maintaining specificity of the pathway by selectively bringing SRP-bound ribosomes near the membrane. Moreover, this suggests that there may be additional interactions between SRP and SR other than between the two NG-domains, that exerts this

mode of regulation. Further studies would be required to elucidate detailed mechanism of regulation of SR compaction.

In addition to membrane targeting, SR compaction is found to be essential for initiating subsequent conformational changes of SRP-SR complex. Our data from mutational studies show that NG-complex detachment from proximal site is inhibited by mutations inhibiting SR compaction (Fig. 2.4E and F,  $\Delta 371$ ). The exact nature of this phenotype is yet to be determined, but based on generated structural model, it seems likely that clash or interaction between X-domain and ribosome induces NG-complex detachment (Fig. S2.5B). In addition, disruption of SR compaction leads to the largest defect in targeting activity (Fig. 2.5A,  $\Delta 371$ ). These data further signify the importance of SR compaction with dual role in mammalian SRP pathway.

SRP-SR NG-complex movement from the proximal site to the distal site is not a feature unique to mammalian system. Similar conformational change has been observed in bacterial system (Kuang Shen et al., 2012). In bacteria, distal conformation was shown to be important for GTPase activation to recycle enzymes (Kuang Shen et al., 2013; Voigts-Hoffmann et al., 2013). Surprisingly, we observed an opposite phenotype in mammalian system, where distal conformation inhibits GTP hydrolysis. Any mutations disrupting NG-complex docking at the distal site, or mutations disrupting interactions at the GTPase active site led to higher GTP hydrolysis activity (Fig. 2.5C, Fig. 2.6E and F). The precise mechanism that exerts this phenotype remains to be elucidated, but this opposite phenotype leads to interesting hypothesis about the evolution of SRP pathway.

Cellular concentration of SRP (~500nM in mammalian cells) is well below the concentration of ribosome (40-50 $\mu$ M) requiring SRP to be efficiently recycled to ensure that all substrates are targeted (Kulak et al., 2014; Zhang & Shan, 2014). On the other hand, premature dissociation from substrate before complete transfer of substrate to Sec61 translocon could expose hydrophobic signal sequence or transmembrane domain to cytosol, which would lead to aggregation. Thus, the timing of SRP dissociation through GTP hydrolysis needs to be precisely controlled for balance between processivity and accuracy. Based on this, we can speculate that in bacteria, substrate engagement of SecYEG translocon may be more efficient requiring less time, allowing SRP to be highly processive. On the other hand, in mammals, substrate engagement of Sec61 translocon may be slow requiring more time. Thus, SRP evolved to inhibit GTP hydrolysis to increase lifetime of SRP-SR complex and provide sufficient time for substrate transfer from SRP to translocon. This could be particularly important for substrates with less-hydrophobic signal sequences as their initial interaction with Sec61 may be even slower. Interestingly, native SRP has been traditionally purified from isolated ER microsomes (Peter Walter & Blobel, 1983) and preliminary studies showed that roughly 40% of SRP is localized on ER membrane (P. Walter, 1983). Moreover,  $k_{\text{cat}}$  of stimulated GTP hydrolysis of mammalian SRP-SR complex is much slower than that of bacterial system (Lee et al., 2018; Peluso et al., 2001), supporting the idea that mammalian SRP has evolved to increase lifetime of targeting intermediate at the ER membrane.

In summary, our work describes a new detailed molecular model for mammalian SRP pathway. Previous studies showed presence of signal sequence pre-organizes SRP into proximal conformation, and this efficiently recruits SR to the proximal site (Lee et al., 2018).

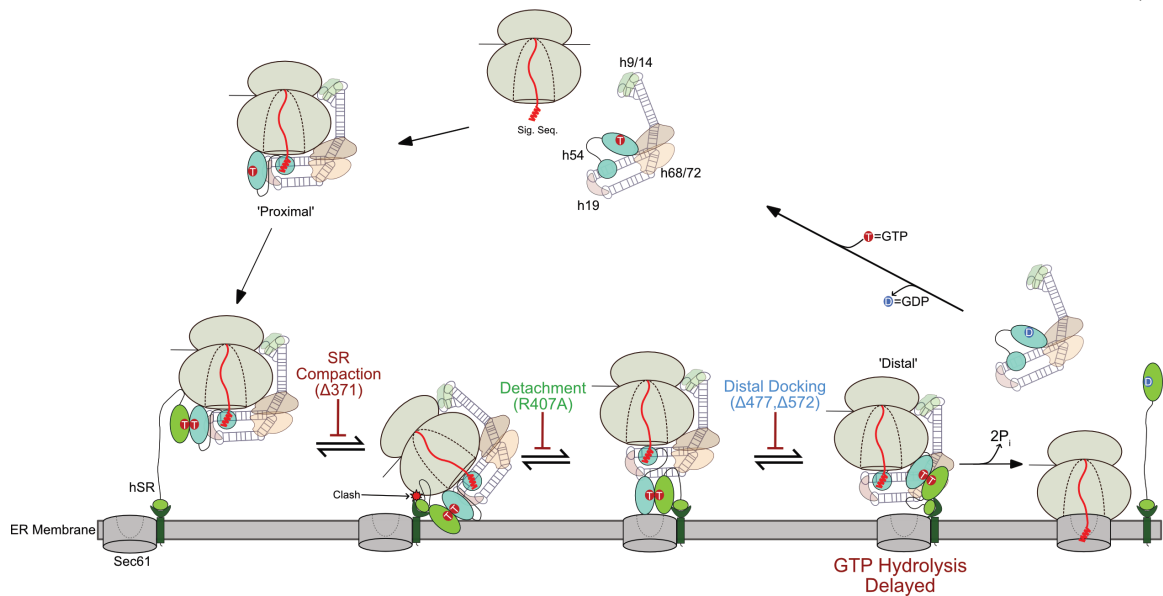


**Figure. 2.7 Model for mammalian SRP pathway.** SRP binds to signal sequence exposed RNC, which pre-organizes SRP into proximal conformation. This conformation rapidly recruits SR $\alpha$ -NG to the proximal site. SRP binding to SR induces compaction (SR Compaction), and this introduces potential clash at the proximal site that induces detachment of NG complex from the proximal site (Detachment). NG-complex can then dock at the distal site (Distal Docking), where multiple protein interactions stabilizes the complex to delay GTP hydrolysis. This delay potentially provides sufficient time-window for substrate transfer from SRP to Sec61 translocon. After transfer, GTP is hydrolyzed and SRP/SR can be recycled for additional rounds of targeting.

Upon SRP-SR interaction, SR compacts to bring the targeting intermediate near the membrane and introduces potential clash between X-domain and ribosome to induce detachment of SRP-SR complex from proximal site (Fig. 2.7). NG-complex then can dock at the distal site to expose Sec61 binding site and allow substrate transfer to the translocon (Fig. 2.7). We find that GTP hydrolysis is delayed through multiple interactions in distal conformation, which may provide sufficient time-window for substrate engagement by Sec61. After transfer, GTP is hydrolyzed to dissociate SRP-SR complex to recycle them for

additional rounds of targeting. Compared to bacterial SRP, mammalian SRP seem to have evolved to increase the lifetime of targeting complex more than the processivity.

## 2.4 MATERIALS AND METHODS

### *Vectors.*

Most vectors used in this study has been described previously (Lee et al., 2018). For fluorescence labeling of SRP68, sfp recognition motif (ybbr6, DSLEFI) was inserted after residue P149 through fastcloning. For fluorescence labeling of SR $\beta$  $\Delta$ TM, longer sfp recognition motif (ybbr11, DSLEFIASKLA) was inserted at the N-terminus through fastcloning. All SR mutants were generated by replacing original residues with residues specified in Fig. 2.4A. SRP72 truncation mutants were generated by removing residues specified in Fig. S2.6A.

### *Biochemical Preparations.*

Human SRP components were prepared as described previously (Lee et al., 2018).

### *Fluorescence Labeling*

Fluorescence labeling of SRP54 (C12), SRP54 (C47), SRP19 (C64), and SR $\alpha$  $\beta$  $\Delta$ TM C-terminus has been described previously (Lee et al., 2018).

*SRP68/72.* A sfp recognition motif (ybbr6, DSLEFI) was inserted right after residue P149 on SRP68. Atto647N maleimide was conjugated to CoA through sulfhydryl group. CoA-Atto647N was attached on underlined serine by sfp. The reaction was done for 20

minutes at room temperature with 0.4 molar ratio of protein to sfp enzyme, in the presence of 2-fold excess of CoA-Atto647N. The salt concentration was maintained below 120mM for efficient labeling. The labeled protein was immediately used for SRP assembly. The labeling efficiency was close to 100%.

*SR $\alpha\beta\Delta$ TM*. C-terminus of SR $\alpha$  was labeled using sortase as described previously (Lee et al., 2018). A sfp recognition motif of 11-residue ybbr-tag (DSLEFIASKLA) (Yin et al., 2006) was inserted at the N-terminus of SR $\beta\Delta$ TM. SR $\alpha\beta\Delta$ TM was doubly labeled by carrying out sfp mediated labeling for 30 minutes at room temperature with 0.4 molar ratio of sfp and 2-fold excess of CoA-Atto647N. Subsequently, sortase mediated labeling was done for 3 hours at room temperature with 5-fold excess of sortase and 10-fold excess of GGGC-Atto550. Unconjugated fluorescent species were removed by purifying reaction mixture on Ni-Sepharose resin. The labeling efficiency for sfp labeling was close to 100%, and the efficiency of sortase labeling was around 60~70%.

### ***Biochemical Assays.***

All proteins except for SRP were centrifuged at 4 °C, 100,000 rpm in TLA100 rotor for 30 minutes to remove aggregates before the assay. GTPase activity and co-translational targeting/translocation activity were measured following same procedures as described previously (Lee et al., 2018).

smFRET measurements was done following similar procedure as before (Kapanidis et al., 2005, 2004; Lee et al., 2018). hSRP-4A10L was diluted to 100-200pM in SRP Assay Buffer (50 mM KHEPES (pH 7.5), 150 mM KOAc, 5 mM Mg(OAc)<sub>2</sub>, 10% glycerol, 2 mM

DTT, and 0.04% Nikkol) containing 200  $\mu$ M non-hydrolysable GTP (GppNHp) and 150nM 80S, and 2 $\mu$ M SR $\alpha\beta\Delta$ TM where indicated. For measuring SR conformation, SR was diluted to 100-200pM in SRP Assay Buffer with 200  $\mu$ M GppNHp, 400nM 80S, and 300nM SRP-4A10L where indicated. The measurement and analysis were done following the same procedures described previously (Ingargiola et al., 2016; Lee et al., 2018).

## 2.5 SUPPLEMENTARY FIGURES

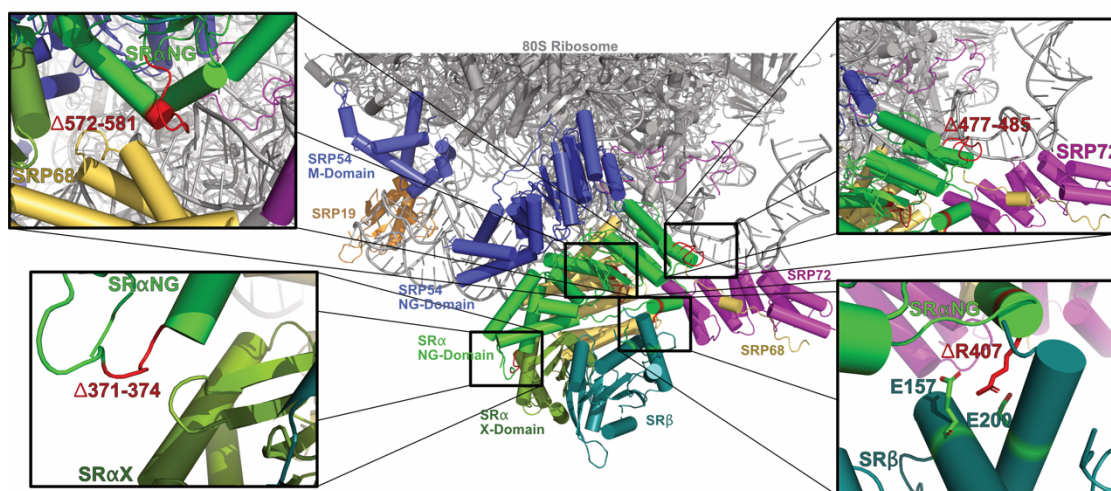


**Figure S2.1. SRP-SR complex in distal conformation with SR mutations highlighted.** Structural view of ternary complex of RNC bound SRP-SR complex in distal conformation with SR mutations highlighted (Kobayashi et al., 2018).

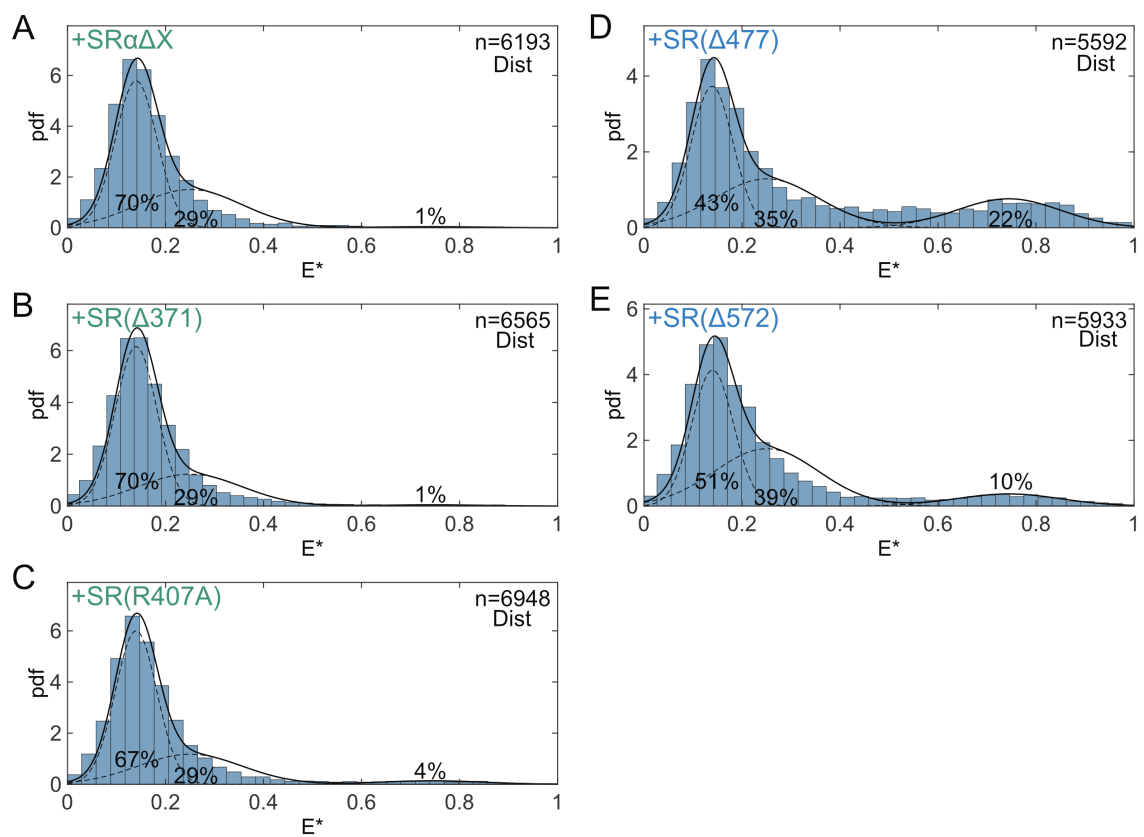


**Figure S2.2. smFRET histograms of distal docking activity of SR mutants. (A-E)** smFRET histograms of signal sequence fused SRP bound to ribosome in the presence of indicated SR mutants measured with distal probes. The measurement conditions were the same as Fig. 2.2.

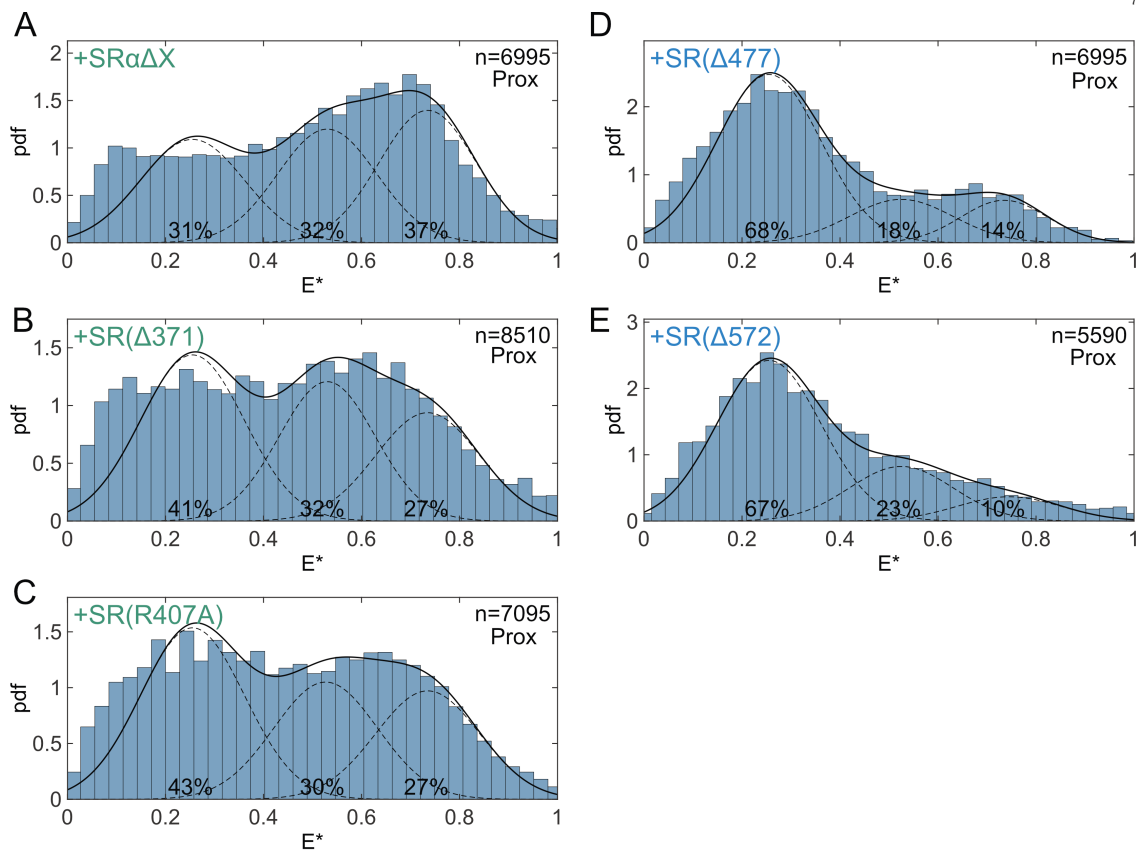


**Figure S2.3. smFRET histograms of NG-complex detachment activity of SR mutants.** (A-E) smFRET histograms of signal sequence fused SRP bound to ribosome in the presence of indicated SR mutants measured with proximal probes. The measurement conditions were the same as Fig. 2.2.

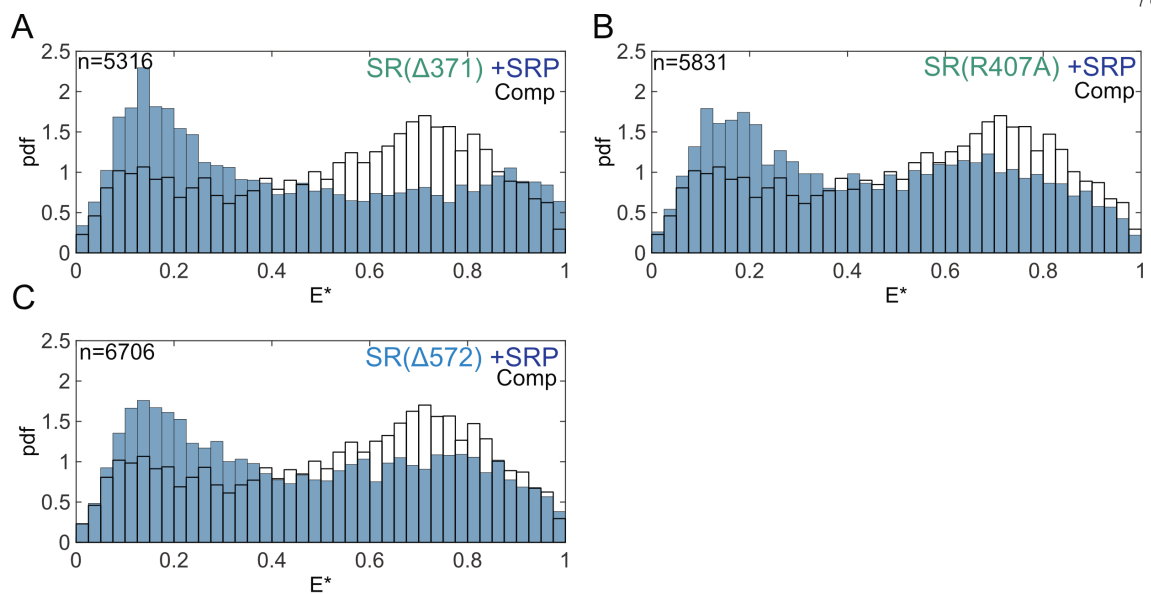


**Figure S2.4. smFRET histograms of SR compaction activity of SR mutants. (A-C)** smFRET histograms of SR mutants in the presence of signal sequence fused SRP bound to ribosomes measured with compaction probes. The measurement conditions were the same as Fig. 2.3.

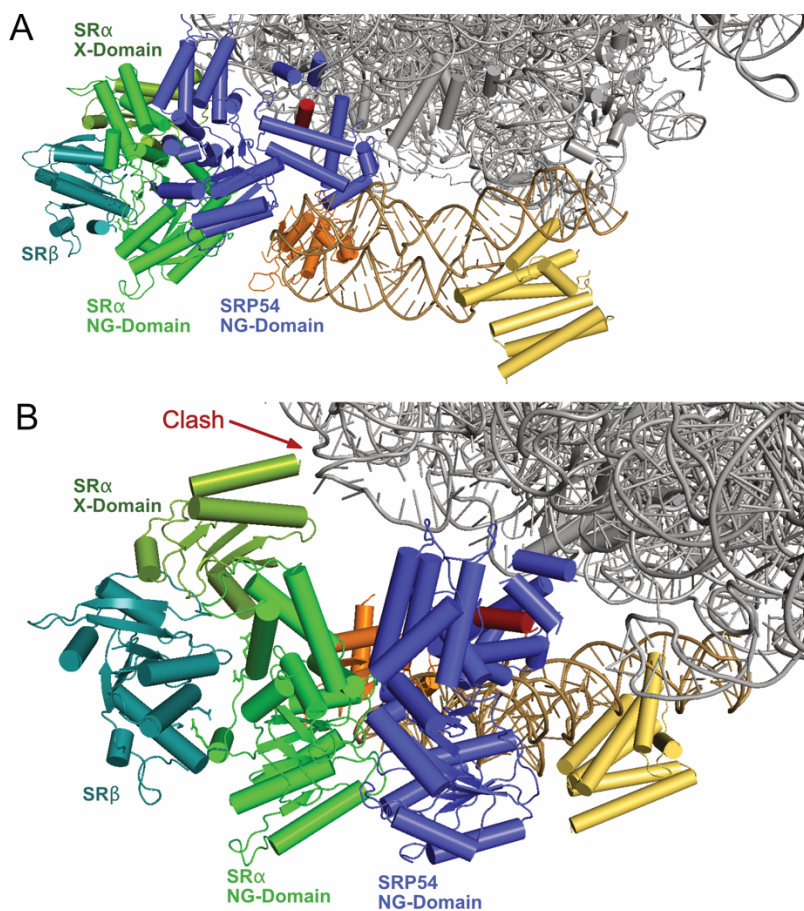


**Figure S2.5. Structural model showing SRP-SR complex docked at the proximal site.** (A) Structural model was generated by aligning SRP-SR complex structure in distal conformation (Kobayashi et al., 2018) to proximal structure (Voorhees & Hegde, 2015) using SRP54 homology. (B) Zoomed-in view of proximal site showing potential clash between X-domain of SR $\alpha$  and ribosome.



## REFERENCES

- Akopian, D., Shen, K., Zhang, X., & Shan, S. (2013). Signal Recognition Particle: An Essential Protein-Targeting Machine. *Annual Review of Biochemistry*.  
<https://doi.org/10.1146/annurev-biochem-072711-164732>
- Alamo, M. del, Hogan, D. J., Pechmann, S., Albanese, V., Brown, P. O., & Frydman, J. (2011). Defining the Specificity of Cotranslationally Acting Chaperones by Systematic Analysis of mRNAs Associated with Ribosome-Nascent Chain Complexes. *PLoS Biology*, *9*(7), e1001100. <https://doi.org/10.1371/journal.pbio.1001100>
- Ataide, S. F., Schmitz, N., Shen, K., Ke, A., Shan, S. -o., Doudna, J. A., & Ban, N. (2011). The Crystal Structure of the Signal Recognition Particle in Complex with Its Receptor. *Science*, *331*(6019), 881–886. <https://doi.org/10.1126/science.1196473>
- Bacher, G., Lütcke, H., Jungnickel, B., Rapoport, T. A., & Dobberstein, B. (1996). Regulation by the ribosome of the GTPase of the signal-recognition particle during protein targeting. *Nature*, *381*(6579), 248–251. <https://doi.org/10.1038/381248a0>
- Berndt, U., Oellerer, S., Zhang, Y., Johnson, A. E., & Rospert, S. (2009). A signal-anchor sequence stimulates signal recognition particle binding to ribosomes from inside the exit tunnel. *Proceedings of the National Academy of Sciences*, *106*(5), 1398–1403.  
<https://doi.org/10.1073/pnas.0808584106>
- Bradshaw, N., Neher, S. B., Booth, D. S., & Walter, P. (2009). Signal Sequences Activate the Catalytic Switch of SRP RNA. *Science*, *323*(5910), 127–130.  
<https://doi.org/10.1126/science.1165971>
- Chartron, J. W., Hunt, K. C. L., & Frydman, J. (2016). Cotranslational signal-independent SRP preloading during membrane targeting. *Nature*, *536*(7615), 224–228.  
<https://doi.org/10.1038/nature19309>
- Connolly, T., Rapiejko, P., & Gilmore, R. (1991). Requirement of GTP hydrolysis for

- dissociation of the signal recognition particle from its receptor. *Science*, 252(5009), 1171–1173. <https://doi.org/10.1126/science.252.5009.1171>
- Costa, E. A., Subramanian, K., Nunnari, J., & Weissman, J. S. (2018). Defining the physiological role of SRP in protein-targeting efficiency and specificity. *Science*, 359(6376), 689–692. <https://doi.org/10.1126/science.aar3607>
- Flanagan, J. J., Chen, J. C., Miao, Y., Shao, Y., Lin, J., Bock, P. E., & Johnson, A. E. (2003). Signal recognition particle binds to ribosome-bound signal sequences with fluorescence-detected subnanomolar affinity that does not diminish as the nascent chain lengthens. *Journal of Biological Chemistry*. <https://doi.org/10.1074/jbc.M300173200>
- Gamerding, M., Hanebuth, M. A., Frickey, T., & Deuerling, E. (2015). The principle of antagonism ensures protein targeting specificity at the endoplasmic reticulum. *Science*, 348(6231), 201–207. <https://doi.org/10.1126/science.aaa5335>
- Gowda, K., Black, S. D., Moeller, I., Sakakibara, Y., Liu, M.-C., & Zwieb, C. (1998). Protein SRP54 of human signal recognition particle: cloning, expression, and comparative analysis of functional sites. *Gene*, 207(2), 197–207. [https://doi.org/10.1016/S0378-1119\(97\)00627-6](https://doi.org/10.1016/S0378-1119(97)00627-6)
- Guimaraes, C. P., Witte, M. D., Theile, C. S., Bozkurt, G., Kundrat, L., Blom, A. E. M., & Ploegh, H. L. (2013). Site-specific C-terminal and internal loop labeling of proteins using sortase-mediated reactions. *Nature Protocols*, 8, 1787. Retrieved from <https://doi.org/10.1038/nprot.2013.101>
- HAINZL, T. (2005). Structural insights into SRP RNA: An induced fit mechanism for SRP assembly. *RNA*, 11(7), 1043–1050. <https://doi.org/10.1261/rna.2080205>
- Hainzl, T., Huang, S., Meriläinen, G., Brännström, K., & Sauer-Eriksson, A. E. (2011). Structural basis of signal-sequence recognition by the signal recognition particle. *Nature Structural & Molecular Biology*, 18, 389. Retrieved from <https://doi.org/10.1038/nsmb.1994>

- Hainzl, T., & Sauer-Eriksson, A. E. (2015). Signal-sequence induced conformational changes in the signal recognition particle. *Nature Communications*, *6*, 7163. Retrieved from <https://doi.org/10.1038/ncomms8163>
- Halic, M. (2006). Signal Recognition Particle Receptor Exposes the Ribosomal Translocon Binding Site. *Science*, *312*(5774), 745–747. <https://doi.org/10.1126/science.1124864>
- Hartl, F. U., Bracher, A., & Hayer-Hartl, M. (2011). Molecular chaperones in protein folding and proteostasis. *Nature*. <https://doi.org/10.1038/nature10317>
- Hessa, T., Kim, H., Bihlmaier, K., Lundin, C., Boeckl, J., Andersson, H., ... von Heijne, G. (2005). Recognition of transmembrane helices by the endoplasmic reticulum translocon. *Nature*, *433*(7024), 377–381. <https://doi.org/10.1038/nature03216>
- Hessa, T., Meindl-Beinker, N. M., Bernsel, A., Kim, H., Sato, Y., Lerch-Bader, M., ... von Heijne, G. (2007). Molecular code for transmembrane-helix recognition by the Sec61 translocon. *Nature*, *450*, 1026. Retrieved from <https://doi.org/10.1038/nature06387>
- Hortsch, M., Avossa, D., & Meyer, D. I. (1985). A structural and functional analysis of the docking protein. Characterization of active domains by proteolysis and specific antibodies. *J Biol Chem*.
- Huck, L. (2004). Conserved tertiary base pairing ensures proper RNA folding and efficient assembly of the signal recognition particle Alu domain. *Nucleic Acids Research*, *32*(16), 4915–4924. <https://doi.org/10.1093/nar/gkh837>
- Hwang Fu, Y.-H., Huang, W. Y. C., Shen, K., Groves, J. T., Miller, T., & Shan, S. (2017). Two-step membrane binding by the bacterial SRP receptor enable efficient and accurate Co-translational protein targeting. *ELife*, *6*. <https://doi.org/10.7554/eLife.25885>
- Ingargiola, A., Lerner, E., Chung, S., Weiss, S., & Michalet, X. (2016). FRETbursts: An Open Source Toolkit for Analysis of Freely-Diffusing Single-Molecule FRET. *PLOS ONE*, *11*(8), e0160716. <https://doi.org/10.1371/journal.pone.0160716>

- Ingolia, N. T., Lareau, L. F., & Weissman, J. S. (2011). Ribosome Profiling of Mouse Embryonic Stem Cells Reveals the Complexity and Dynamics of Mammalian Proteomes. *Cell*, *147*(4), 789–802. <https://doi.org/10.1016/j.cell.2011.10.002>
- Jadhav, B., McKenna, M., Johnson, N., High, S., Sinning, I., & Pool, M. R. (2015). Mammalian SRP receptor switches the Sec61 translocase from Sec62 to SRP-dependent translocation. *Nature Communications*, *6*, 10133. Retrieved from <https://doi.org/10.1038/ncomms10133>
- Jan, C. H., Williams, C. C., & Weissman, J. S. (2014). Principles of ER cotranslational translocation revealed by proximity-specific ribosome profiling. *Science*, *346*(6210), 1257521–1257521. <https://doi.org/10.1126/science.1257521>
- Jomaa, A., Fu, Y.-H. H., Boehringer, D., Leibundgut, M., Shan, S., & Ban, N. (2017). Structure of the quaternary complex between SRP, SR, and translocon bound to the translating ribosome. *Nature Communications*, *8*, 15470. <https://doi.org/10.1038/ncomms15470>
- Jungnickel, B., & Rapoport, T. A. (1995). A posttargeting signal sequence recognition event in the endoplasmic reticulum membrane. *Cell*, *82*(2), 261–270. [https://doi.org/10.1016/0092-8674\(95\)90313-5](https://doi.org/10.1016/0092-8674(95)90313-5)
- Kapanidis, A. N., Laurence, T. A., Lee, N. K., Margeat, E., Kong, X., & Weiss, S. (2005). Alternating-Laser Excitation of Single Molecules. *Accounts of Chemical Research*, *38*(7), 523–533. <https://doi.org/10.1021/ar0401348>
- Kapanidis, A. N., Lee, N. K., Laurence, T. A., Doose, S., Margeat, E., & Weiss, S. (2004). Fluorescence-aided molecule sorting: Analysis of structure and interactions by alternating-laser excitation of single molecules. *Proceedings of the National Academy of Sciences*, *101*(24), 8936–8941. <https://doi.org/10.1073/pnas.0401690101>
- Karpinets, T. V, Greenwood, D. J., Sams, C. E., & Ammons, J. T. (2006). RNA:protein ratio of the unicellular organism as a characteristic of phosphorous and nitrogen stoichiometry and of the cellular requirement of ribosomes for protein synthesis. *BMC Biology*, *4*(1), 30. <https://doi.org/10.1186/1741-7007-4-30>

- Kobayashi, K., Jomaa, A., Lee, J. H., Chandrasekar, S., Boehringer, D., Shan, S., & Ban, N. (2018). Structure of a prehandover mammalian ribosomal SRP·SRP receptor targeting complex. *Science*, *360*(6386), 323–327. <https://doi.org/10.1126/science.aar7924>
- Kulak, N. A., Pichler, G., Paron, I., Nagaraj, N., & Mann, M. (2014). Minimal, encapsulated proteomic-sample processing applied to copy-number estimation in eukaryotic cells. *Nature Methods*, *11*, 319. Retrieved from <https://doi.org/10.1038/nmeth.2834>
- Lauffer, L., Garcia, P. D., Harkins, R. N., Coussens, L., Ullrich, A., & Walter, P. (1985). Topology of signal recognition particle receptor in endoplasmic reticulum membrane. *Nature*, *318*(6044), 334–338. <https://doi.org/10.1038/318334a0>
- Lauring, B., Kreibich, G., & Weidmann, M. (1995). The intrinsic ability of ribosomes to bind to endoplasmic reticulum membranes is regulated by signal recognition particle and nascent-polypeptide-associated complex. *Proceedings of the National Academy of Sciences*, *92*(21), 9435–9439. <https://doi.org/10.1073/pnas.92.21.9435>
- Lee, J. H., Chandrasekar, S., Chung, S., Hwang Fu, Y.-H., Liu, D., Weiss, S., & Shan, S. (2018). Sequential activation of human signal recognition particle by the ribosome and signal sequence drives efficient protein targeting. *Proceedings of the National Academy of Sciences*, *115*(24), E5487–E5496. <https://doi.org/10.1073/pnas.1802252115>
- Mandon, E. C., Jiang, Y., & Gilmore, R. (2003). Dual recognition of the ribosome and the signal recognition particle by the SRP receptor during protein targeting to the endoplasmic reticulum. *The Journal of Cell Biology*, *162*(4), 575–585. <https://doi.org/10.1083/jcb.200303143>
- Mary, C., Scherrer, A., Huck, L., Lakkaraju, A. K. K., Thomas, Y., Johnson, A. E., & Strub, K. (2010). Residues in SRP9/14 essential for elongation arrest activity of the signal recognition particle define a positively charged functional domain on one side of the protein. *RNA*, *16*(5), 969–979. <https://doi.org/10.1261/rna.2040410>
- Menichelli, E., Isel, C., Oubridge, C., & Nagai, K. (2007). Protein-induced Conformational

- Changes of RNA During the Assembly of Human Signal Recognition Particle. *Journal of Molecular Biology*, 367(1), 187–203. <https://doi.org/10.1016/j.jmb.2006.12.056>
- Mercier, E., Holtkamp, W., Rodnina, M. V., & Wintermeyer, W. (2017). Signal recognition particle binds to translating ribosomes before emergence of a signal anchor sequence. *Nucleic Acids Research*, 45(20), 11858–11866. <https://doi.org/10.1093/nar/gkx888>
- Meyer, D. I. (1982). Characterization of molecules involved in protein translocation using a specific antibody. *The Journal of Cell Biology*, 92(2), 579–583. <https://doi.org/10.1083/jcb.92.2.579>
- Nilsson, I., Lara, P., Hessa, T., Johnson, A. E., von Heijne, G., & Karamyshev, A. L. (2015). The Code for Directing Proteins for Translocation across ER Membrane: SRP Cotranslationally Recognizes Specific Features of a Signal Sequence. *Journal of Molecular Biology*, 427(6), 1191–1201. <https://doi.org/10.1016/j.jmb.2014.06.014>
- Nir, E., Michalet, X., Hamadani, K. M., Laurence, T. A., Neuhauser, D., Kovchegov, Y., & Weiss, S. (2006). Shot-Noise Limited Single-Molecule FRET Histograms: Comparison between Theory and Experiments †. *The Journal of Physical Chemistry B*, 110(44), 22103–22124. <https://doi.org/10.1021/jp063483n>
- Nyathi, Y., Wilkinson, B. M., & Pool, M. R. (2013). Co-translational targeting and translocation of proteins to the endoplasmic reticulum. *Biochimica et Biophysica Acta (BBA) - Molecular Cell Research*, 1833(11), 2392–2402. <https://doi.org/10.1016/j.bbamcr.2013.02.021>
- Ogg, S. C., Barz, W. P., & Walter, P. (1998). A Functional GTPase Domain, but not its Transmembrane Domain, is Required for Function of the SRP Receptor  $\beta$ -subunit. *The Journal of Cell Biology*, 142(2), 341–354. <https://doi.org/10.1083/jcb.142.2.341>
- Pechmann, S., Chartron, J. W., & Frydman, J. (2014). Local slowdown of translation by nonoptimal codons promotes nascent-chain recognition by SRP in vivo. *Nature Structural & Molecular Biology*, 21, 1100. Retrieved from <https://doi.org/10.1038/nsmb.2919>

- Peluso, P., Shan, S., Nock, S., Herschlag, D., & Walter, P. (2001). Role of SRP RNA in the GTPase Cycles of Ffh and FtsY †. *Biochemistry*, *40*(50), 15224–15233.  
<https://doi.org/10.1021/bi011639y>
- Powers, T. (1997). Co-translational protein targeting catalyzed by the Escherichia coli signal recognition particle and its receptor. *The EMBO Journal*, *16*(16), 4880–4886.  
<https://doi.org/10.1093/emboj/16.16.4880>
- Powers, T., & Walter, P. (1995). Reciprocal stimulation of GTP hydrolysis by two directly interacting GTPases. *Science*, *269*(5229), 1422–1424.  
<https://doi.org/10.1126/science.7660124>
- Shan, S., Chandrasekar, S., & Walter, P. (2007). Conformational changes in the GTPase modules of the signal reception particle and its receptor drive initiation of protein translocation. *The Journal of Cell Biology*, *178*(4), 611–620.  
<https://doi.org/10.1083/jcb.200702018>
- Sharma, A., Mariappan, M., Appathurai, S., & Hegde, R. S. (2010). In Vitro Dissection of Protein Translocation into the Mammalian Endoplasmic Reticulum (pp. 339–363).  
[https://doi.org/10.1007/978-1-60327-412-8\\_20](https://doi.org/10.1007/978-1-60327-412-8_20)
- Shen, K., Arslan, S., Akopian, D., Ha, T., & Shan, S. (2012). Activated GTPase movement on an RNA scaffold drives co-translational protein targeting. *Nature*, *492*(7428), 271–275.  
<https://doi.org/10.1038/nature11726>
- Shen, K., Wang, Y., Hwang Fu, Y.-H., Zhang, Q., Feigon, J., & Shan, S. (2013). Molecular Mechanism of GTPase Activation at the Signal Recognition Particle (SRP) RNA Distal End. *Journal of Biological Chemistry*, *288*(51), 36385–36397.  
<https://doi.org/10.1074/jbc.M113.513614>
- Shen, K., Zhang, X., & Shan, S. -o. (2011). Synergistic actions between the SRP RNA and translating ribosome allow efficient delivery of the correct cargos during cotranslational protein targeting. *RNA*, *17*(5), 892–902. <https://doi.org/10.1261/rna.2610411>

- Siegel, V., & Walter, P. (2018). The affinity of signal recognition particle for presecretory proteins is dependent on nascent chain length. *The EMBO Journal*.  
<https://doi.org/10.1002/j.1460-2075.1988.tb03007.x>
- Torella, J. P., Holden, S. J., Santoso, Y., Hohlbein, J., & Kapanidis, A. N. (2011). Identifying Molecular Dynamics in Single-Molecule FRET Experiments with Burst Variance Analysis. *Biophysical Journal*, *100*(6), 1568–1577. <https://doi.org/10.1016/j.bpj.2011.01.066>
- Travers, K. J., Boyd, N., & Herschlag, D. (2007). Low specificity of metal ion binding in the metal ion core of a folded RNA. *RNA*, *13*(8), 1205–1213.  
<https://doi.org/10.1261/rna.566007>
- Verma, R., Oania, R. S., Kolawa, N. J., & Deshaies, R. J. (2013). Cdc48/p97 promotes degradation of aberrant nascent polypeptides bound to the ribosome. *ELife*, *2*.  
<https://doi.org/10.7554/eLife.00308>
- Voigts-Hoffmann, F., Schmitz, N., Shen, K., Shan, S., Ataide, S. F., & Ban, N. (2013). The Structural Basis of FtsY Recruitment and GTPase Activation by SRP RNA. *Molecular Cell*, *52*(5), 643–654. <https://doi.org/10.1016/j.molcel.2013.10.005>
- von Loeffelholz, O., Jiang, Q., Ariosa, A., Karuppasamy, M., Huard, K., Berger, I., ... Schaffitzel, C. (2015). Ribosome–SRP–FtsY cotranslational targeting complex in the closed state. *Proceedings of the National Academy of Sciences*, *112*(13), 3943–3948.  
<https://doi.org/10.1073/pnas.1424453112>
- Voorhees, R. M., & Hegde, R. S. (2015). Structures of the scanning and engaged states of the mammalian SRP-ribosome complex. *ELife*, *4*. <https://doi.org/10.7554/eLife.07975>
- Walker, K. P., Black, S. D., & Zwieb, C. (1995). Cooperative Assembly of Signal Recognition Particle RNA with Protein SRP19. *Biochemistry*, *34*(37), 11989–11997.  
<https://doi.org/10.1021/bi00037a041>
- Walter, P. (1983). Subcellular distribution of signal recognition particle and 7SL-RNA

- determined with polypeptide-specific antibodies and complementary DNA probe. *The Journal of Cell Biology*, 97(6), 1693–1699. <https://doi.org/10.1083/jcb.97.6.1693>
- Walter, P., & Blobel, G. (1983). [53] Signal recognition particle: A ribonucleoprotein required for cotranslational translocation of proteins, isolation and properties (pp. 682–691). [https://doi.org/10.1016/S0076-6879\(83\)96057-3](https://doi.org/10.1016/S0076-6879(83)96057-3)
- Wild, K., Bange, G., Motiejunas, D., Kribelbauer, J., Hendricks, A., Segnitz, B., ... Sinning, I. (2016). Structural Basis for Conserved Regulation and Adaptation of the Signal Recognition Particle Targeting Complex. *Journal of Molecular Biology*, 428(14), 2880–2897. <https://doi.org/10.1016/j.jmb.2016.05.015>
- Yin, J., Lin, A. J., Golan, D. E., & Walsh, C. T. (2006). Site-specific protein labeling by Sfp phosphopantetheinyl transferase. *Nature Protocols*, 1(1), 280–285. <https://doi.org/10.1038/nprot.2006.43>
- Zhang, X., Kung, S., & Shan, S. (2008). Demonstration of a Multistep Mechanism for Assembly of the SRP·SRP Receptor Complex: Implications for the Catalytic Role of SRP RNA. *Journal of Molecular Biology*, 381(3), 581–593. <https://doi.org/10.1016/j.jmb.2008.05.049>
- Zhang, X., Rashid, R., Wang, K., & Shan, S. O. (2010). Sequential checkpoints govern substrate selection during cotranslational protein targeting. *Science*, 328(5979), 757–760. <https://doi.org/10.1126/science.1186743>
- Zhang, X., Schaffitzel, C., Ban, N., & Shan, S. (2009). Multiple conformational switches in a GTPase complex control co-translational protein targeting. *Proceedings of the National Academy of Sciences*. <https://doi.org/10.1073/pnas.0808573106>
- Zhang, X., & Shan, S. (2014). Fidelity of Cotranslational Protein Targeting by the Signal Recognition Particle. *Annual Review of Biophysics*, 43(1), 381–408. <https://doi.org/10.1146/annurev-biophys-051013-022653>